PB82-249186

Augmentation of Fine Particle Collection in the EPxP Scrubber

Air Pollution Technology, Inc.
San Diego, CA

Prepared for

Industrial Environmental Research Lab.
Research Triangle Park, NC

May 82

U.S. Department of Commerce
National Technical Information Service
NTIS

United States
Environmental Protection
Agency

EPA-600/7-82-044
May 1982

EPA

Research and Development

PB82-249186

AUGMENTATION OF FINE PARTICLE COLLECTION IN THE EPxP SCRUBBER

Prepared for

Office of Air Quality Planning and Standards

Prepared by

Industrial Environmental Research
Laboratory
Research Triangle Park NC 27711

REPRODUCED BY
NATIONAL TECHNICAL
INFORMATION SERVICE
U.S. DEPARTMENT OF COMMERCE
SPRINGFIELD, VA. 22161

IERL-RTP-1315

TECHNICAL REPORT DATA
(Please read Instructions on the reverse before completing)

1. REPORT NO. EPA-600/7-82-044	2.	3. RECIPIENT'S ACCESSION NO. PB82 249186
4. TITLE AND SUBTITLE Augmentation of Fine Particle Collection in the EPxP Scrubber		5. REPORT DATE May 1982 6. PERFORMING ORGANIZATION CODE
7. AUTHOR(S) Shui-Chow Yung, Toai Le, Ronald Patterson, and Seymour Calvert		8. PERFORMING ORGANIZATION REPORT NO.
9. PERFORMING ORGANIZATION NAME AND ADDRESS Air Pollution Techology, Inc. 4901 Morena Boulevard, Suite 402 San Diego, California 92117		10. PROGRAM ELEMENT NO. 11. CONTRACT/GRANT NO. 68-02-3102
12. SPONSORING AGENCY NAME AND ADDRESS EPA, Office of Research and Development Industrial Environmental Research Laboratory Research Triangle Park, NC 27711		13. TYPE OF REPORT AND PERIOD COVERED Final; 8/77-8/80 14. SPONSORING AGENCY CODE EPA/600/13

15. SUPPLEMENTARY NOTES IERL-RTP project officer is Dennis C. Drehmel, Mail Drop 62, 919/541-7505.

16. ABSTRACT The report gives results of a study of the A. P. T. electrostatically augmented particle by particle (EPxP) dry scrubber. It is analogous to a venturi scrubber except that it uses relatively large solid particles (instead of water drops) as collection centers for the fine particles in the gas stream. It is a novel device for controlling fine particle emissions at high temperatures and pressures. Bench scale (0.5 and 1.1 A cu m/min) and pilot scale (4.8 A cu m/min) experiments were run at 20-820 C to determine the performance characteristics of the system. Experimental results show that the EPxP dry scrubber can operate at high temperatures and that its particle collection efficiency can be increased by precharging the particles and by polarizing the solid collectors. The report describes both the system and the experimental results.

17. KEY WORDS AND DOCUMENT ANALYSIS

a. DESCRIPTORS	b. IDENTIFIERS/OPEN ENDED TERMS	c. COSATI Field/Group
Pollution	Pollution Control	13B
Dust	Stationary Sources	11G
Aerosols	EPxP Dry Scrubber	07D
Scrubbers	Particulate	07A, 13I
Electrostatics		20C
High Temperature Tests		14B
High Pressure Tests		

18. DISTRIBUTION STATEMENT Release to Public	19. SECURITY CLASS *(This Report)* Unclassified	21. NO. OF PAGES 137
	20. SECURITY CLASS *(This page)* Unclassified	22. PRICE

EPA Form 2220-1 (9-73)

AUGMENTATION OF FINE PARTICLE COLLECTION IN THE PxP SCRUBBER

by

Shui-Chow Yung, Toai Le, Ronald Patterson,
and Seymour Calvert

A.P.T. Inc.
4901 Morena Boulevard, Suite 402
San Diego, California 92117

Contract No. 68-02-3102

EPA Project Officer: Dennis C. Drehmel

Industrial Environmental Research Laboratory
Office of Environmental Engineering and Technology
Research Triangle Park, NC 27711

COLOR ILLUSTRATIONS REPRODUCED
IN BLACK AND WHITE

CONTENTS

Page

Abstract i
Figures iv
Tables vii
Nomenclature viii
List of Abbreviations xi
Acknowledgement xii

Sections

1. Summary and Conclusions 1
   - Summary 1
   - Results 2
   - Experimental Results 3
   - Conclusions 5

2. Introduction 7

3. Theory 13
   - Pressure Drop 14
   - Particle Collection 15

4. Preliminary Experiments 31
   - Collector Charging 31
   - Preliminary EPxP Study 35
   - Bench Scale EPxP 39
   - Comparison Between Theory and Data. 54

5. Auxiliary Experiments 57
   - Pneumatic Transport Experiments 56
   - Collector Injection 59
   - Collector Cleaning Experiments. 69
   - Collector Attrition Experiments 72

6. High Temperature Bench Scale Experiments 74
   - High Temperature Particle Charging Experiments 77
   - Experiments 81
   - Particle Collection Experiments 81

7. Pilot Scale Studies 94
   - Pilot Plant Design 94

CONTENTS (Continued)

8. Evaluations 100

HTP Cleanup Requirements 100
Emissions from PFBC 101
Performance Evaluation 103

9. Recommendations 106

References 107

Appendices

A. Experimental Grade Penetration Curves of The Hot Bench Scale EPxP Scrubber A-1

FIGURES

Number Page

1. Functional diagram of A.P.T. PxP dry scrubber process 8
2. Assembly diagram of a PxP scrubber 10
3. Delta arrangement of 12 PxPs for HTP gas cleaning 11
4. Target efficiency results of various investigators 18
5. Single collector collection efficiencies for inertialess particles 24
6. Single drop collection efficiency versus electrostatic parameter with inertial impaction parameter as parameter. 25
7. Single drop collection efficiency versus inertial impaction parameter with electrostatic parameter as parameter 25
8. Single drop collection efficiency versus inertial impaction parameter with Coulombic force parameter as parameter 27
9. $n^{0.5}$ versus K_p for different values of K_{ic} for charged particle image force with potential field. 28
10. $n^{0.5}$ versus K_p for different values of K_{ip} for the charged collector image force with potential field 29
11. $n^{0.5}$ versus K_p for different values of K_{icp} for the electric dipole interaction force with potential flow 30
12. Impaction charging apparatus 32
13. Charge transferred in 240 s with and without collector granules. 33
14. Impaction charging apparatus designed to have low corona charge 34
15. Charge transfer to collector granules 36
16. Electrostatically augmented PxP scrubber experiment 37
17. Current versus applied voltage. 38
18. Bench scale EPxP experimental apparatus 40
19. Methylene blue particle size distribution (scrubber inlet). 43

FIGURES (continued)

Number Page

20. Experimental grade penetration curves 48

21. Experimental grade penetration curves 49

22. Experimental grade penetration curves of the E PxP. 50

23. Effects of pressure drop on PxP penetration 51

24. Experimental grade penetration curves forr PxP scrubber 52

25. Performance comparison between long throat and short throat 53

26. Predicted and measured PxP performance 55

27. Apparatus for studying pneumatic transport 58

28. Inclined transport pipe solid handing capacity 61

29. Sand flow experimental setup 65

30. Experimental collector discharge rate 66

31. Experimental collector discharge rate 67

32. Experimental collector discharge rate 68

33. Study of sand cleaning bustle 70

34. Measured fraction of fly ash as a function of cycle number 71

35. Particle size distribution zirconium T sand before and after grinding 73

36. Hot EPxP bench scale system 75

37. Particle charger design 76

38. Calculated values of d/c vs. b/c for Wire-Plate Geometry (Cooperman 1960) 79

39. Calculated corona-starting voltage vs. relative air density for wire-plate geometry 80

FIGURES (continued)

Number Page

40. Measured negative corona current-voltage curves at various gas temperatures in the bench-scale, EpxP particle charger 82

41. Faraday Cup for charge measurements 83

42. Dilution and Faraday cup for high-temperature charge measurements 84

43. Experimental charge to mass ratio vs. gas temperature in the bench-scale EPxP wire-plate particle charger, at the obtainable operating negative corona applied voltage 85

44. Measured EPxP penetration 90

45. Measured EPxP penetration 91

46. Effect of temperature on penetration 92

47. Effect of particle type on EPxP penetration 93

48. EPxP process flow diagram. 95

49. Measured EPxP inlet and outlet particle concentrations with no coal feed to combustor 97

50. Measured EPxP penetration 99

51. Projected turbine tolerance 102

52. Particle size distribution in gas stream from secondary cyclone 104

53. Maximum allowable penetration to meet GE's turbine requirements 105

TABLES

Number Page

1. Properties of regular grade Florida Zircon sand 42
2. Bench scale EPxP experimental data 46
3. Pneumatic transport experimental data 60
4. Coefficients C_W and C_o 64
5. Hot bench scale EPxP test summary 86

NOMENCLATURE

A = duct cross-sectional area, cm^2

A_g = empirical constant, kV/cm

B_g = empirical constant, $kV/cm^{0.5}$

b = wire-to-plate spacing, cm

C' = Cunningham slip correction factor, dimensionless

C_{Do} = drag coefficient at the throat entrance, dimensionless

C_o = constant, dimensionless

C_w = constant, dimensionless

c = dust concentration, g/cm^3

c = one half of wire-to-wire spacing, cm

d = characteristic dimension, cm

d_c = collector diameter, cm

d_h = hydraulic diameter of duct, cm

d_{or} = orifice diameter, cm

d_p = particle diameter, cm

d_{pa} = aerodynamic particle diameter, μmA

d_{pg} = mass median diameter, μmA or cm

E_c = corona starting field strength, kV/cm

E_c = particle charging field strength, V/cm

E_o = uniform external electric field strength

E_p = polarizing field strength, V/cm

F_e = electrostatic force, $g\text{-}cm/s^2$

F_s = discharge rate of solid, g/s

f = friction factor, dimensionless

f_e = spatial dependence of the electrostatic force in terms of dimensionless coordinates, dimensionless

NOMENCLATURE (Cont.)

K_c = Coulombic corce parameter, dimensionless

K_e = electrostatic force parameter, dimensionless

K_{ex} = external electric field force parameter, dimensionless

K_{ic} = charged particle image force parameter, dimensionless

K_{icp} = electric dipole interaction force parameter, dimensionless

K_{ip} = charged collector image force parameter, dimensionless

L = dense phase transport pipe length, cm

ℓ_t = throat length, cm

m_c = collector mass flow rate, g/s

m_G = gas mass flow rate, g/s

$\overline{Pt}$ = overall penetration, fraction

Pt_d = penetration for particle diameter d_{pa}, fraction

p = pressure, dyne/cm^2

Δp = pressure drop, cm W.C.

Q_c = collector charge, C

Q_c = collector volumetric flow rate, cm^3/s

Q_G = gas volumetric flow rate, cm^3/s

Q_p = particle charge, C

u_c = collector velocity, cm/s

u_c = collector velocity at the throat exit, dimensionless

u_{ce} = collector velocity at throat exit, cm/s

u_G = gas velocity, cm/s

u_G = gas velocity with respect to the collector, cm/s

u_G^* = gas velocity, dimensionless

u_{Gt} = gas velocity at the throat, cm/s

u_o = undisturbed upstream velocity, cm/s

NOMENCLATURE (Cont.)

u_p = particle velocity, cm/s

u_p = particle velocity with respect to collector, cm/s

u_p^* = particle velocity, dimensionless

T_G = gas temperature, ^oC

t = time, s

r_o = wire radius, cm

V_c = corona starting voltage, kV

y_o = distance of the limiting streamline from the axis of collector motion, cm

z = rectangular coordinate in the direction of flow, cm

Greek

δ = relative gas density, dimensionless

η = single collector efficiency, dimensionless

μ_G = gas viscosity, g/cm-s

σ = bulk density of solid, g/cm^3

σ_c = collector density, g/cm^3

σ_G = gas density, g/cm^3

σ_g = geometric standard deviation, dimensionless

σ_p = particle density, g/cm^3

ε = void fraction, fraction

ε_c = dielectric constant of the collector, F/cm

ε_p = dielectric constant of the particle, F/cm

ε_o = dielectric constant of gas, F/cm

θ_r = repose angle, degree

LIST OF ABBREVIATIONS

AFBC - Atmospheric fluidized bed combustor
EPxP - Electrostatically augmented A.P.T. PxP dry scrubber
PxP - A.P.T. particle-by-particle dry scrubber
NSPS - New source performance standard
UP/NC - Uncharged particle/non-polarized collector
CP/NC - Charged particle/non-polarized collector
UP/PC - Uncharged particle/polarized collector
CP/PC - Charged particle/polarized collector
HTP - High temperature and high pressure
PFBC - Pressurized fluidized bed coal combustor

ACKNOWLEDGEMENT

A.P.T., Inc. greatly appreciates the following individuals' contributions during this study:

Mr. James Abbott	Chief, Particulate Technology Branch EPA, IERL/RTP
Dr. Dennis C. Drehmel	Project Officer EPA, IERL/RTP

Section 1

SUMMARY AND CONCLUSIONS

SUMMARY

The A.P.T. PxP (particle collection by particles) scrubber is analogous to a Venturi scrubber except that relatively large solid granules are used as fine particle collectors instead of liquid drops. It is a novel device especially suitable for controlling fine particle emissions from advanced energy processes, such as pressurized fluidized bed coal combustors. By properly selecting collector granules and structural materials, the PxP scrubber is capable of operating at any temperature and pressure encountered in advanced energy processes.

In a PxP scrubber, particle collection by inertial impaction on individual collector granules is the principal collection phenomenon. Collection by impaction is less effective for sub-micron particles than larger ones, but several approaches may be used to improve it and electrostatic augmentation is one of them. This report describes a research program in which the feasibility and performance characteristics of the EPxP (electrostatically augmented PxP) scrubber were determined experimentally in bench and pilot scale units under ambient and high temperature conditions.

Preliminary Bench Scale Study

To evaluate the feasibility of electrostatically augmenting the PxP, an EPxP scrubber system was built of Plexiglass. It consisted of blower, particle precharger, EPxP contactor, gravity settler for collector separation, particle generator, collector storage hopper, and various flow and pressure measuring instruments. The contactor was inclined at an angle of 60° with the horizon to allow vertical collector injection and a continuous flow system of three contactors in a "delta" arrangement.

Two EPxP throat configurations were tested, the first with a round cross-section. Throat diameter was 1.6 cm and the throat length was 5 cm (from collector injection point to throat exit). The other throat had a square cross-section. Each side was 1.6 cm and the throat length was 28 cm.

There was no attempt to precharge the collector granules in the bench scale apparatus but some triboelectric charging occurred. The collector granules could be polarized with an external field. When using the long square throat, the polarizer, consisting of two oppositely charged parallel plates, was located at the throat. When using the round throat, the polarizer was located in the lift pipe after the contactor.

The apparatus was operated at ambient temperatures and pressures and under forced-draft conditions. Test particles were injected into the air stream upstream of the particle charger. After the particle charging section, the air and particles flowed into the EPxP, where contact with collector granules occurred.

The collector granules were regular grade Florida zircon sand with a mass median diameter of about 0.11 mm. The sand was passed through the system on a once-through basis.

After the contactor, the granules were lifted by the cleaned air to a gravity settler. In the settler an expanding cross section slowed the gas to less than the settling velocity of the collector granules. The air was vented to the atmosphere after the collector separator.

Results

Both methylene blue and fly ash particles were used in the experiments. Particle samples were taken simultaneously at the inlet and outlet of the EPxP with cascade impactors. The inlet sampling point is located after the particle precharger so the measured EPxP collection did not include collection by the particle charger.

The EPxP contactor was operated in the following modes:

1. UP/NC (uncharged particle/non-polarized collector)
2. CP/NC (charged particle/non-polarized collector)
3. UP/PC (uncharged particle/polarized collector)
4. CP/PC (charged particle/polarized collector)

It should be noted that "uncharged" and "non-polarized" mean that the natural charges on the particles and the granules were not neutralized. The granules and particles might actually carry charges. This is especially true for the collector granules since they can acquire charges by friction.

Experimental results showed the particle collection efficiency could be increased either by precharging the particles or by polarizing the collectors. The particle collection efficiency was further increased by simultaneoulsy precharging the particles and polarizing the collectors. Due to its longer throat length and inclusion of the polarizer, the square throat showed a higher collection efficiency than the round throat.

High Temperature Bench Scale Experiments

In order to obtain design information for the particle charger, contactor, collector separator, and EPxP under high temperature conditions, a bench scale scrubber system was built from 309 s.s. It was similar to the room temperature bench scale EPxP except it had a furnace for producing the hot gas and a quencher for cooling the gas. The system was designed for a maximum volumetric gas flow rate of 1.1 Am^3/min (38 ACFM) and a maximum collector mass/gas volume ratio of 8 kg/ m^3.

The furnace had a natural gas burner for heating the air to desired temperatures. Fly ash particles were injected into the flame to deagglomerate and mix the particles. The particles next entered the wire-and-plate particle charger which was made from machinable ceramic. The particle charger was followed by the EPxP contactor which was also made from machinable ceramic. Two opposite surfaces were covered with 309 s.s. so that a high electrical potential could be applied to one of the plates to polarize the contactor. The collector granules were injected into the contactor downstream of the throat entrance.

The granules and the collected particles were separated from the gas stream in a baffled, gravity settler. Downstream from the collector separator were a quencher to cool the gas and a liquid entrainment separator to remove the water drops from the quencher before the gas was vented to the atmosphere.

Thermocouples and pressure gauges were installed at each process step of the system for monitoring the gas temperatures and pressures. Gas flow rates were monitored with a Venturi meter and an electronic flow meter.

Experimental Results

The particle charger did not show any operational problems at temperatures up to 800°C. The negative corona current-voltage characteristics of the bench scale hot EPxP particle charger were then determined for various temperatures. It is generally observed that the corona starting voltage operating range between the corona starting voltage and the spark-over voltage decreases with gas density decreases. Present results agreed with these findings. The measured spark-over voltage decreased from 19kV at 20°C to 7.5 kV at 450°C and to 5 kV at 650°C.

A Faraday cup, which consisted of a shielded, insulated, glass fiber filter connected to an electrometer, was used to measure the charge/mass ratios at various temperatures. It was 7×10^{-2} C/kg at ambient temperatures and 1×10^{-2} C/kg at 800°C for fly ash particles with a mass median diameter of about 1.5 μmA and a "σ_g" (geometric standard deviation) about 2.0. Even though the obtainable charge level at high temperatures is 7 times lower than that at low temperatures, it is still acceptable.

Particle penetration was determined for the EPxP scrubber at several gas temperatures. Results confirmed that the particle collection efficiency of the PxP scrubber could be increased by augmenting the scrubber with electrostatic forces, even under high temperature conditions. The improvement was greater with small particles. For particles larger than 5 μmA diameter, the improvement was minimal.

The measured collection efficiency decreased with increasing temperature. This is consistent with the findings of Calvert and Parker (1977) that high temperature particle collection is more difficult than that at low temperatures.

Comparison of the experimental penetration with that computed from Venturi scrubber design equations for UP/NC conditions revealed that the measured performance is worse than predicted. The higher penetration of the scrubber could be due to:

1. particle bounce
2. attrition of collectors, and
3. dirty collectors.

The test particles used in the experiments were re-dispersed power plant fly ash. The properties of power plant fly ash are different from that of pressurized fluidized-bed combuster (PFBC) fly ash which is sticky. Particle bounce would be less with PFBC particles. To determine the performance of the EPxP scrubber on sticky particles, experiments were done on titanium dioxide aerosol. Experimental results indicated that the scrubber was more efficient in removing titanium dioxide particles than on power plant fly ash. Titanium dioxide is used to simulate PFBC fly ash.

The collector granules used in the experiments are regular grade Florida zircon sand which is irregular in shape and contains a large amount of fine dust. Particle samples collected by cascade impactors showed two distinct colors, black in the lower impactor stages and sandy brown in the upper. This indicates either attrition or re-entrainment of fine dust contained in the sand. Cleaning the sand by passing it through the system several times helped but did not completely alleviate the problem.

Pilot Scale EPxP System

A 4.8 Am^3/min (170 ACFM) pilot scale EPxP was built for controlling the particle emissions from an A.P.T. atmospheric fluidized-bed coal combuster. The pilot plant contained an integral collector cleaning system for removing collected particles. The collector granules were continuously recirculating in the system; i.e. the granules from the collector separator were cleaned and reinjected into the EPxP contactor. The pilot plant was operated for several days at 870°C (1,600°F) without problems.

The attrition problem mentioned earlier prevented particle collection efficiency determination. Several alternative collector granules were evaluated and it was found that high density alumina spheres were the best. They were able to stand high temperatures with little attrition. However, only one manufacturer produces small, 100 μm diameter alumina spheres in limited amounts. Since the spheres are not mass produced, they are expensive and not yet economically feasible.

CONCLUSIONS

The EPxP is capable of operating under high temperature conditions. The particle collection efficiency of the EPxP can be greatly increased by precharging the particles and polarizing the collector granules.

Experimental results at ambient conditions indicate that the EPxP is capable of cleaning the gas to meet the GE projected turbine requirement (0.1 g/Nm^3) at a scrubber pressure drop of 51 to 65 cm W.C. when the particles are charged and the collector granules are polarized. The EPxP cannot meet the cleanup requirement with the same pressure drop at high temperatures. To meet the cleanup requirement, it is necessary to operate the EPxP at a higher pressure drop. Since neither a reliable mathematical model nor experimental data at high pressure drops are available, the required scrubber pressure drop is not known.

To evaluate the EPxP under high temperature conditions, attrition resistant granules are needed. Such a material is currently not available at a reasonable cost.

Section 2

INTRODUCTION

Fine particle removal from gases at the high temperatures and pressures encountered in fluidized-bed combustors and various fuel conversion processes places severe requirements on the gas cleaning system. The environment of reactive gas mixtures, temperatures up to 1,100°C and pressures up to 1,520 kPa (15 atmospheres) can be withstood by only a few structural materials. Particle collection efficiency must be high to meet the NSPS (new source performance standard) and turbine requirements if the gas is to be expanded through a gas turbine.

Only a few developmental control devices are capable of operating at these extreme temperatures and pressures. The A.P.T. Dry Scrubbing System, which we call the "PxP" system (for "particle collection by particles"), is one of the devices. The PxP system is a patented device (Calvert, 1979) which uses relatively large particles as collection bodies for the fine particles in the gas stream. The large particles (collector granules) introduced to the gas stream can collect fine particles by mechanisms such as diffusion, inertial impaction, interception, and electrophoresis. The larger size of the granules allows easy separation from the gas stream by methods such as cyclones, entrainment separators, and gravitational settling.

Figure 1 is a functional diagram of the process steps for a representative PxP system. The process steps on this diagram could occur simultaneously in one device, or separately in several pieces of equipment. In the first step the collector granules are introduced into the gas stream by pneumatic or mechanical injection. Then in the second step the contact between the collector granules and the gas is improved to encourage the movement of the fine particles to the collectors. A Venturi device can be used for the contactor, in which case the PxP system would be analogous to a Venturi scrubber except that solid collectors are used instead of liquid drops.

The next process step is to remove the collector granules in a separator after allowing capture of the fine particles in the contactor. At this stage, the large size and mass of the collector particles is utilized to sepa-

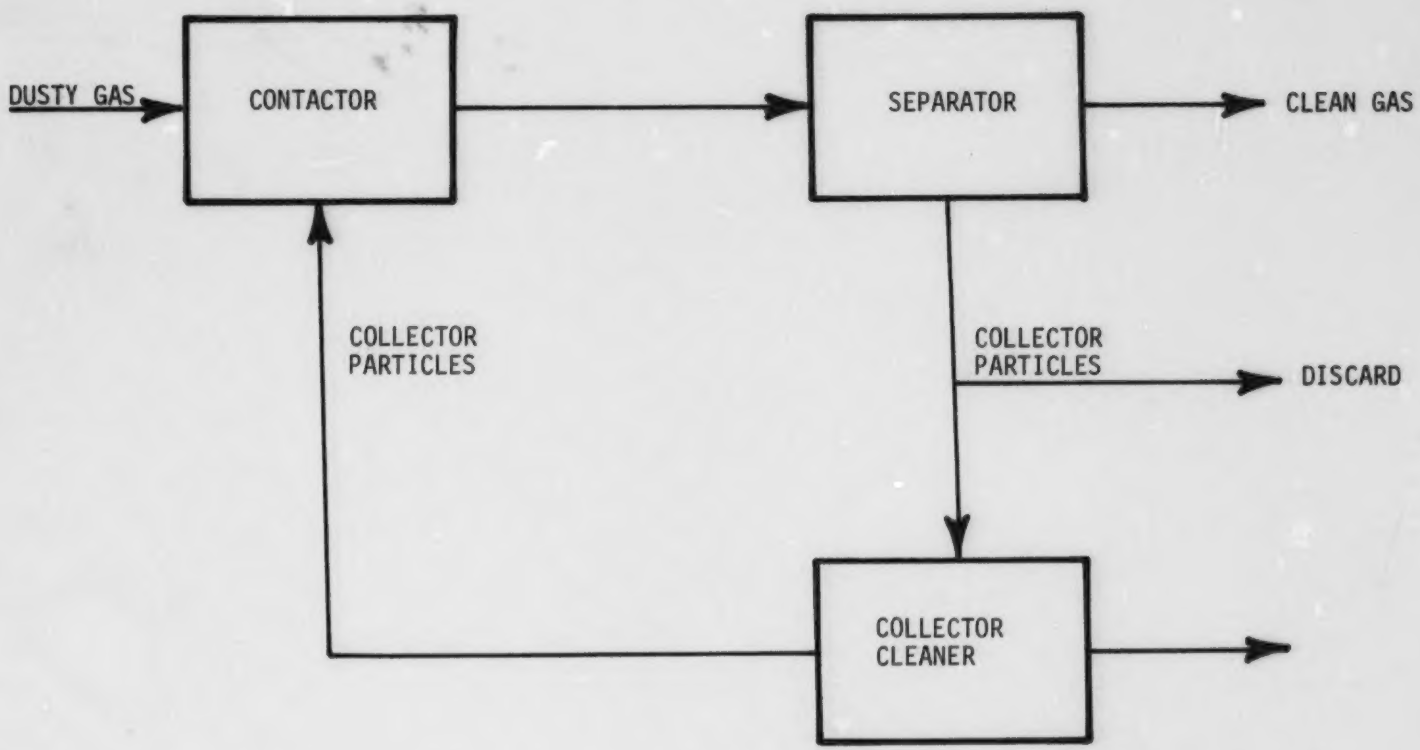
DUSTY GAS
CONTACTOR
SEPARATOR
CLEAN GAS
COLLECTOR PARTICLES
COLLECTOR PARTICLES
DISCARD
COLLECTOR CLEANER

Figure 1. Functional diagram of A.P.T. PxP Dry Scrubber process.

rate them from the gas. Two streams are shown leaving the separator: the cleaned gas leaves the process at this point, and the second stream represents the flow of collector particles to the next step. The final process involves either discarding the collector particles or cleaning them for recycle and disposing of the fine particles collected from the gas stream.

Patterson et al. (1980) evaluated several possible PxP designs and concluded that the systems presented in Figures 2 and 3 are feasible. In this design, twelve PxP's are arranged in four "delta" units for controlling the emissions from a typical pressurized fluidized-bed coal combustor. Each PxP contactor has an angle of 60° or more to the horizon. The solid collector granules are injected at the contactor entrance and are transported to a baffled collector separator.

Collector granules are separated from the gas and are recycled through a vertical downcomer to the next contactor. The dense flow of the collectors in the downcomer and the rubbing of collectors against each other causes the collected particles to be released. A bleed stream of gas from the downcomer carries the small particles into a separate cleaning process at low temperature and pressure. As a result the collector particles are continuously cleaned just before introduction into the contactor.

Advantages

This design:

1. Maximizes the flow of collector by having a vertical downcomer.
2. Eliminates the requirement for an external collector lifting system.
3. Provides an integral method for collector cleaning.

Particle collection in the PxP scrubber is achieved principally through the mechanism of inertial impaction. Particle penetration through the scrubber increases as the particle aerodynamic diameter decreases. Although the penetration can be decreased by operating at higher collector loadings, greater power is required to accelerate the collector granules.

The performance of the PxP scrubber relies on its ability to collect particles with minimal reentrainment. Adhesion of the particles to the collector granule surface is a function of the London-Van der Waals forces and naturally occurring electrostatic attractive forces. Collision with the

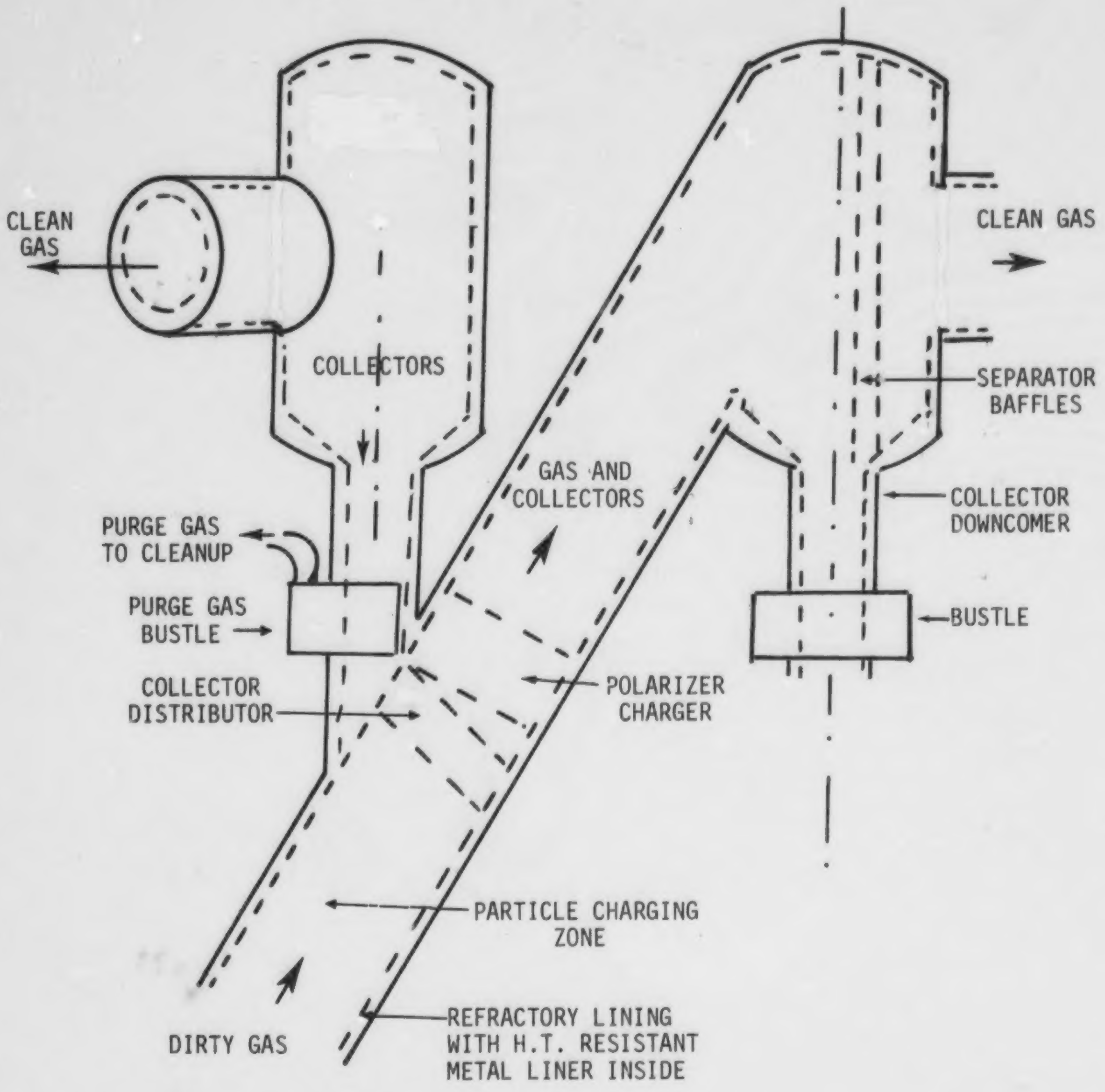
CLEAN GAS
CLEAN GAS
COLLECTORS
SEPARATOR BAFFLES
GAS AND COLLECTORS
COLLECTOR DOWNCOMER
PURGE GAS TO CLEANUP
PURGE GAS BUSTLE
BUSTLE
COLLECTOR DISTRIBUTOR
POLARIZER CHARGER
PARTICLE CHARGING ZONE
DIRTY GAS
REFRACTORY LINING WITH H.T. RESISTANT METAL LINER INSIDE

Figure 2. Assembly diagram of a PxP scrubber.

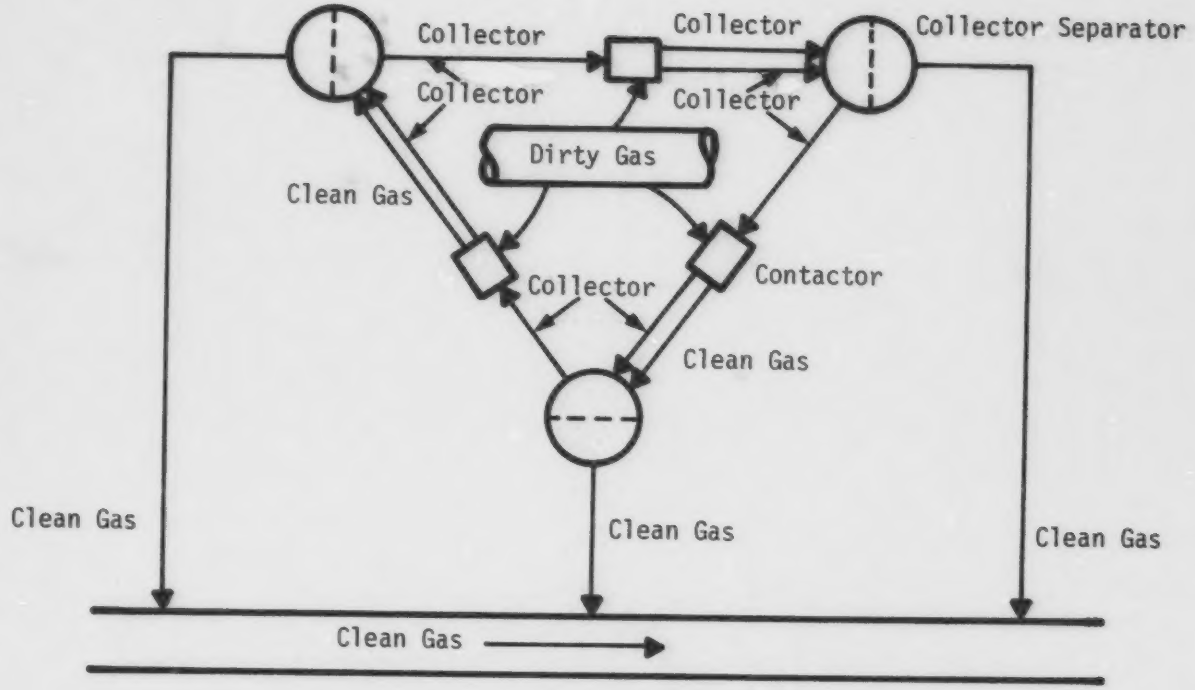
Collector
Collector
Collector Separator
Collector
Collector
Dirty Gas
Clean Gas
Collector
Contactor
Clean Gas
Clean Gas
Clean Gas
Clean Gas
Clean Gas

Figure 3. Delta arrangement of 3 P x P.

scrubber wall and with other granules can produce forces large enough to overcome the attractive forces and dislodge collected particles.

Many approaches could be used to overcome the limitations of inertial impaction and the problems of premature granule unloading. Patterson et al. (1980) recommended electrostatic augmentation, such as by charging the particles and collector granules to opposite polarities.

The feasibility, performance characteristics, and energy requirements of an EPxP (electrostatically augmented PxP) scrubber were determined in the present study. This report presents the results of a theoretical and experimental investigation of the particle collection efficiency of the A.P.T. EPxP Dry Scrubber.

Section 3

THEORY

The basic equations for particle collection in a PxP scrubber are the same as those for Venturi scrubbers (Calvert, 1968, 1970, Boll, 1973, Yung et al., 1977). The equations for penetration, drag on the collector granules, and gas pressure drop after rearrangement read:

$$\frac{dc}{c} = \frac{1.5\ |u_p - u_c|}{u_c\ d_c}\ \frac{Q_c}{Q_G}\ \eta\ dz \tag{1}$$

$$\frac{d\ u_c}{dz} = \frac{3}{4}\ \frac{\rho_G}{\rho_c}\ \frac{(u_G - u_c)^2}{d_c\ \ u_c}\ C_D \tag{2}$$

$$\frac{dp}{dz} = \rho_G u_G \frac{du_G}{dz} - \frac{3}{4}\ \frac{\rho_G}{\rho_c}\ \frac{C_D}{d_c}\ \frac{(u_G - u_c)^2}{u_c}\ \frac{m_c}{A} - \frac{(m_c + m_G)}{m_G}\ \frac{f \rho_G u_G^2}{2d_h} \tag{3}$$

The initial conditions are:

at $z = 0$, $c = c_o$; $u_c = u_{co}$; $u_G = u_{Go}$; $p = p_o$

where c = dust concentration, g/cm^3
C_D = drag coefficient, dimensionless
d_c = collector diameter, cm
Q_c = volumetric flow rate of collectors, cm^3/s
u_c = collector velocity, cm/s
u_G = gas velocity, cm/s
u_p = particle velocity, cm/s
z = rectangular coordinate in the direction of flow, cm
ρ_c = collector density, g/cm^3
ρ_G = gas density, g/cm^3
η = single collector efficiency, dimensionless
Q_G = volumetric flow rate of gas, cm^3/s

p = pressure, dyne/cm^2
m_c = collector mass flow rate, g/s
m_G = gas mass flow rate, g/s
A = duct cross-sectional area, cm^2
d_h = hydraulic diameter of duct, cm
f = friction factor, dimensionless.

The following assumptions were used in the derivation of these equations:

1. The flow is one-dimensional, incompressible and isothermal.
2. Collector particles are uniformly spread across the duct.
3. Collectors are of uniform diameter.
4. There is no attrition of collector granules.
5. Each particle that contacts a collector sticks to it.
6. Collector fraction is small at any cross-section of the scrubber. Therefore, at any location, the gas velocity can be calculated based on total cross-sectional area.

PRESSURE DROP

Calvert (1968, 1970) solved equations (2) and (3) for the Venturi throat by neglecting the wall frictional loss and obtained an explicit expression for predicting the pressure drop. Yung et al. (1977) modified his equation as follows:

$$\Delta p = 1.0 \times 10^{-3}\, u_c^* \; u_{Gt}^2 \; \frac{\rho_c\, Q_c}{Q_G} \tag{4}$$

where u_{Gt} = gas velocity in the throat, cm/s
u_c^* = dimensionless collector velocity at the throat exit, dimensionless
Q_c = collector volumetric flow rate, cm^3/s
Q_G = gas volumetric flow rate, cm^3/s
ρ_c = collector density, g/cm^3
Δp = pressure drop, cm W.C.

The dimensionless collector velocity at the throat exit is calculated from the following equations:

$$u_c^* = \frac{u_{ce}}{u_{Gt}} = 2[1 - x^2 + (x^4 - x^2)^{0.5}] \tag{5}$$

$$x = \frac{3\ell_t\ C_{DO}\ \rho_G}{16\ d_c\ \rho_c} + 1 \tag{6}$$

where u_c^* = dimensionless collector velocity at the throat exit, dimensionless

u_{ce} = collector velocity at the throat exit, cm/s

u_{Gt} = gas velocity at the throat, cm/s

ℓ_t = throat length, cm

d_c = collector diameter, cm

C_{DO} = drag coefficient at the throat entrance, dimensionless

ρ_c = collector density, g/cm^3

ρ_G = gas density, g/cm^3

The drag coefficient at the throat entrance is obtained from the standard curve for spheres.

Yung et al. (1977) also applied equations (2) and (3) to other sections of the Venturi scrubber and presented graphs for estimating the pressure drops in those sections.

PARTICLE COLLECTION

The particle penetration for the PxP scrubber can be predicted from equations (1) and (2) if the single collector efficiency "η" is known.

The single collector collection efficiency is defined as the ratio of the number of particles collected to the number of particles initially contained in the volume swept by the collector. To the extent that one can rationally predict the behavior of the particles as they flow around and onto the collector, one can say that a particle of given diameter and density will strike the collector if it lies initially within a certain distance "y_o" of the axis of motion of the collector. If the particle lies farther away from the axis than "y_o", it will pass by the collector and not be collected. The above reasoning does not apply to mechanism of diffusional collection.

If the particles are uniformly distributed throughout the approaching gas stream, then the collection efficiency equals the ratio of area swept clean to the cross-sectional area of the collector, i.e.,

$$\eta = \frac{\pi y_o^2 \sigma}{\pi d_c^2/4} = \frac{4\sigma y_o^2}{d_c^2} \tag{7}$$

where η = single collector collection efficiency, fraction
σ = attachment coefficient, fraction
d_c = collector diameter, cm
y_o = distance of the limiting streamline from the axis of collector motion, cm

If it is assumed that all particles stick to the collector upon striking it, $\sigma = 1$.

The distance of the limiting particle trajectory from the axis of collector motion, y_o, can be predicted from Newton's law of motion if the velocity distribution of the gas flowing by the collector and the forces acting on the particle are specified. When considering the viscous and electrostatic forces only, the equation of motion for a spherical particle of diameter d_p, density ρ_p and for particle Reynolds number less than one, is given by a momentum balance as:

$$\frac{1}{6} \pi d_p^3 \rho_p \frac{du_p}{dt} = - \frac{3\pi\mu_G d_p}{C'} (u_p - u_G) F_e \tag{8}$$

where d_p = particle diameter, cm
ρ_p = particle density, g/cm^3
u_G = gas velocity with respect to the collector, cm/s
u_p = particle velocity with respect to collector, cm/s
C' = Cunningham slip correction factor, dimensionless

μ_G = gas viscosity, g/cm-s
F_e = electrostatic force, g-cm/s^2
t = time, s

Case 1. Neutral Collector and Neutral Particle

When both the particle and collector are neutral, there is no electrostatic force, i.e., $F_e = 0$. Equation (8) in dimensionless form becomes:

$$K_p \frac{du_p^*}{dt^*} = (u_G^* - u_p^*) \qquad (9)$$

where $K_p = \dfrac{C' \rho_p d_p^2 u_o}{9 \mu_G d_c}$ = inertial impaction parameter, dimensionless

$u_G^* = \dfrac{u_G}{u_o}$ = dimensionless gas velocity with respect to the collector, dimensionless

$u_p^* = \dfrac{u_p}{u_o}$ = dimensionless particle velocity with respect to the collector, dimensionless

$t^* = \dfrac{2 u_o t}{d_d}$ = dimensionless time, dimensionless

u_o = undisturbed upstream velocity, cm/s
d_c = collector diameter, cm
d_p = particle diameter, cm
ρ_p = particle density, g/cm^3
μ_G = gas viscosity, g/cm-s

The solutions to equation (9) depend upon the assumed velocity field around the collector. Langmuir and Blodgett (1946) solved equation (9) for potential flow. Herne (1960) solved it for both potential and viscous flows. Their results are plotted in Figure 4.

The calculations of Herne (1960) for potential flow have been fitted by Knettig and Beeckmans (1974) to

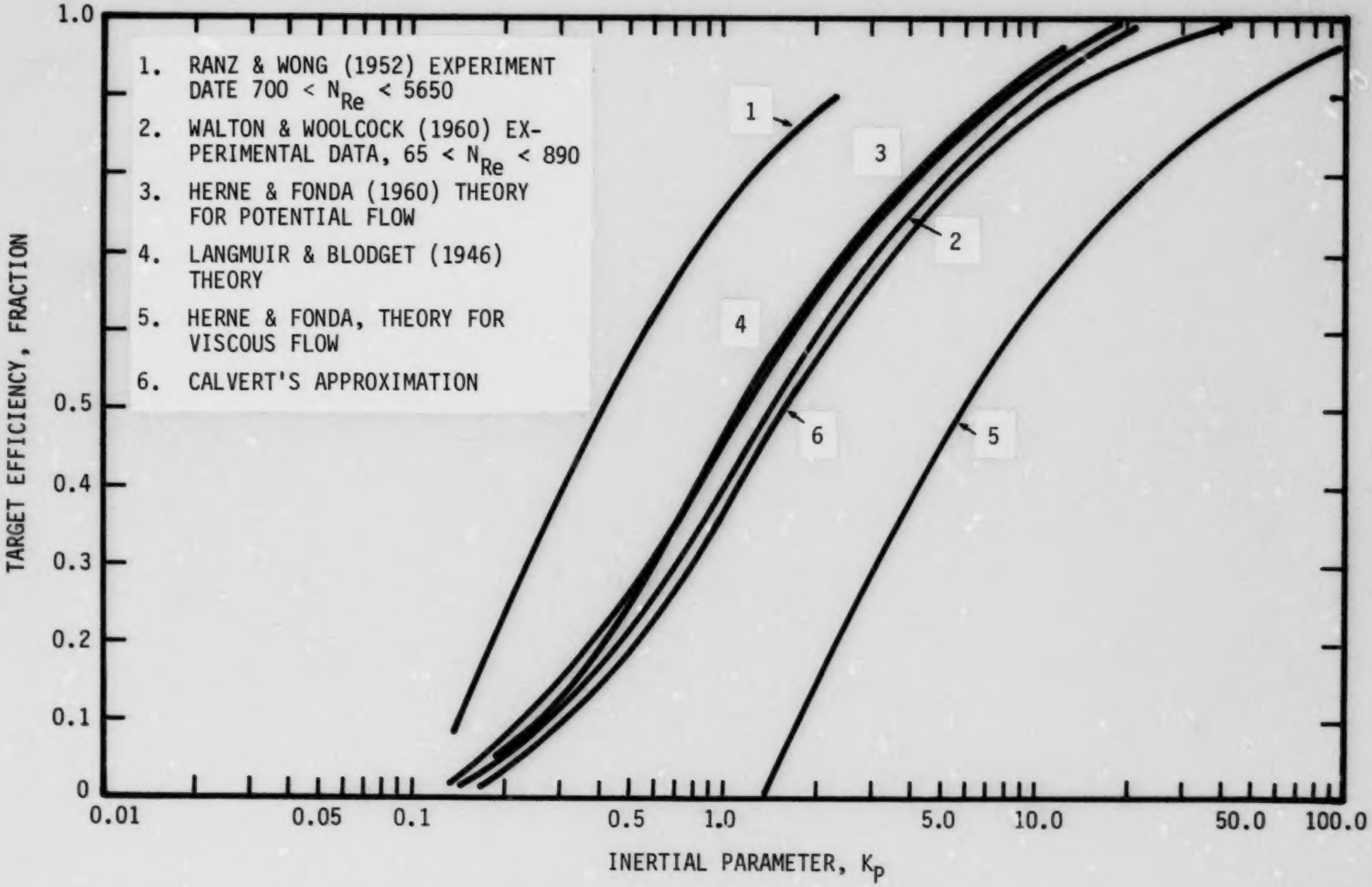

Figure 4. Target efficiency results of various investigators.

$$\eta = 0.00376 - 0.232\ K_p + 2.42\ K_p^2 - 2.025\ K_p^3 \qquad (10)$$

for $0.0832 \leq K_p \leq 0.6$, and

$$\eta = \frac{4\ K_p^2}{(2\ K_p + 1)^2}\ , \text{ for } K_p > 0.6 \qquad (11)$$

where η = single drop collection efficiency, fraction

K_p = inertial impaction parameter, dimensionless

For intermediate Reynolds numbers, single collector collection efficiency can be determined by interpolation between the theoretical curves for viscous and potential flows. Langmuir (1948) gave the following empirical interpolation formula:

$$\eta = \frac{\eta_v + \eta_p \dfrac{N_{Re}}{60}}{1 + \dfrac{N_{Re}}{60}} \qquad (12)$$

where η = single collector collection efficiency, fraction

η_v = viscous flow single collector collection efficiency, fraction

η_p = potential flow single collector collection efficiency, fraction

N_{Re} = collector Reynolds number, dimensionless

Single collector collection efficiency has been measured experimentally by Ranz and Wong (1952) and Walton and Woolcock (1960). Their results are plotted in Figure 4 along with theoretical curves.

Data of Ranz and Wong (1952) show a higher efficiency than those predicted from potential flow. The deviations could be due to errors in estimating the average particle size.

Walton and Woolcock (1960) used a methylene blue aerosol (2.5 μm and 5 μm diameter) impacting on a water drop (500 μm, 1,000 μm, and 2,000 μm diameter) at flow velocities of 2.0, 3.9, and 6.7 m/s to measure particle collection efficiencies. The range of "K_p" was 0.06 to 2.18 and the collector

Reynolds numbers were 65 to 890. Their data agree quite well with theoretical calculations of Langmuir and Blodgett (194) and Herne (1960) for potential flow. That Walton and Woolcock's collector Reynolds numbers often fell substantially below the criterion for potential flow was apparently unimportant. For potential flow and for values of "K_p" greater than 0.2, the experimental values of inertial collection efficiency for spheres can be approximated by the correlation suggested by Calvert (1970):

$$\eta = \frac{K_p}{K_p + 0.7}^{2} \tag{13}$$

Since most of the particle collection in a Venturi scrubber occurs in the throat, Yung et al. (1977) applied equations (1), (2), and (13) to the throat and obtained the following equation for predicting the particle penetration:

$$\begin{aligned} \frac{\ln Pt_d}{B} = {} & \frac{1}{K_{po}(1-u_c^*) + 0.7} [4K_{po}(1-u_c^*)^{1.5} + 4.2\,(1-u_c^*)^{0.5} \\ & -5.02\,K_{po}^{0.5}(1-u_c^* + \frac{0.7}{K_{po}})\tan^{-1}\frac{(1-u_c^*)\,K_{po}}{0.7}^{0.5}] \\ & - \frac{1}{K_p + 0.7}[4K_{po} + 4.2 - 5.02\,K_{po}^{0.5}\,(1 + \frac{0.7}{K_{po}})\tan^{-1}\frac{K_{po}}{0.7}^{0.5}] \end{aligned} \tag{14}$$

where: Pt_d = penetration for particles with diameter "d_{pa}", fraction.

$B = \frac{Q_c\ \rho_c}{Q_G\ \rho_G}\ \frac{1}{C_{DO}}$, dimensionless

Q_c = volumetric flowrate of collector granules, cm^3/s

Q_G = volumetric flowrate of gas, cm^3/s

ρ_c = density of collector, g/cm^3

ρ_G = density of gas, g/cm^3

C_{DO} = drag coefficient at the throat entrance, dimensionless

u_c^* = dimensionless throat exit velocity of collector, dimensionless

K_{po} = inertial impaction parameter at the throat entrance, dimensionless

The dimensionless throat exit velocity of collector is calculated from equation (5).

Case 2. Electrostatically Augmented Collector and/or Particle

Where there is electrostatic force, equation (8) in dimensionless form becomes

$$K_p \frac{du_G^*}{dt^*} = (u_G^* - u_p^*) + K_e f_e \tag{15}$$

where K_e = dimensionless electrostatic force parameter, dimensionless

f_e = spatial dependence of the electrostatic force in terms of dimensionless coordinates, dimensionless

K_p = inertial impaction parameter, dimensionless

u_G^* = dimensionless gas velocity, dimensionless

u_p^* = dimensionless particle velocity, dimensionless

t^* = dimensionless time, dimensionless

The electrical forces on the particle may be due to:

1. The Coulombic force between a charged particle and a charged collector,
2. The electrical image force between a charged particle and a neutral collector,
3. The electrical image force between a neutral particle and a charged collector,
4. The force on a charged particle in the presence of a neutral collector by a uniform external electric field directed parallel to the flow field, and
5. The electric dipole interaction force between a neutral particle and a neutral collector, both polarized by a uniform external electric field directed parallel to the flow field.

The dimensionless electrostatic force parameters for the above five conditions are defined as:

$$K_c = \frac{Q_c \; Q_p \; C'}{3 \; \pi^2 \; \varepsilon_o \; \mu_G \; u_o \; d_c^2 \; d_p} \tag{16}$$

$$K_{ic} = \frac{\varepsilon_c - \varepsilon_o}{\varepsilon_p + 2 \; \varepsilon_o} - \frac{Q_p^2 \; C'}{3 \; \pi^2 \; \rho_o \; \mu_G \; u_o \; d_c^3 \; d_p} \tag{17}$$

$$K_{ip} = \frac{\varepsilon_p - \varepsilon_o}{\varepsilon_p + 2 \; \varepsilon_o} \; \frac{2 \; Q_d^2 \; d_p^2 \; C'}{3 \; \pi^2 \; \varepsilon_o d_c^5 \; \mu_G \; u_o} \tag{18}$$

$$K_{ex} = \frac{Q_p \; E_o \; C'}{3 \; \pi \; \mu_G \; u_o \; d_p} \tag{19}$$

$$K_{icp} = \frac{\varepsilon_p - \varepsilon_o}{\varepsilon_p + 2 \; \varepsilon_o} \left(\frac{\varepsilon_c - \varepsilon_o}{\varepsilon_c + 2 \; \varepsilon_o} \right)^2 \frac{\varepsilon_o \; d_p^2 \; E_o^2 \; C'}{d_c \; \mu_G \; u_o} \tag{20}$$

where K_c = Coulombic force parameter, dimensionless
K_{ic} = charged particle image force parameter, dimensionless
K_{ip} = charged collector image force parameter, dimensionless
K_{ex} = external electric field force parameter, dimensionless
K_{icp} = electric dipole interaction force parameter, dimensionless
Q_c = collector charge, C
Q_p = particle charge, C
C' = Cunningham slip correction factor, dimensionless
d_c = collector diameter, cm
d_p = particle diameter, cm
u_o = undisturbed upstream velocity, cm/s
E_o = uniform external electric field strength, V/cm
μ_G = gas viscosity, g/cm-s
ε_c = dielectric constant of the collector, F/cm
ε_p = dielectric constant of the particle, F/cm
ε_o = dielectric constant of gas, F/cm

Kraemer and Johnstone (1955) solved equation (15) numerically and obtained approximate collection efficiencies for potential flow and Stokes flow around a spherical collector in the absence of particle inertia. For the collection of a charged aerosol by a charged collector, considering only the Coulombic force, the collection efficiency is:

$$\eta = -4 K_c \tag{21}$$

For the collection of uncharged aerosol particles by a charged spherical collector, considering only the induced charge on the particles, the collection efficiency is:

$$\eta = \left(\frac{15}{8} \pi K_{ip}\right)^{0.4} \tag{22}$$

Nielsen (1974) and Nielsen and Hill (1976a) solved equation (15) numerically on a digital computer for the collection of inertialess particles on spheres with electrical force. Their calculations reveal that the collection efficiency of inertialess particle under the influence of Coulombic and external electric field forces is the same for potential flow and viscous flow. Their result for collection efficiency under the influence of Coulombic force is identical to that reported by Kraemer and Johnstone (1955). The collection efficiency for external electric field force is:

$$\eta = \left(1 + 2\,\frac{\varepsilon_c - \varepsilon_o}{\varepsilon_c + 2\varepsilon_o}\right) \frac{K_{ex}}{1 + K_{ex}} \tag{23}$$

The flow field does affect the collection efficiencies for the image force cases. Their results are plotted in Figure 5 for potential and viscous flows.

George and Poehlein (1974) numerically calculated the target efficiencies for the collection of fine particles by a single spherical collector in a gaseous flow field under the combined influences of particle inertia and electrical forces. Their results are presented in Figures 6 and 7.

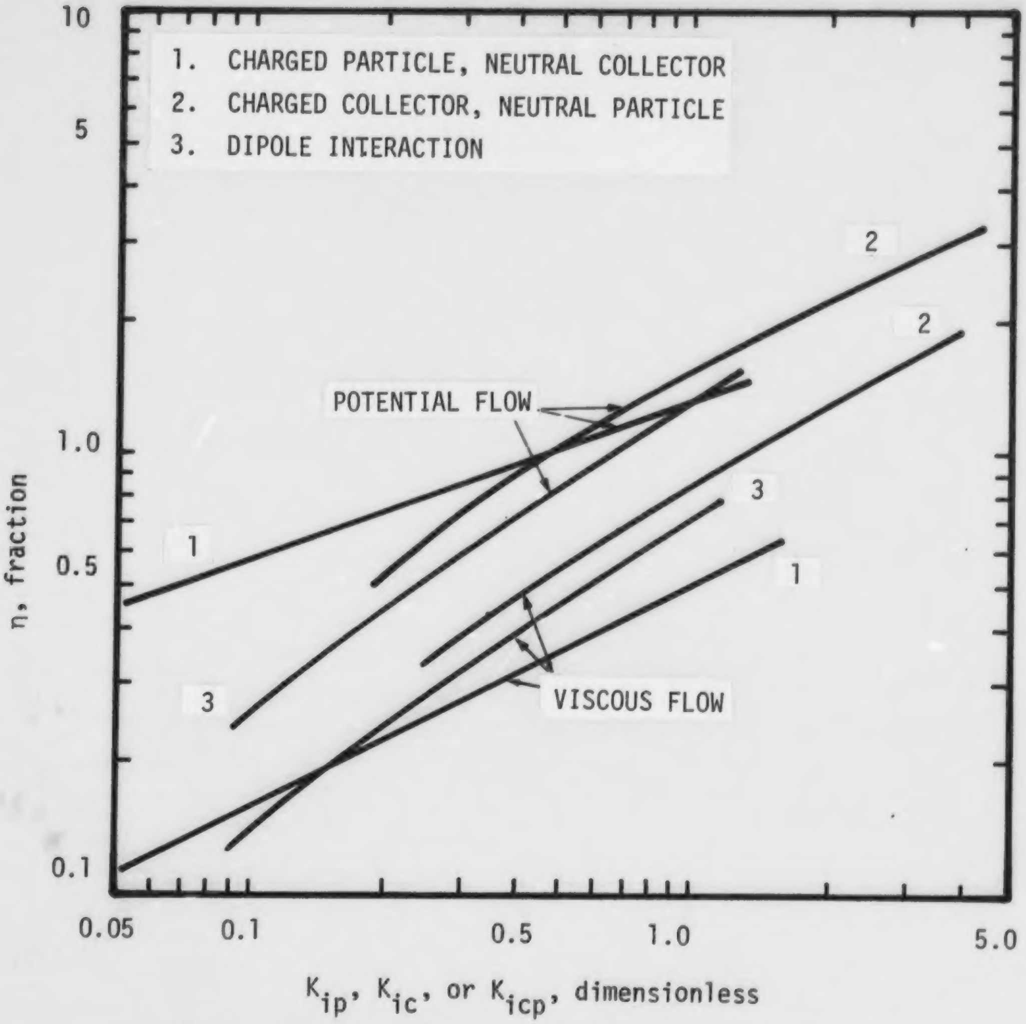

K_{ip}, K_{ic}, or K_{icp}, dimensionless

Figure 5. Single collector collection efficiencies for inertialess particles.

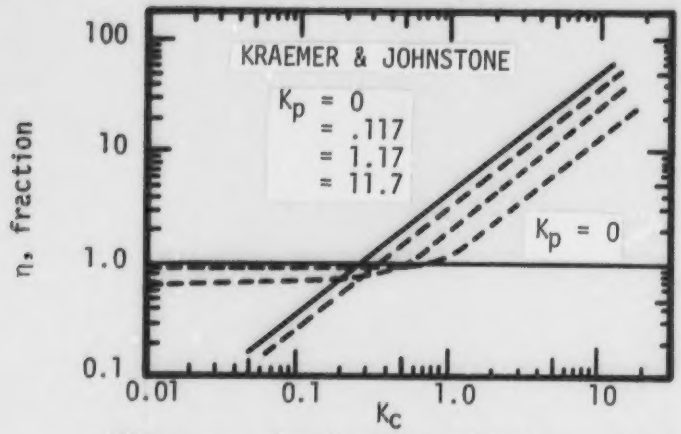

Figure 6. Single drop collection efficiency versus electrostatic parameter with inertial impaction parameter as parameter.

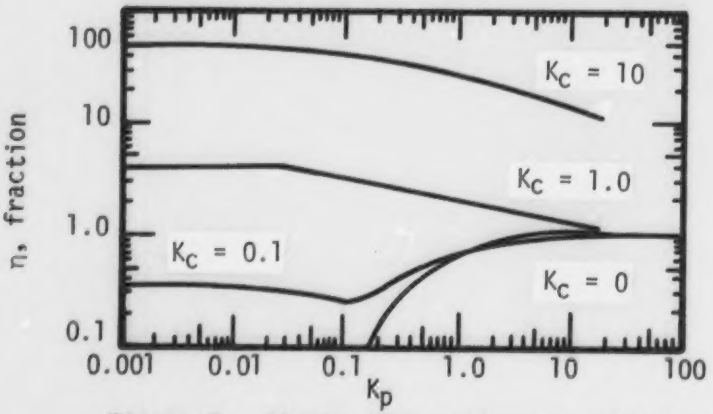

Figure 7. Single drop collection efficiency versus inertial impaction parameter with electrostatic parameter as parameter.

Nielsen and Hill (1974) demonstrated that the convergence criteria used in George and Poehlein's calculations were not adequate for the computation of some particle trajectories. Nielsen (1974) and Nielsen and Hill (1976b) repeated the calculations. Their results are shown in Figures 8 through 11.

Since no explicit expressions were available for estimating the single collector efficiencies with electrostatic force, equation (1) can not be solved analytically. In predicting particle penetration, it is necessary to integrate equation (1) numerically or graphically.

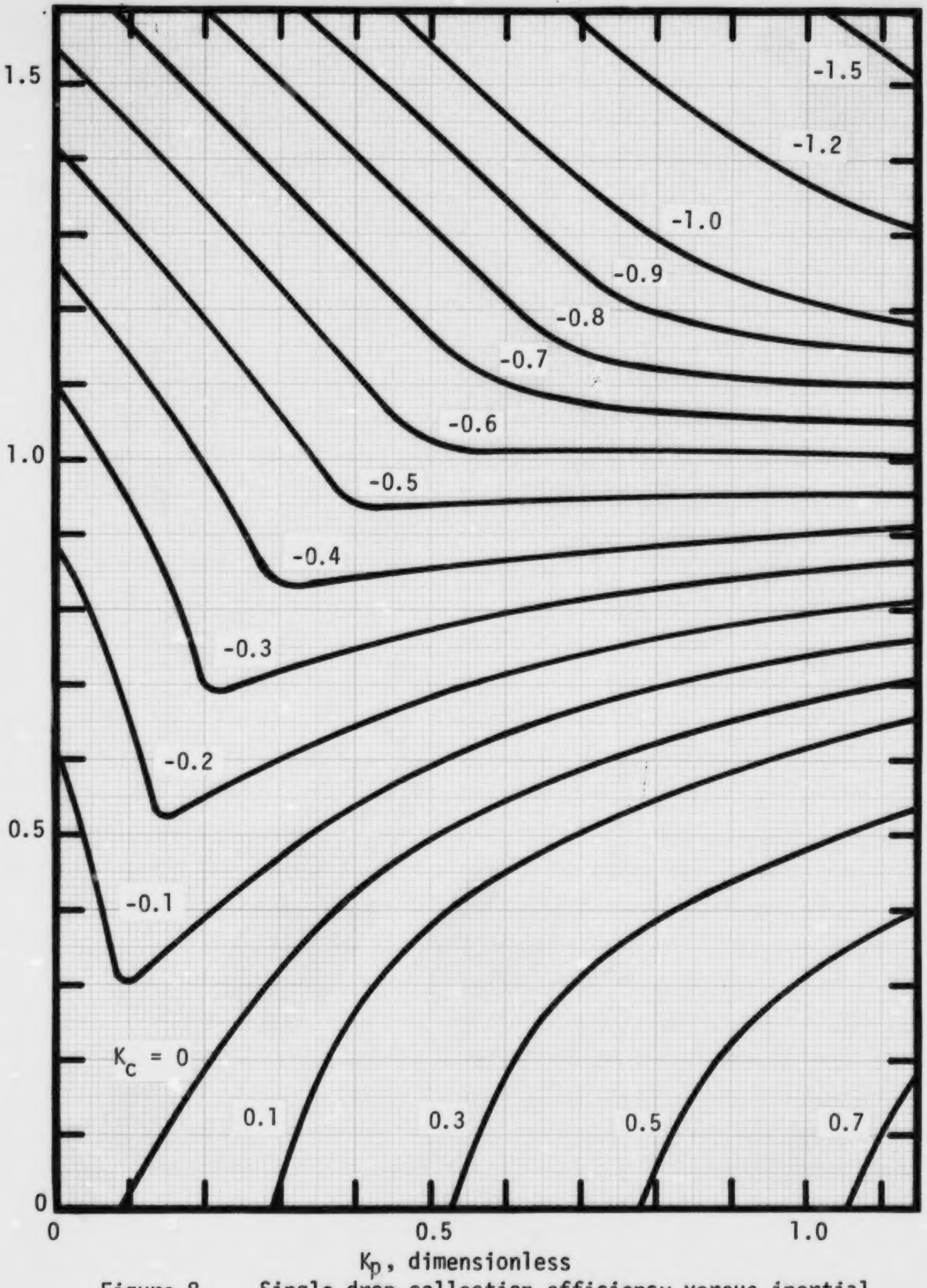

Figure 8. Single drop collection efficiency versus inertial impaction parameter with Coulombic force parameter as parameter.

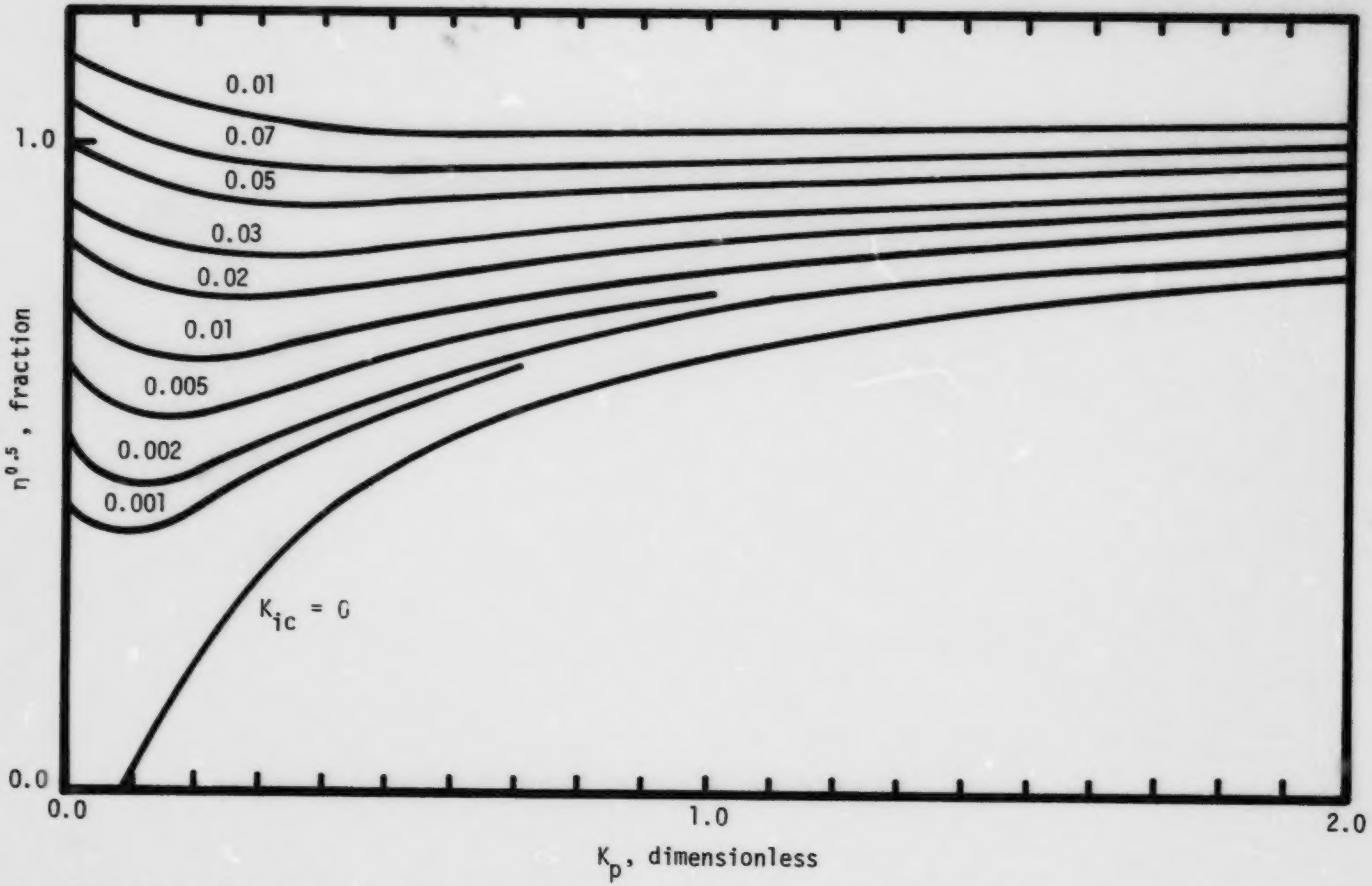

Figure 9. $\eta^{0.5}$ versus K_p for different values of K_{ic} for charged particle image force with potential field.

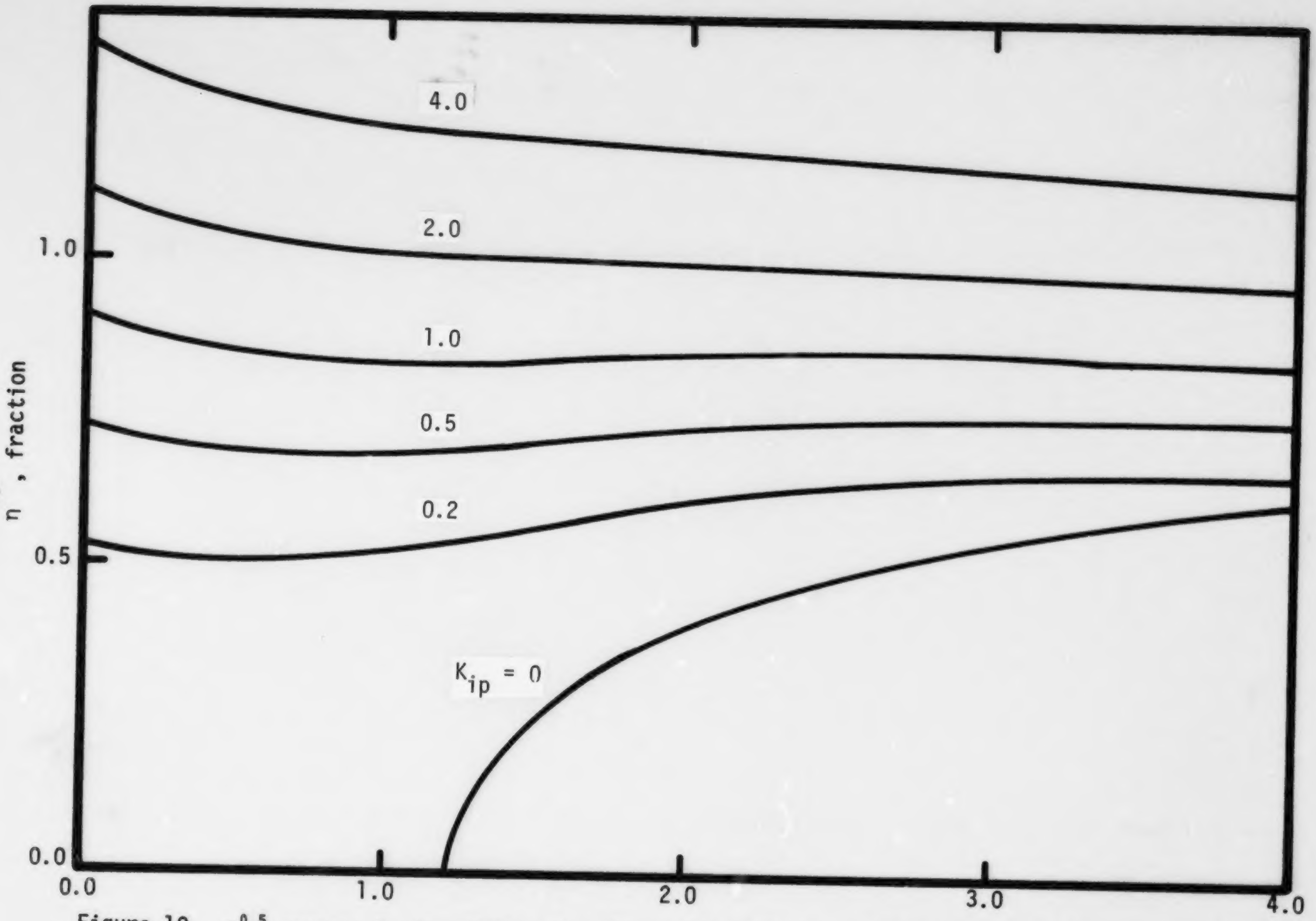

Figure 10. $\eta^{0.5}$ versus K_p for different values of K_{ip} for the charged collector image force with potential field.

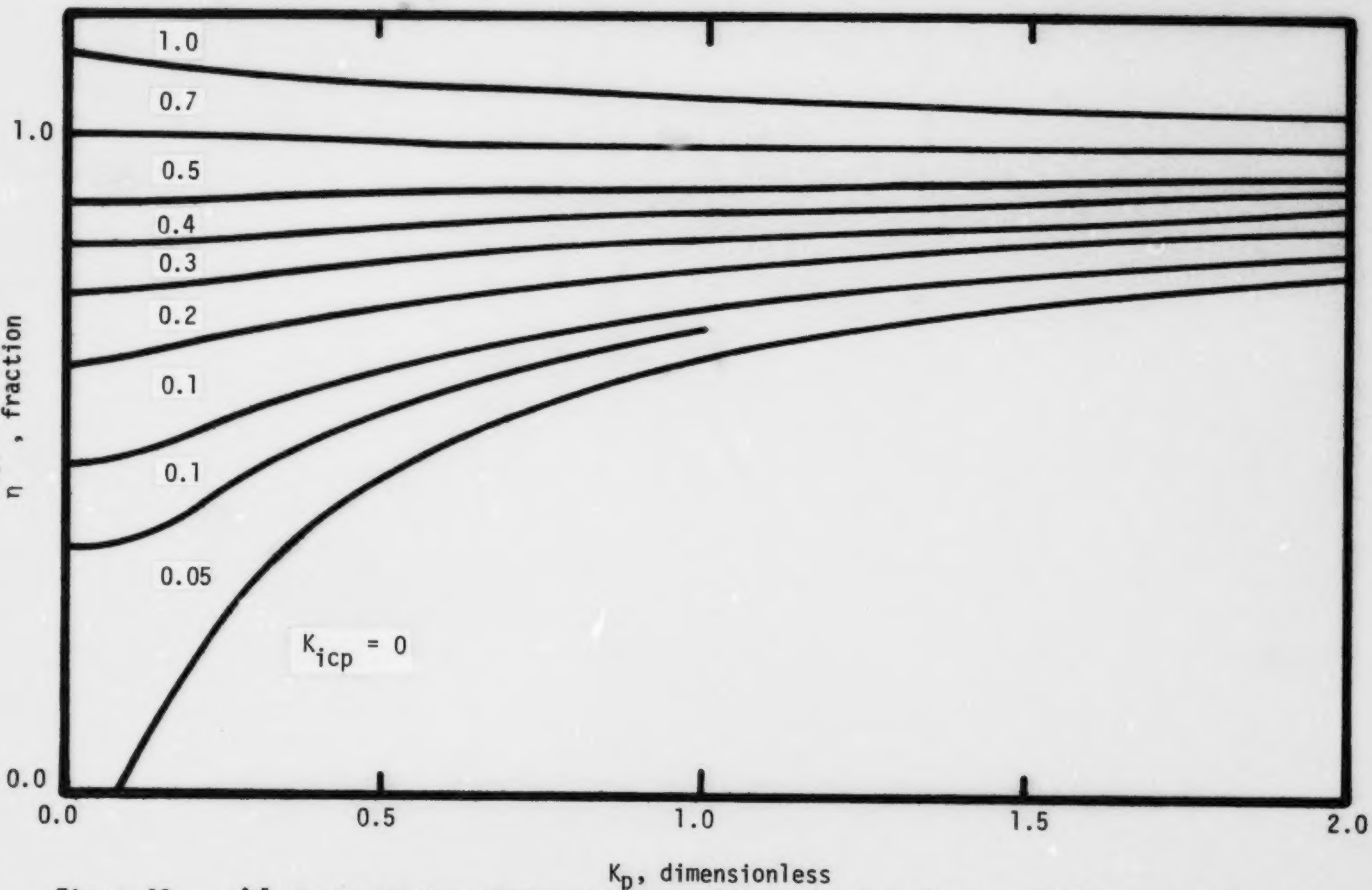

Figure 11. $\eta^{0.5}$ versus K_p for different values of K_{icp} for the electric dipole interaction force with potential flow.

Section 4

PRELIMINARY EXPERIMENTS

COLLECTOR CHARGING

The EPxP scrubber is most efficient when particles and collector granules are charged to opposite polarities. Particle charging could be accomplished with corona wires. The same technique could not be applied to charging the granules because it is necessary to maintain a dense flow in the collector injection line to minimize gas by-pass. However, it is feasible to charge the collector granules by contact charging.

Some small scale experiments were done to develop methods for charging the collector granules in the PxP scrubber. Figure 12 is a schematic drawing of an impaction device. Collector particles are held in the hopper and are allowed to fall through an adjustable nozzle towards a conducting impaction plate. The plate is held at high electric potential with respect to ground. Depending upon the electrical properties of the collectors, they may or may not become charged in the process of bouncing off the plate.

The collectors then fall into a metal container which is insulated from the ground and from the impaction plate. The container is connected through a Coulomb meter to ground for measuring the current due to the charged collectors entering it. A Coulomb meter is used rather than an ammeter since the Coulomb meter integrates out the rapid fluctuations in current.

With the impaction plate connected to ground (an applied potential of zero volts), a current of on the order of nanoamperes was measured for a collector particle flow rate of 1 cm^3/s. The collector particles obtained the charge levels shown in Figure 13 when the voltage on the impaction plate was increased from zero to -20kVDC.

The corona current from the impaction plate, through the metal container, to ground is also shown in Figure 13 for the case when no collectors were flowing. This shows that the corona current approached that of the collectors at an applied voltage of -20 kVDC.

The apparatus shown in Figure 14 was used for additional collector charging experiments. In this case the collectors contacted a metal sphere which was used to decrease the corona current. The amount of charge accumulated by

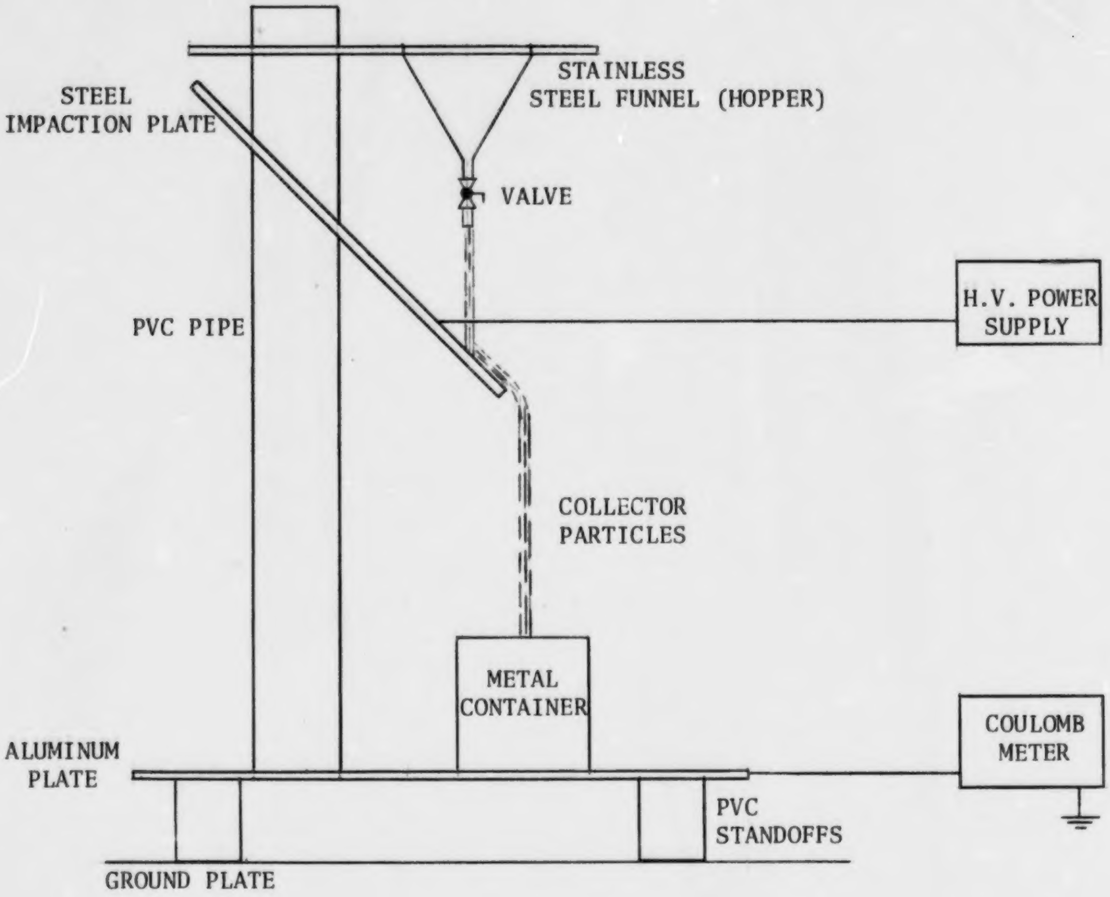
STEEL
IMPACTION PLATE
STAINLESS
STEEL FUNNEL (HOPPER)
VALVE
PVC PIPE
H.V. POWER
SUPPLY
COLLECTOR
PARTICLES
METAL
CONTAINER
ALUMINUM
PLATE
COULOMB
METER
PVC
STANDOFFS
GROUND PLATE

Figure 12. Impaction charging apparatus.

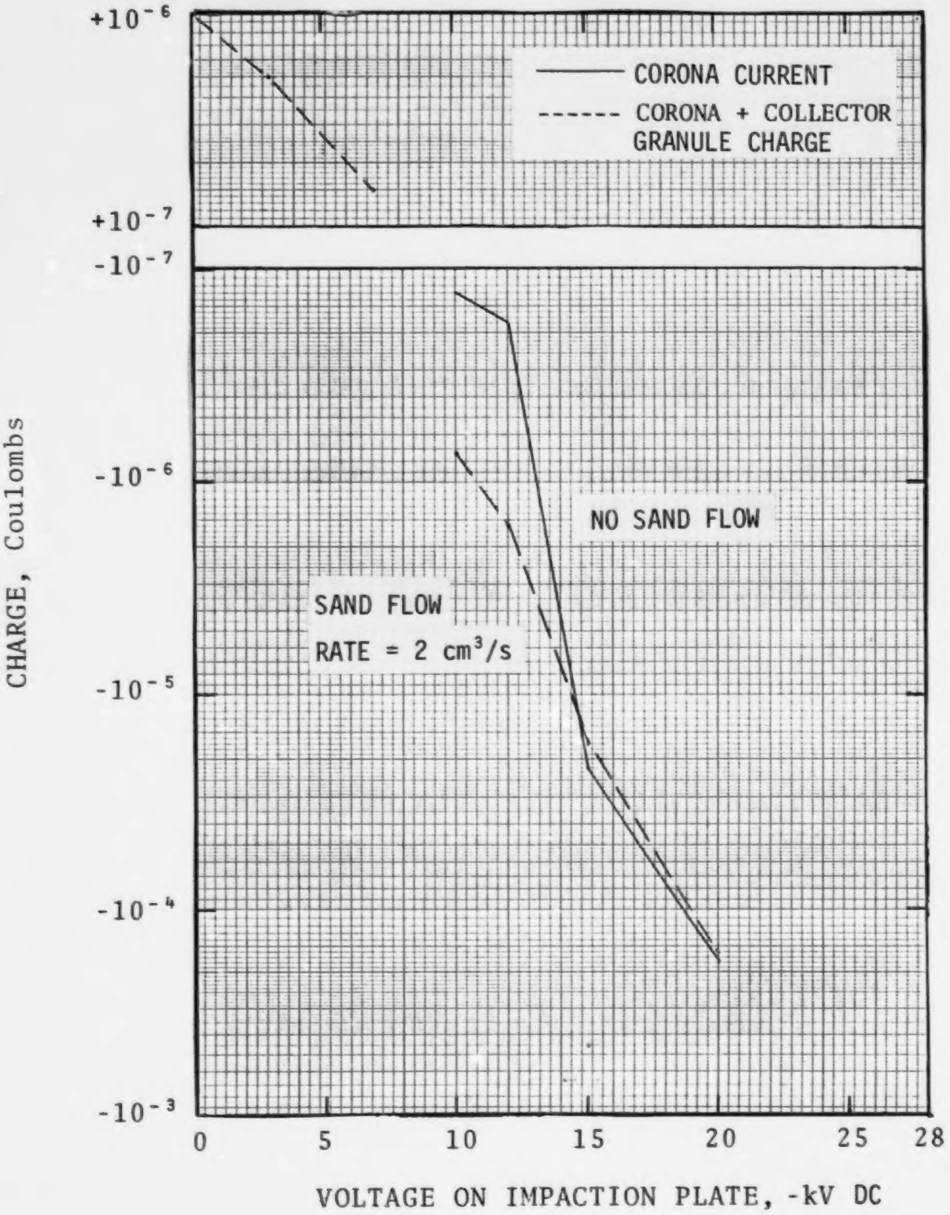

Figure 13. Charge transferred in 240 s with and without collector granules.

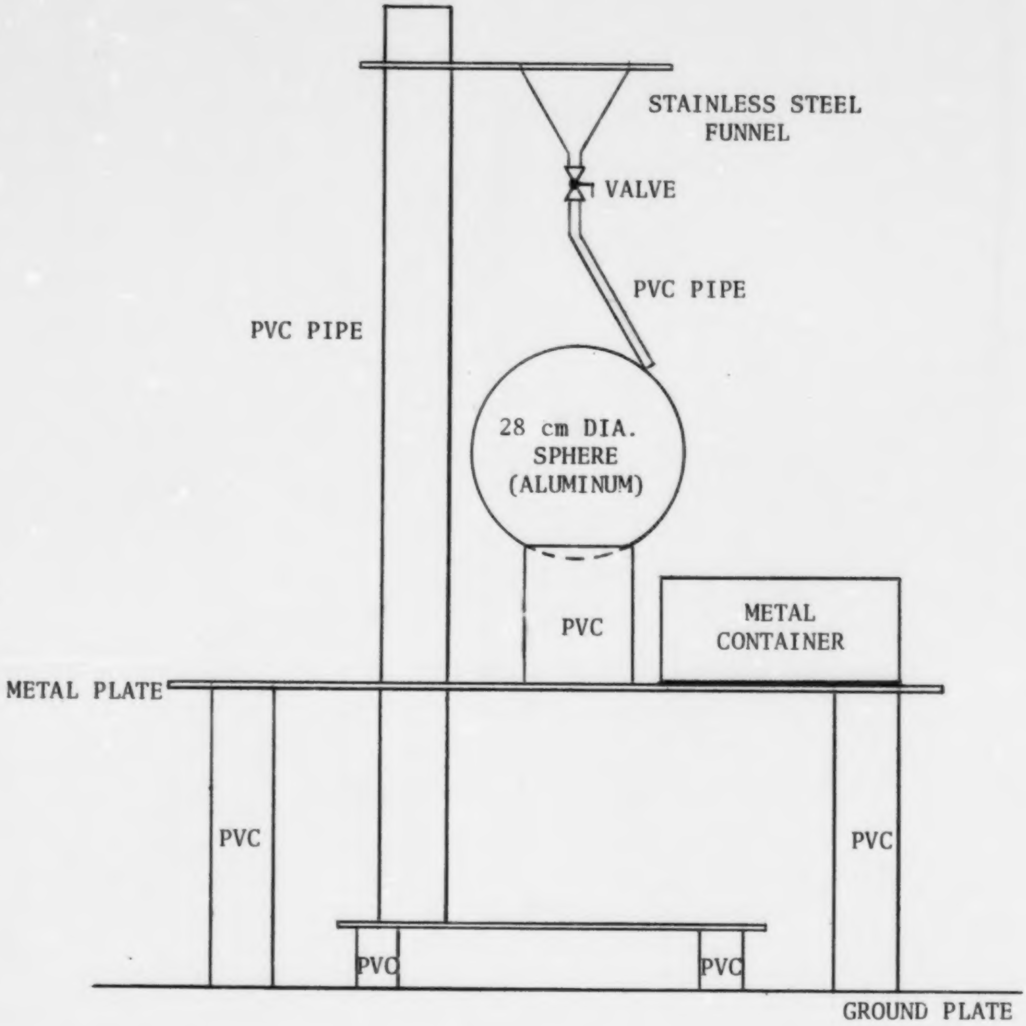
STAINLESS STEEL
FUNNEL
VALVE
PVC PIPE
PVC PIPE
28 cm DIA.
SPHERE
(ALUMINUM)
PVC
METAL
CONTAINER
METAL PLATE
PVC
PVC
PVC
PVC
GROUND PLATE

Figure 14. Impaction charging apparatus designed to have low corona charge.

the collectors is shown in Figure 15 for a range of applied voltages. The figure also shows that the corona current for this apparatus was much less than the previous one.

PRELIMINARY EPxP STUDY

A preliminary electrostatically augmented PxP scrubber was built using the collector charger mentioned above. Figure 16 shows a schematic of the system. The scrubber operated at room temperature and pressure and at flow rates of up to 0.37 m^3/min. (13 CFM). The gas containing the particles was injected into the scrubber through the throat at the bottom. The maximum air flow velocity in the throat was 50 m/s.

The collector granules were 105 μm diameter Florida zircon sand and were held in the bottom of the scrubber assembly surrounding the nozzle. The collectors were entrained into the high velocity gas stream along with the surrounding air. Particle collection occurs in the throat. The collector granules were removed from the air stream in the disengagement section and were returned to the nozzle by falling down the space between the throat and the vessel.

The nozzle could be charged electrically either positive or negative. A ground plate surrounding the nozzle maintained a strong radial electric field at the edge of the nozzle through which entraining sand had to pass. Corona ions surrounding the nozzle charged the collector granules as they passed through. After traveling through the Venturi, the charged granules contacted a metal funnel in the disengagement section before falling back towards the nozzle.

The current carried by the collector granules flowing between the nozzle and the disengagement section was measured with a nanoammeter connected to the disengagement funnel. The collector current for various air flow rates and nozzle voltages is shown in Figure 17. The corona current was much smaller than collector current and did not vary as a function of air flow rate.

Several particle collection experiments were done. The collection efficiency was low due to collector feeding problems. The collector feed rate was not steady causing surging and by-passing. This EPxP design was subsequently abandoned.

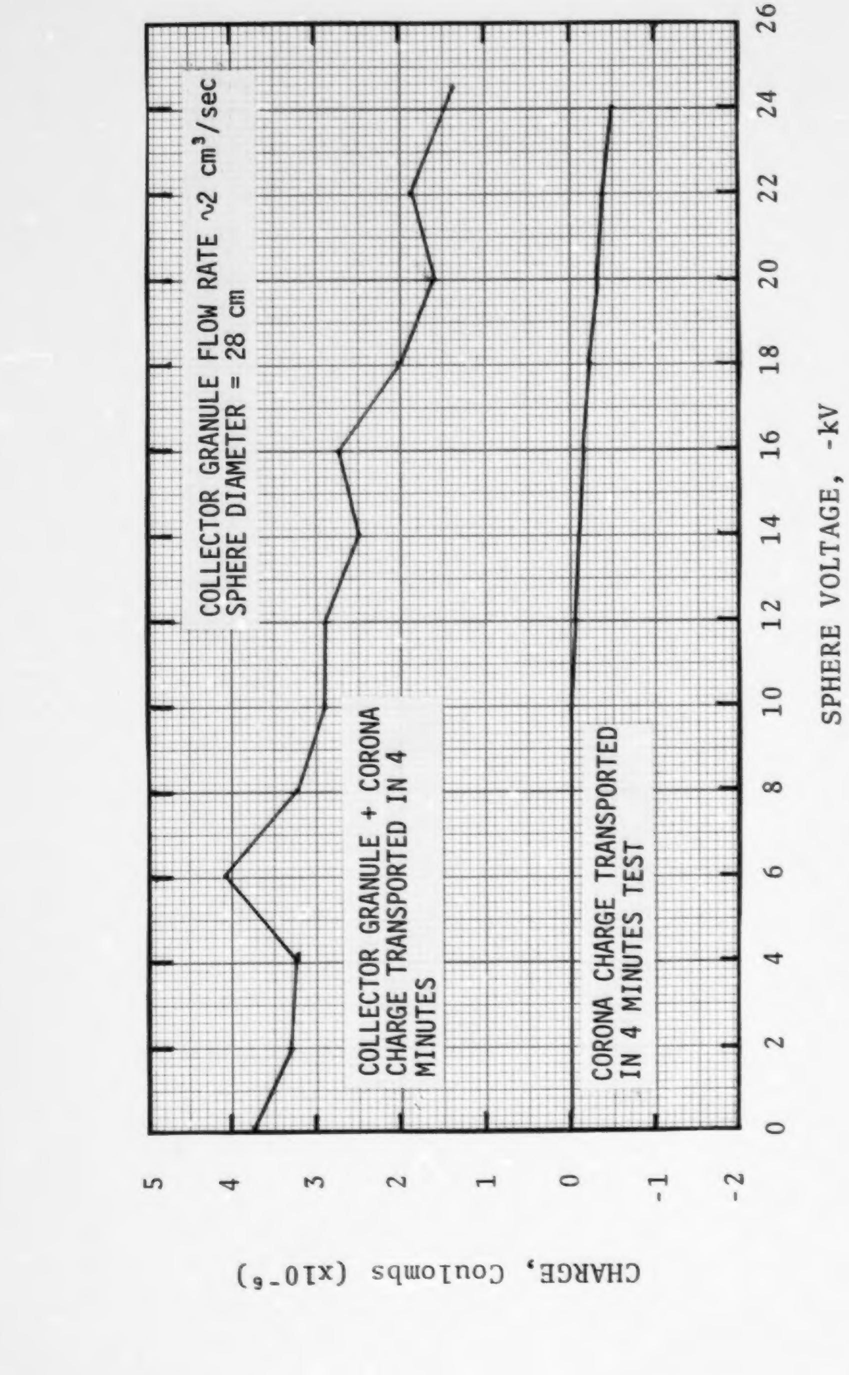

Figure 15. Charge transfer to collector granules.

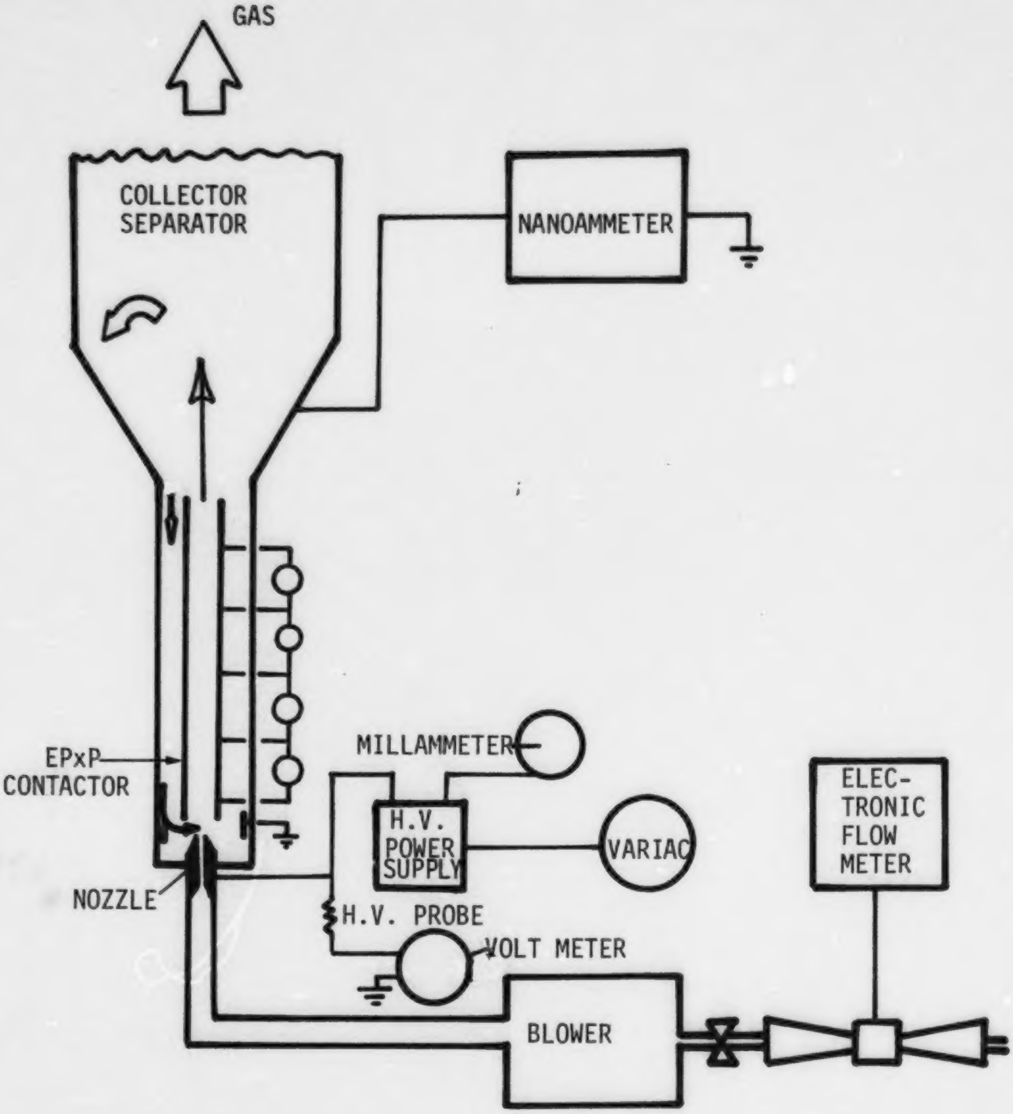
GAS
COLLECTOR
SEPARATOR
NANOAMMETER
EPxP
CONTACTOR
NOZZLE
MILLAMMETER
H.V.
POWER
SUPPLY
VARIAC
H.V. PROBE
VOLT METER
BLOWER
ELEC-
TRONIC
FLOW
METER

Figure 16. Electrostatically augmented PxP scrubber experiment.

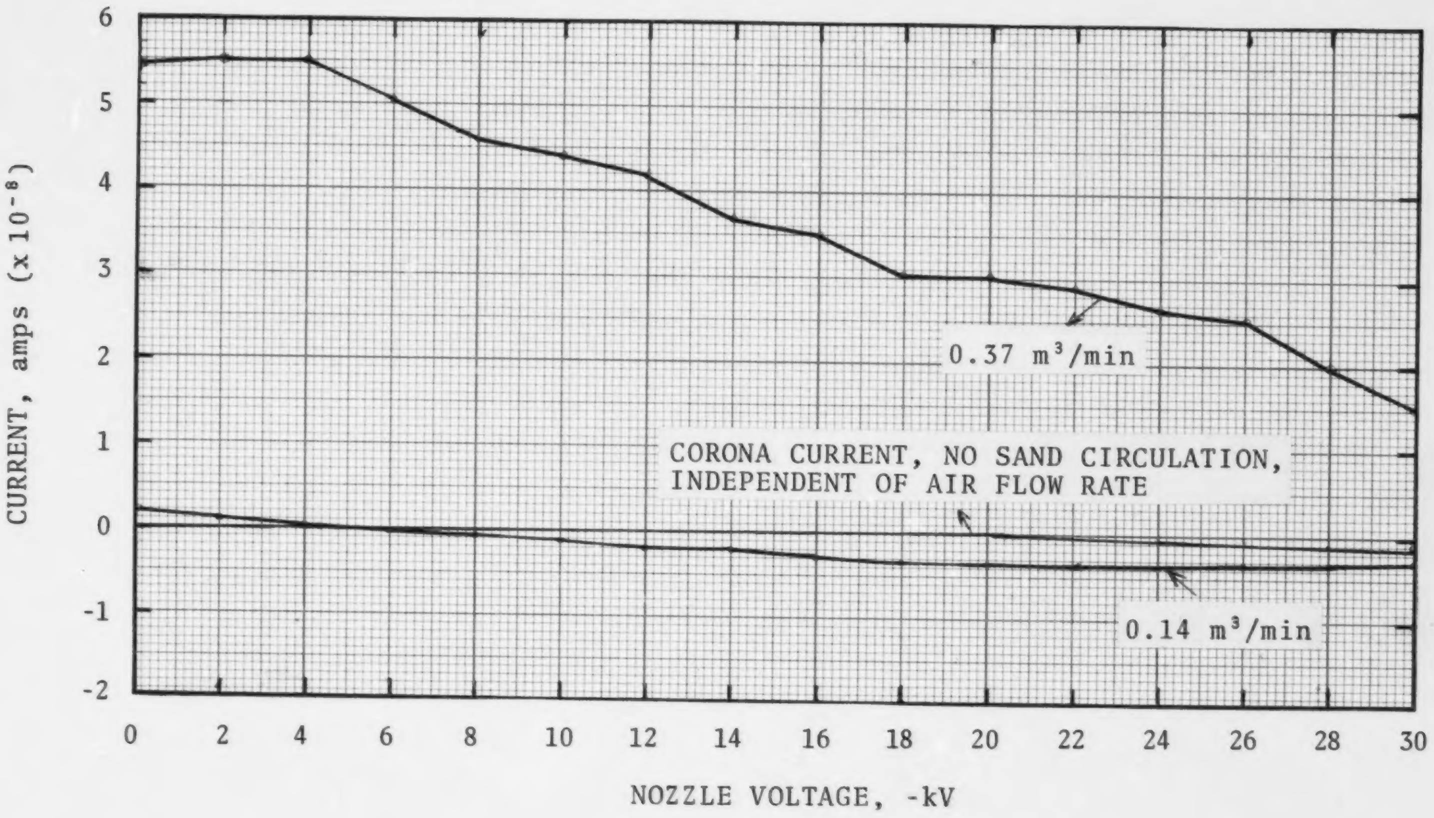

Figure 17. Current versus applied voltage.

BENCH SCALE EPxP

It can be seen from Figure 17 that the collector charge level due to frictional charging was greater than that due to nozzle contact charging. The granules were charged even without the application of a high voltage. Therefore, it is not necessary to have a collector "precharger" to charge the collector granules.

Since the granules can be charged by friction, it is possible to further increase their charge by applying a polarizing field. The polarizer could be simply two parallel plates charged to opposite polarities. The electric field between the plates establishes an nonhomogeneous electric field around each of the collector granules. This nonhomogeneous field will interact with particles. The net result is additional particle collection and better retention of the collected particles by the granules.

To evaluate this possibility, the bench scale EPxP system shown in Figure 18 was built. The configuration of the system is similar to that recommended by Patterson et al (1980). It was made of Plexiglas for visual observation of collector flow pattern.

The bench scale EPxP system consisted of a blower, a particle precharger which had two corona wires, an EPxP contactor, a gravity settler for collector separation, a particle generator, a collector storage hopper, and various flow and pressure measuring instruments. The contactor was inclined at an angle of 60° with the horizon to allow vertical collector injection.

Two EPxP throat configurations were tested. The first one had a round cross-section of 1.6 cm diameter and 5 cm length (from collector injection point to throat exit). The other configuration had a 1.6 cm square cross-section and 28 cm throat length. The polarizer, which consisted of two oppositely charged parallel plates, was part of the long square throat. When using the round throat, the polarizer was located in the lift pipe at the end of the diffuser.

The apparatus was operated at room temperature under ambient pressures and forced-draft conditions. Test particles, which were either methylene blue or re-dispersed fly ash, were injected into the air stream upstream of the particle charger. After the particle charging section, the air and particles flowed into the EPxP where they contacted the collector granules.

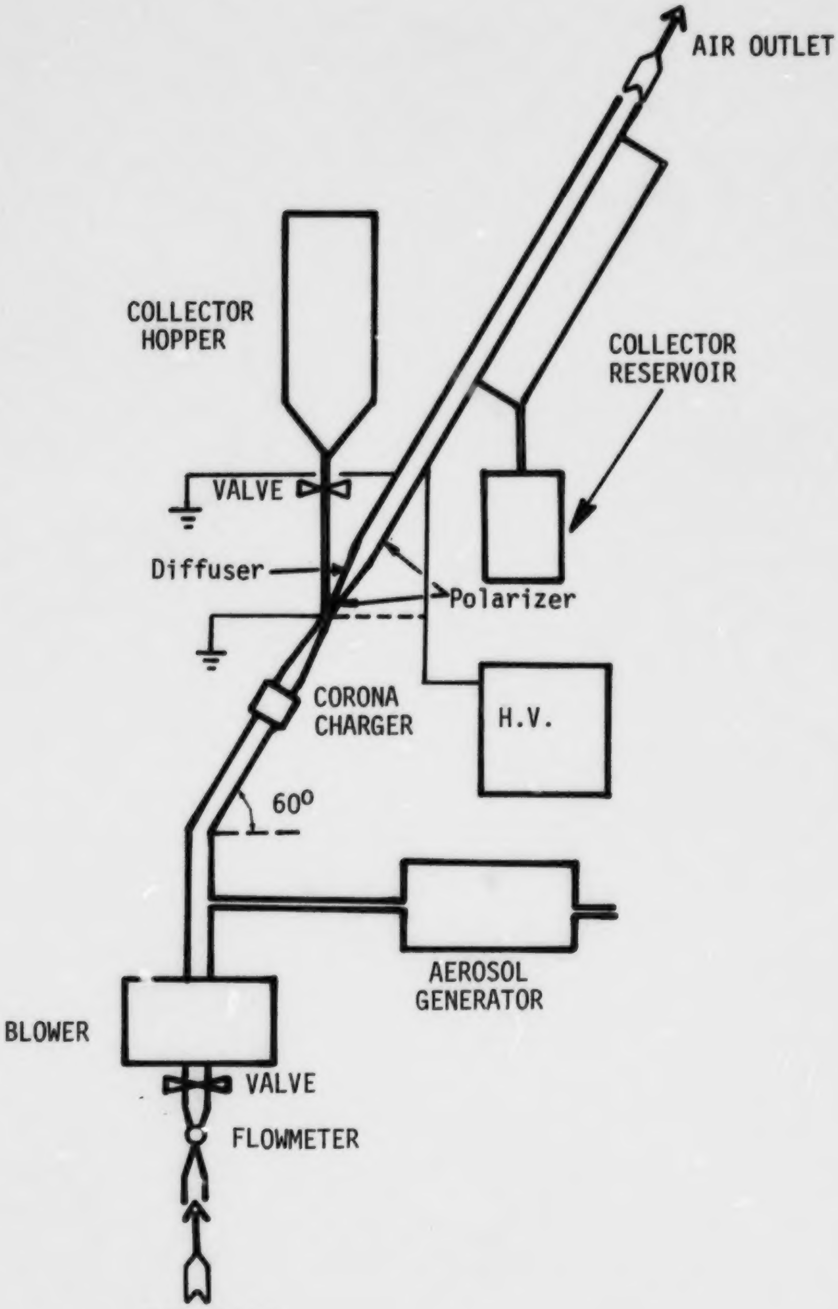
AIR OUTLET
COLLECTOR HOPPER
COLLECTOR RESERVOIR
VALVE
Diffuser
Polarizer
CORONA CHARGER
H.V.
60°
AEROSOL GENERATOR
BLOWER
VALVE
FLOWMETER
AIR INLET

Figure 18. Bench scale EPxP experimental apparatus.

The collector granules were regular grade Florida zircon sand. The collector size distribution and physical properties are shown in Table 1. The granules were stored in an overhead hopper and flowed vertically by gravity into the throat of the EPxP contactor.

Downstream from the contactor, the granules were lifted by the clean air to a gravity settler. The settler had an expanding cross section which slowed the gas below the settling velocity of the collector granules. The air was vented to the atmosphere after collector separation.

In full scale EPxP scrubbers, the granules will be cleaned and recycled. In the present bench scale system, the collectors were used on a once-through basis.

Experiments

Particle Generator

Methylene blue and redispersed fly ash particles were used as test particles. Methylene blue particles were produced by atomizing a 1% by wt. solution of methylene blue dye with a pneumatic atomizing nozzle. The dye was atomized at an accurately controlled rate of 30 cm^3/min with a constant flow rate of air under a regulated pressure of 275 kPa. After atomization, the larger drops were removed by impaction and the smaller drops were dried to solid particles of methylene blue by mixing with a stream of dry air in a heated tube. The particles were then injected into the inlet air stream of the EPxP scrubber.

The methylene blue aerosol generator performed reproducibly. Figure 19 shows the measured size distribution for four runs. The mass median diameter of the methylene blue particles was about 0.4 μmA and the geometric standard deviation (σ_g) was 1.9.

The fly ash particle generator was a small fluidized bed particle generator. It was a batch system. At the beginning of a sampling run, fly ash

TABLE 1. PROPERTIES OF REGULAR GRADE FLORIDA ZIRCON SAND

Typical Screen Analysis

U.S.A. Sieve No.	% Retained on Sieve
50	< 1
70	2
100	15
140	48
200	33
270	1
Pan	< 1

Typical Mineral Composition

Zircon	97%
Kyanite	2.0%
Raetile	< 0.35 %
Misc.	< 1.0 %

Nominal Chemical Composition

ZrO_2	65% (min.)
Fe_2O_3	0.05 % (max.)
TiO_2	0.35 % (max.)
Al_2O_3	2.00 % (max.)
Free Silica	0.2 % (max.)

Range of Physical properties

Bulk density: 3,094 - 3,142 kg/m^3

Specific gravity: 4.64 - 4.65

Hardness (Mohs scale): 7.0 - 7.5

Melting point: 2,100 - 2,300°C

Coefficient of Expansion: 4.0×10^4

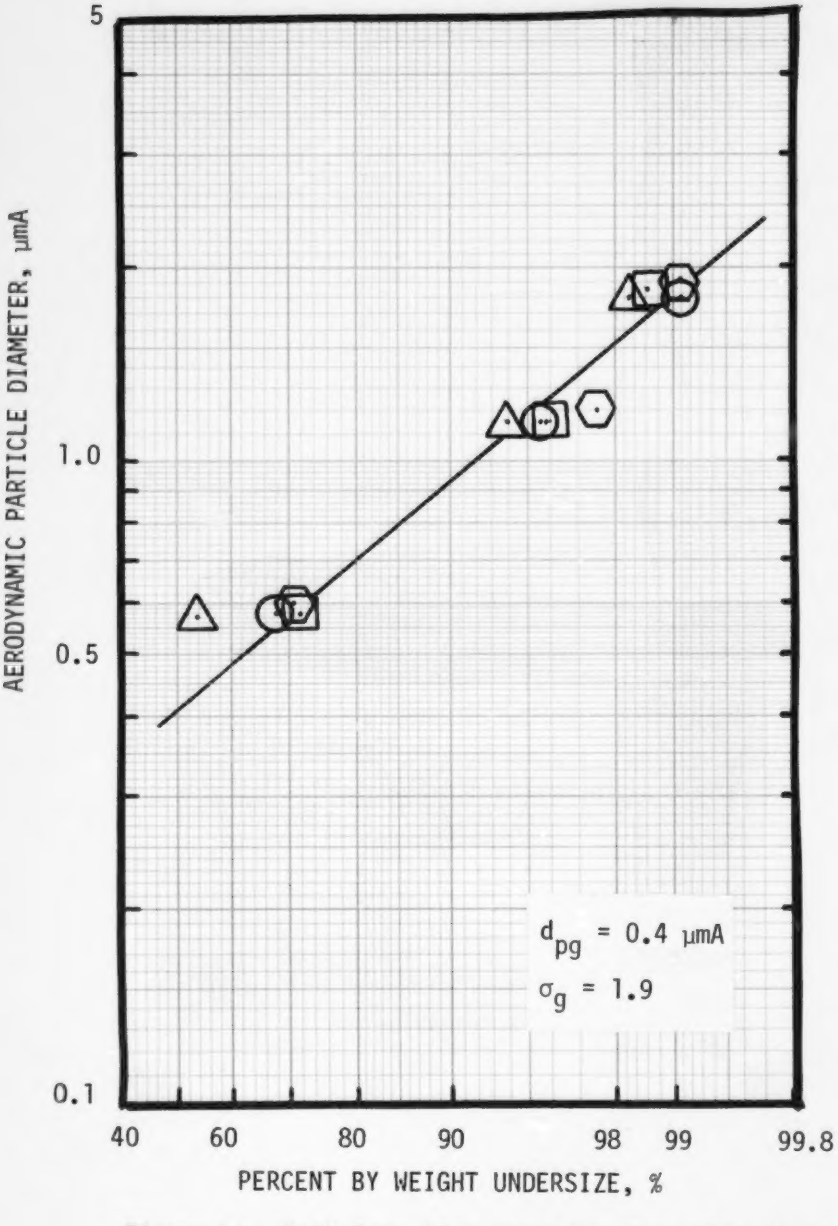

Figure 19. Methylene blue particle size distribution (scrubber inlet).

mixed with bed materials (100-140 μm diameter nickel powder) was loaded into a fluidization column. The bed was fluidized with compressed air and the fly ash particles were deagglomerated by the nickel powder. The particles were elutriated out of the column and were injected into the scrubber system.

Sampling Method

Particle samples were taken simultaneously at the inlet and outlet of the EPxP. In determining the overall collection efficiency with methylene blue particles, nuclepore filters were used. Gas samples were withdrawn through the filters using an EPA Method 5 sampling train. The concentration of the aerosol was determined by relating the amount of methylene blue on the filter with the volume of air sampled through the filter.

The weight of the samples was determined by washing the filter with a known volume of distilled water. After complete washing, the solution was analyzed by a calibrated Bausch and Lomb Spectronic 20 colorimeter at a wavelength of 620 nm.

Cascade impactor sampling runs were also done. The cascade impactor substrates were greased aluminum foil. Sampling and sample handling were the same as for the total filter runs with methylene blue test particles. With fly ash test particles, sample weights were determined with an analytical balance.

The cascade impactor data were reduced into plots of penetration versus aerodynamic particle diameter. The penetration for a given particle diameter is equal to the ratio of outlet and inlet slopes of the cumulative mass concentration curves at the same particle diameter. The slopes of the cumulative mass plot were determined by the following three methods:

1. visual judgment,
2. spline fit, and
3. finite difference.

Visual Judgment - Cumulative mass concentrations were plotted against aerodynamic particle diameters. A curve was fitted to the data points visually. Slopes were then obtained graphically.

Spline Fit - A cubic spline function was used to estimate the derivatives at the data points. The derivatives for other points were calculated by interpolation. Details of this techniques have been presented by Lawless (1978).

Finite Difference - This method has been discussed in detail by Smith et al. (1977). The derivative was calculated by drawing a straight line between two neighboring data points. The derivative was assumed to be the slope of the geometric mean of the two neighboring impactor stage cut diameters. Slopes for other diameters were calculated by interpolation.

Slopes were determined for several "d_{pa}" values in the range of 0.4 to 10 µmA. The fractional penetrations were then determined from the ratio of the slopes, as described above. The fractional penetrations were plotted against particle diameters. The curve is termed "grade penetration" curve.

The grade penetration curve for each cascade impactor run was determined by all three methods. In general, the curves obtained by visual and finite difference methods were close to each other. The curve determined by spline fit method had peaks and valleys. The grade penetration curve presented in this report was the average of the three methods. A smooth curve was visually fitted to the calculated penetration points to eliminate fluctuations.

Particle Data

A total of twenty eight sampling runs were done. Table 2 shows a summary of the experiments. Most of the runs were obtained with the round throat and with methylene blue particles. All experiments were done at room temperature and pressure. The EPxP contactor was operated in the following modes:

1. UP/NC (uncharged particle/non-polarized collector)
2. CP/NC (charged particle/non-polarized collector)
3. UP/PC (uncharged particle/polarized collector)
4. CP/PC (charged particle/polarized collector)

It should be noted that "uncharged" and "non-polarized" mean that the natural charges on the granules or the particles were not neutralized. The granules and particles might actually carry charges. This is especially true for the collector granules since they can pick up charges by friction.

Runs 39/12/1 through 39/12/7 are total filter sampling runs with methylene blue particles and Runs 39/12/12 through 39/12/19 are runs with fly ash particles. The short, round throat was used in these experiments. The gas velocity in the throat was maintained at 34 m/s. The collector-mass to gas-

BENCH SCALE EPxP EXPERIMENTAL DATA

Run No.	Throat Conf.	Q_G, m^3/min	u_{Gt}, m/s	$\frac{\rho_c Q_c}{Q_G}$ kg/m^3	ΔP cm	Particle Chg. Field Strength kV/cm	Polarizing Field Strength kV/cm	Test Particles	Particle Conc., mg/m^3 Inlet	Outlet	$\overline{Pt}$, Fraction
39/12/1	Round	0.42	34	2.6	[illegible]	[illegible]	[illegible]	[illegible]	[illegible]	[illegible]	[illegible]
39/12/2	Round	0.42	34	0	[illegible]	[illegible]	[illegible]	[illegible]	[illegible]	[illegible]	[illegible]
39/12/3	Round	4.2	34	2.6	[illegible]	[illegible]	[illegible]	[illegible]	[illegible]	[illegible]	[illegible]
39/12/4	Round	0.42	34	2.6	[illegible]	[illegible]	[illegible]	[illegible]	[illegible]	1.2	0.20
39/12/5	Round	0.42	34	0	-	7	4	M.B.	5.5	2.3	0.41
39/12/6	Round	0.42	34	0	-	7	0	M.B.	5.8	4.0	0.69
39/12/7	Round	0.42	34	0	-	0	4	M.B.	5.8	4.7	0.81
39/12/8	Round	0.42	34	2.6	7.6	0	0	M.B.	5.7	3.9	0.68
39/12/9	Round	0.42	34	2.6	7.6	7	4	M.B.	5.6	1.7	0.30
39/12/10	Round	0.42	34	2.6	7.6	7	0	M.B.	4.7	2	0.42
39/12/11	Round	0.42	34	2.6	7.6	0	4	M.B.	4.8	3.1	0.64
39/12/12	Round	0.42	34	2.6	7.6	7	4	Fly ash	24.7	5.7	0.23
39/12/13	Round	0.42	34	2.6	7.6	7	4	Fly ash	25.4	6.0	0.24
39/12/14	Round	0.42	34	2.6	7.6	7	4	Fly ash	21.2	4.6	0.22
39/12/15	Round	0.42	34	2.6	7.6	0	0	Fly ash	28.8	26.5	0.68
39/12/16	Round	0.42	34	2.6	7.6	7	0	Fly ash	70.6	27.5	0.39
39/12/17	Round	0.42	34	2.6	7.6	0	0	Fly ash	247.2	144.8	0.59
39/12/18	Round	0.42	34	2.6	7.6	7	4	Fly ash	196.8	21.5	0.11
39/12/19	Round	0.42	34	2.6	7.6	7	4	Fly ash	254.6	32.2	0.13
39/12/20	Round	0.42	34	2.6	7.6	0	0	Fly ash	336.3	191.1	0.57
39/12/21	Round	0.42	34	2.6	7.6	7	4	Fly ash	39.4	19.8	0.50
39/13/12	Round	0.57	47	8.0	38	0	0	M.B.			0.3
39/13/3	Round	0.57	47	8.0	38	7	0	M.B.			0.1
39/13/4	Round	0.57	47	8.0	38	7	4	M.B.			0.034
39/13/5	Round	0.57	47	8.0	38	0	4	M.B.			0.15
39/13/6	Square	0.57	37.5	7.0	38	7	0	M.B.			0.038
39/13/7	Square	0.57	37.5	7.0	38	0	0	M.B.			0.26
39/13/8	Square	0.57	37.5	7.0	38	0	0	Fly ash			0.034

volume ratio was 2.6 kg/m^3. The pressure drop across the contactor was 7.6 cm W.C. As can be seen from Table 2, there is a definite decrease in particle penetration by charging the particles and/or polarizing the collectors.

The same trend was observed with fly ash particles. Due to a larger particle diameter compared to methylene blue, the measured penetrations were lower.

Figures 20 and 21 show the measured grade penetration for the round throat with methylene blue and fly ash particles, respectively. The gas velocity in the throat was 34 m/s. The pressure drop was 7.6 cm W.C. With methylene blue particles, the portion of the grade penetration curve above 1.5 μmA was not reliable because there were few particles in this range. As can be seen from Figure 20, by polarizing the granules or pre-charging the particles, the efficiency of the contactor is increased. The efficiency was increased further by polarizing the collectors and charging the particles at the same time. The increase was greater for small particles (d_{pa} < 3 μmA). For particles with diameters larger than 3 μmA, the improvement was small.

Figure 22 shows experimental results at a higher pressure drop. The gas velocity in the throat and collector-mass/gas-volume ratio were increased to 47 m/s and 8 kg/m^3, respectively, to obtain a pressure drop of 38 cm W.C. (15 inches W.C.). As can be seen, the trends exhibited in Figures 20 and 21 were still observed. When the particles and the collector granules were both electrostatically charged, the particle collection efficiency of the EPxP was very high. The overall collection efficiency was better than 90% for the particle diameters and the experimental conditions used in the present study.

Figure 23 shows the effects of pressure drop on scrubber performance. As expected, scrubber collection efficiency increases with scrubber pressure drop. Scrubber pressure drop can be increased by increasing the gas throat velocity and/or collector flow rate.

Figure 24 shows the results for the square throat. The same sort of results were obtained with this throat as with the round throat. The long, square throat had a better performance than the short, round throat at the same pressure drop as shown in Figure 25. This may be due to the longer contacting time and better collector distribution with the long, square throat or to the proximity of the polarizer. To obtain the same pressure

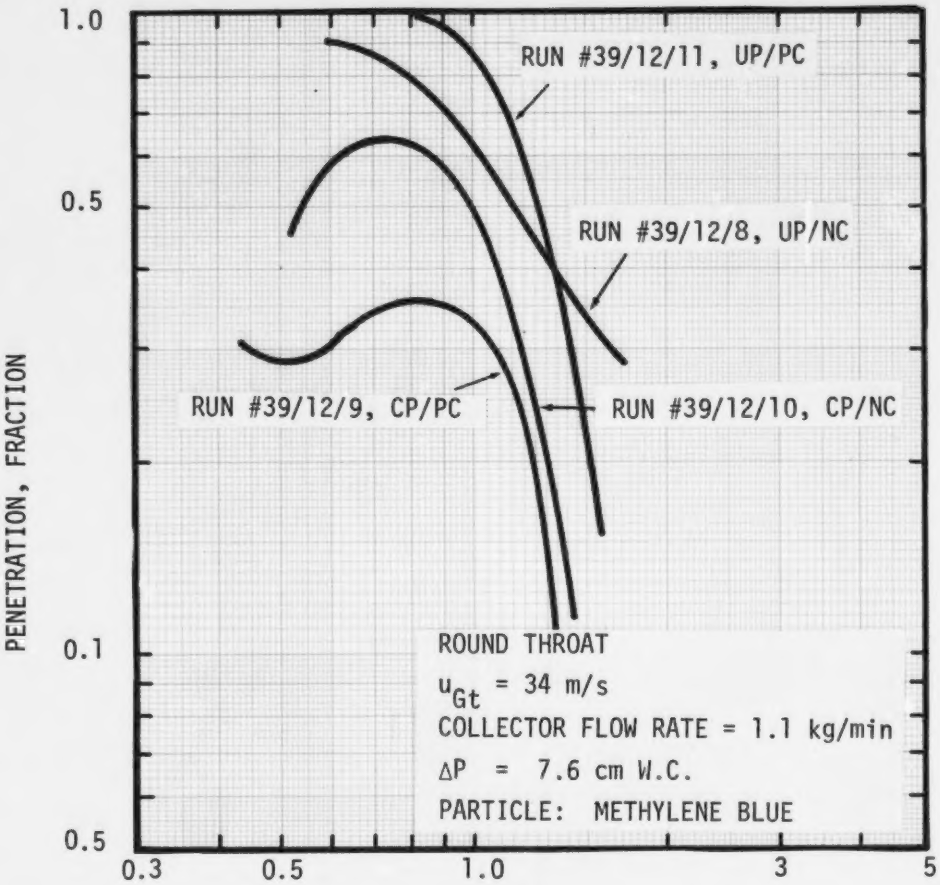

AERODYNAMIC PARTICLE DIAMETER, μmA

Figure 20. Experimental grade penetration curves.

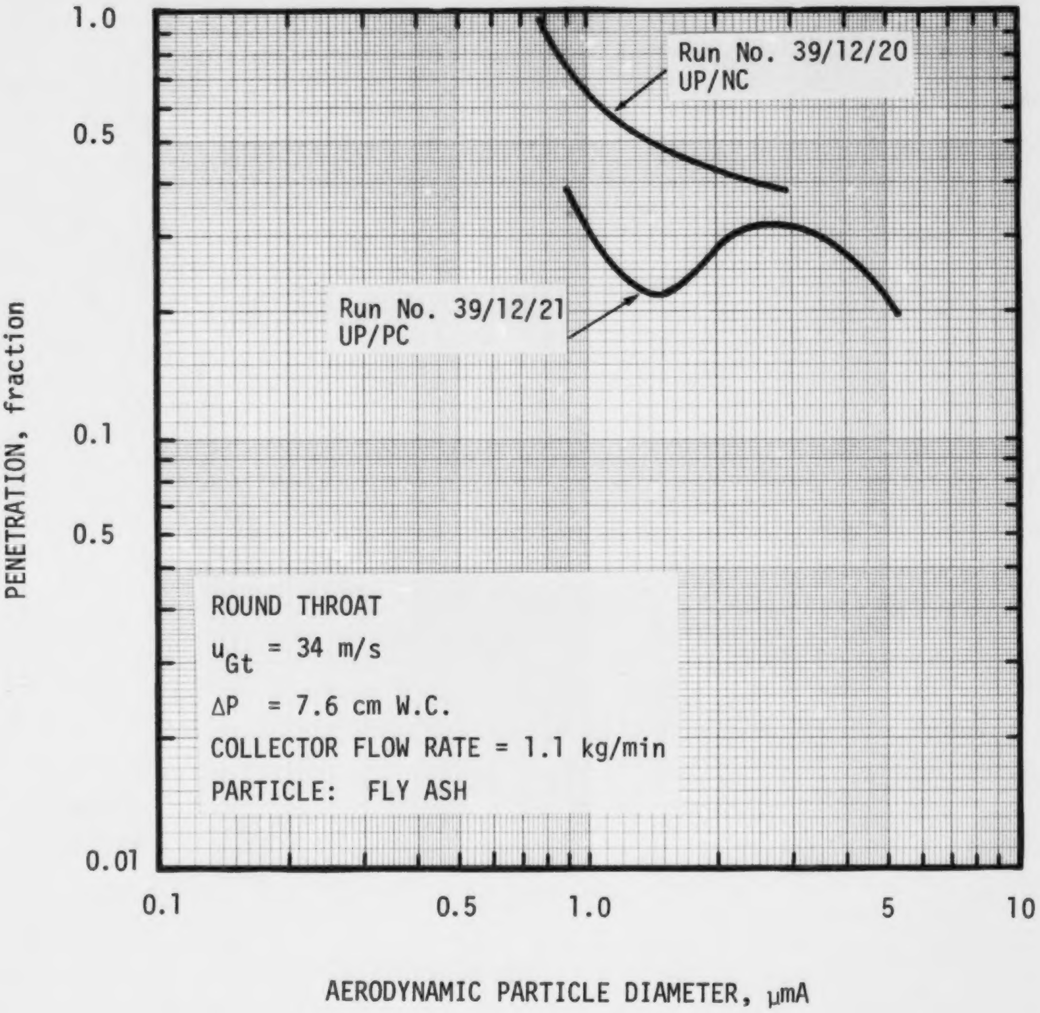

Figure 21. Experimental grade penetration curves.

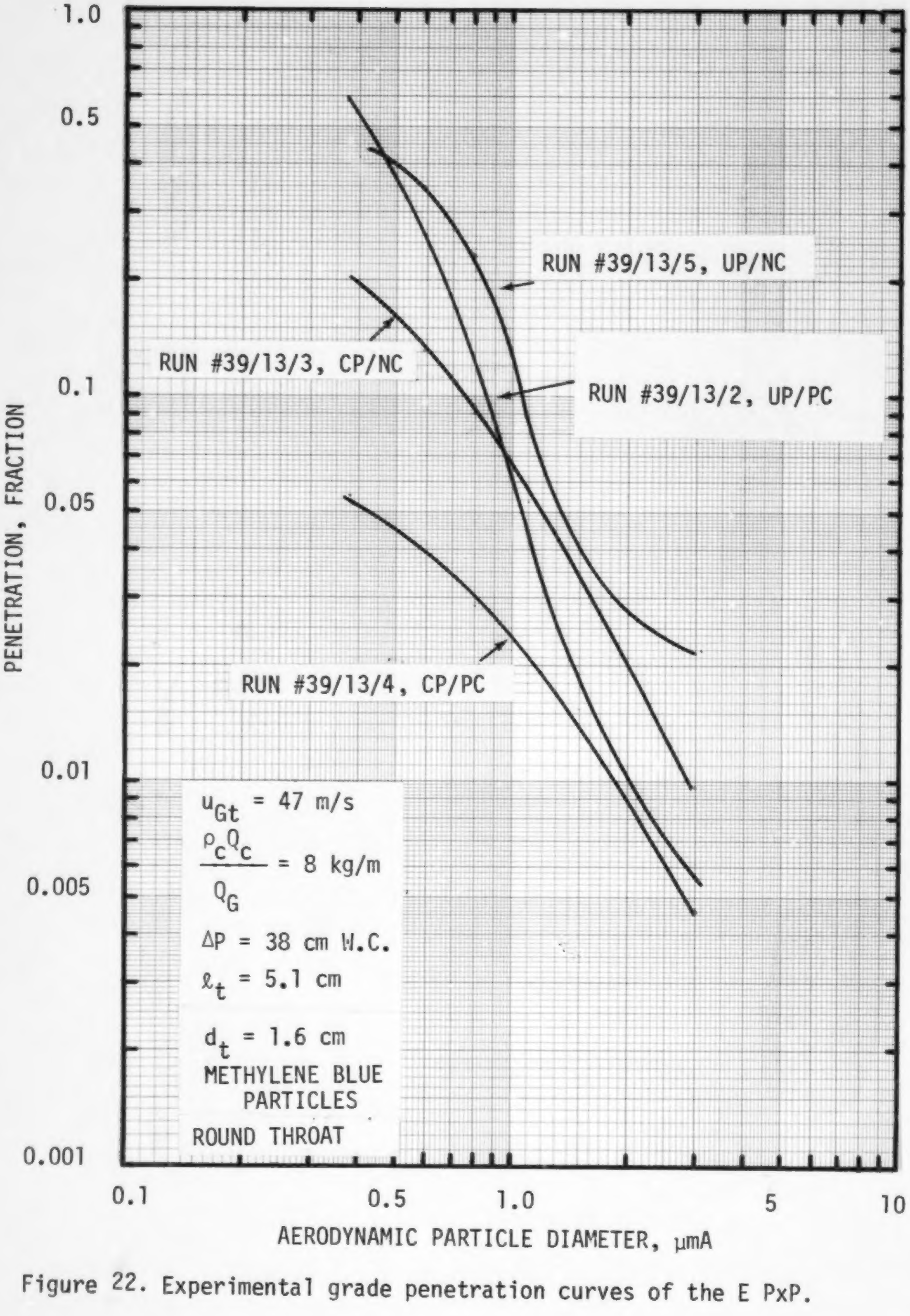

Figure 22. Experimental grade penetration curves of the E PxP.

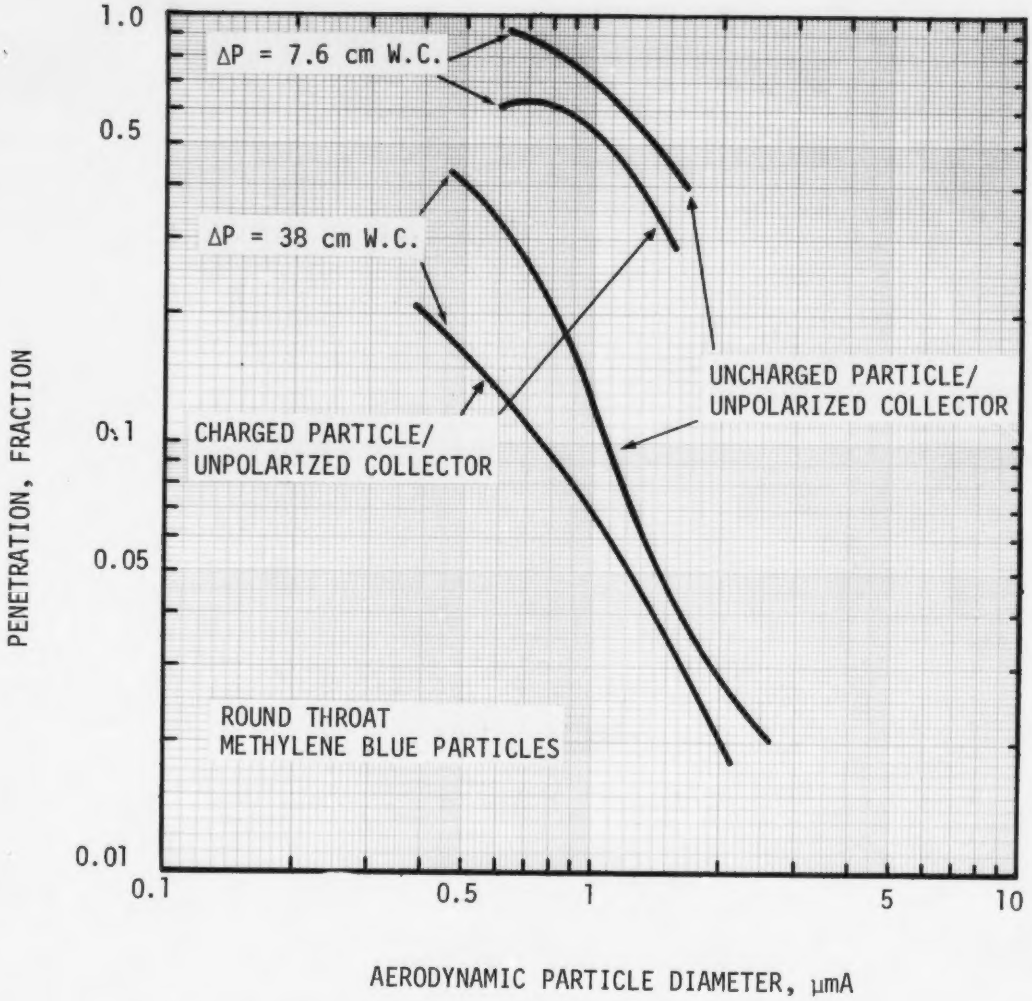

Figure 23. Effects of pressure drop on PxP penetration.

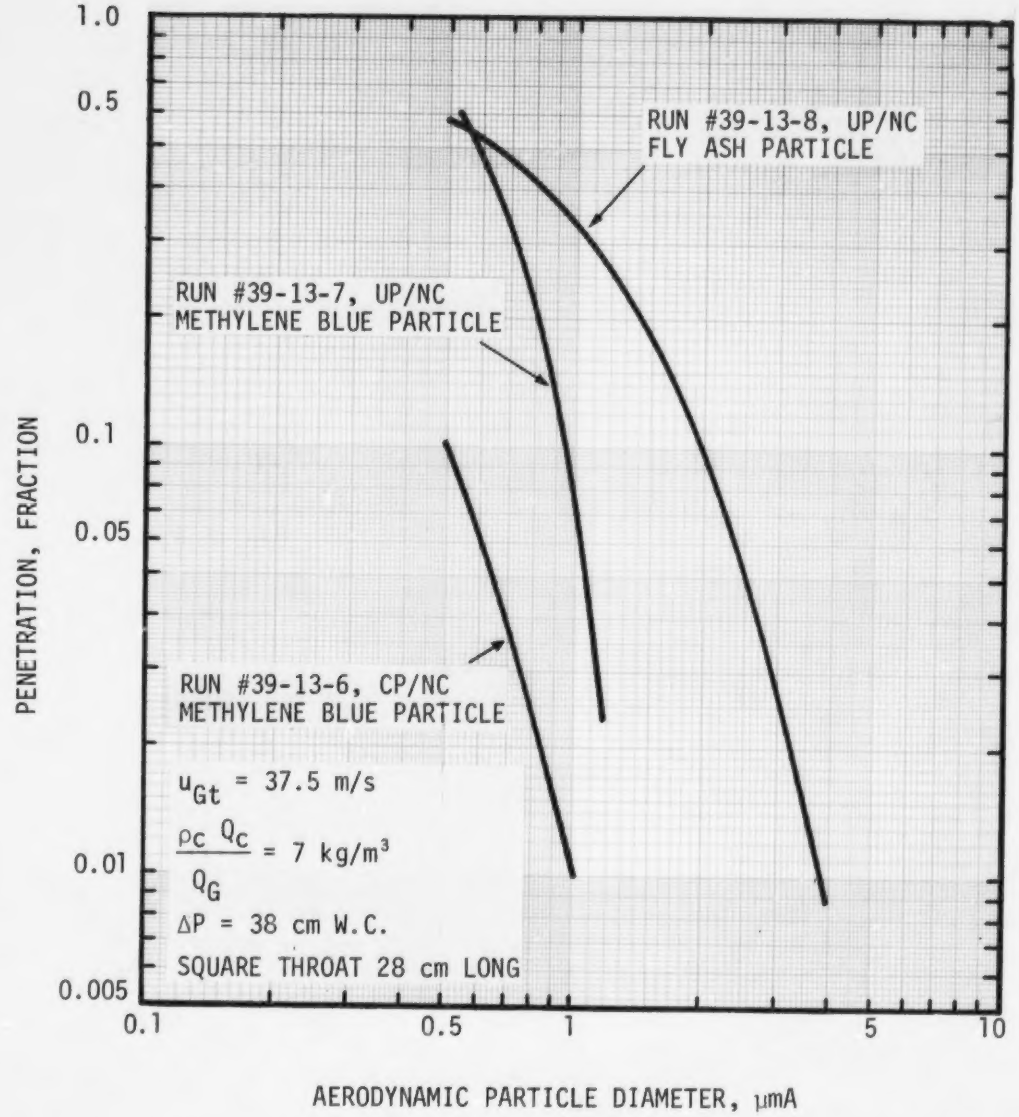

Figure 24. Experimental grade penetration curves for PxP scrubber.

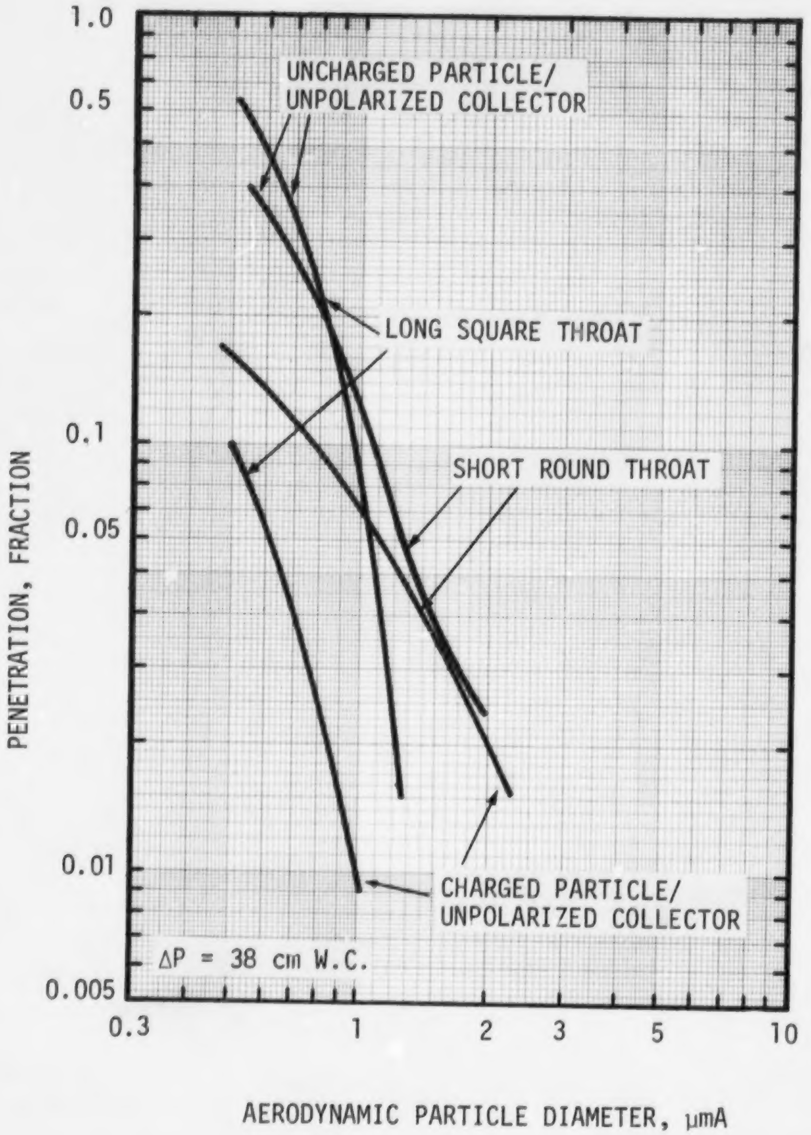

Figure 25. Performance comparison between long throat and short throat.

drop, the long, square throat also operated at a lower gas throat velocity and a lower collector-mass/gas-volume ratio than the short, round throat.

The scrubber efficiency was higher with methylene blue particles than with fly ash particles, as shown in Figure 23. This could be due to particles bouncing off the collector granules upon impaction, or attrition, or particle reentrainment from the dirty collectors. In the present experiments, Florida zircon sand was used as-received without first cleaning it to remove the dust. The as-received sand was measured to contain about 2 to 5 mg/DNm^3 of fine particles between 1 to 5 μmA in diameter. In later experiments, the sand was cleaned by passing it through the PxP system several times before taking particle data.

COMPARISON BETWEEN THEORY AND DATA

The theories presented in Section 3 were used to predict the performance of the bench scale EPxP scrubber. The predicted pressure drops for the three gas velocity and collector-mass/gas-volume ratio combinations are compared with measurements in the following table. The predicted pressure drops are about 20 to 30% higher than experiments. The discrepancy could be due to non-uniform collector distribution across the duct, which caused by-passing.

			Δp, cm W.C.	
u_{Gt}, m/s	$\frac{\rho_c Q_c}{Q_G}$, kg/m^3	ℓ_t, cm	Measured	Predicted
34	2.6	5.1	7.6	9.0
47	8.0	5.1	38	53.0
37.5	7.0	28.0	38	53.0

Figure 26 shows the penetrations calculated from equation 14 and from the cut/power relationship reported by Calvert (1974) for the non-augmented condition. The experimental penetration for methylene blue particles agrees with prediction from the cut/power relation but not with Equation 14. This is another indication of non-uniform collector distribution and gas by-passing. For fly ash particles, the agreement between experiment and prediction is poor.

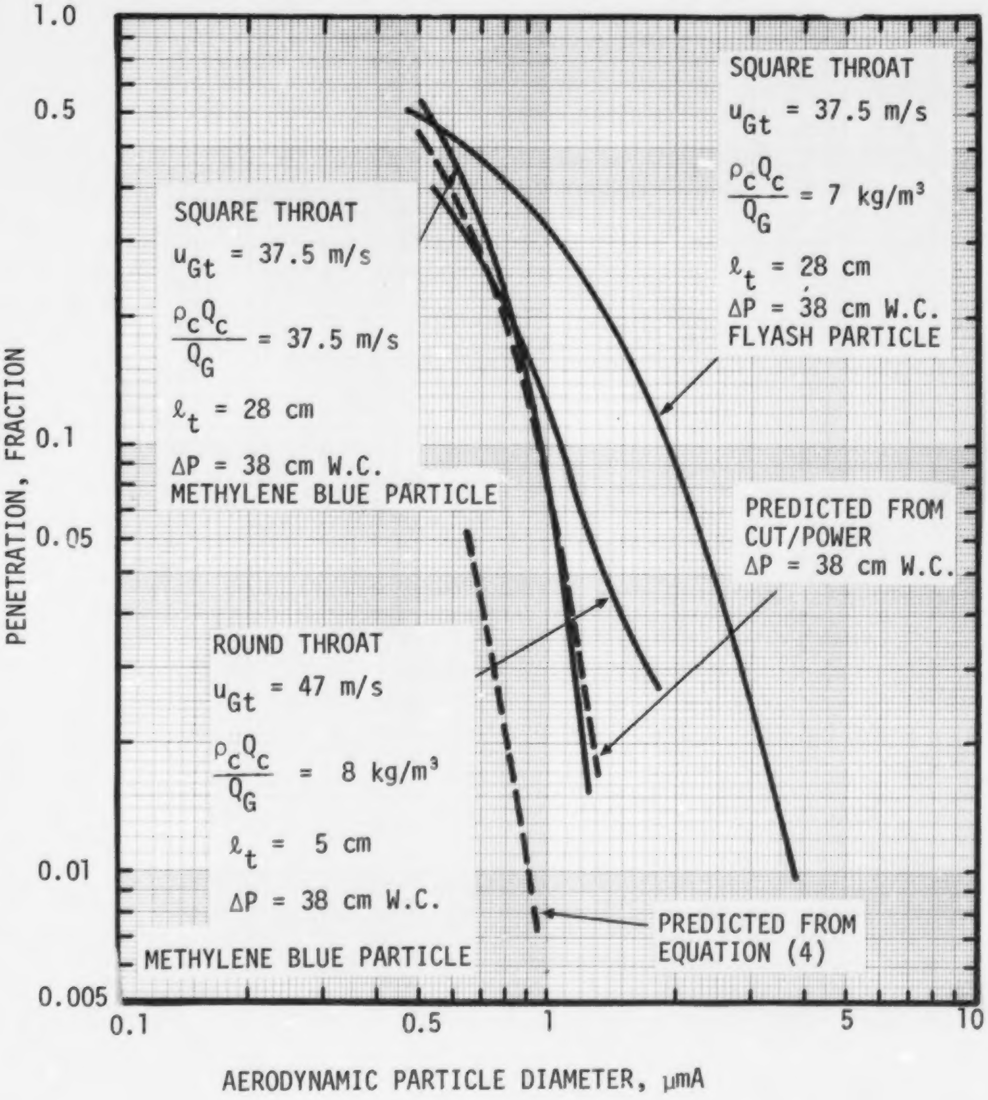

Figure 26. Predicted and measured PxP performance.

For electrostatically augmented conditions, the particle penetration was calculated graphically from equation 1 with "η" determined from Figures 8 through 11. The calculated penetrations were identical to those calculated for non-augmented conditions. This means that there should be no improvement in performance when particles are charged and/or collectors are polarized. This is contrary to experimental findings. A better mathematical model for the electrostatically augmented PxP (EPxP) scrubber is needed.

Section 5

AUXILIARY EXPERIMENTS

It has been shown in the last section that the EPxP design shown in Figure 18 is workable and has satisfactory performance at ambient temperature and pressure. More research work was carried out on the designs of collector injection, and separation systems, and on the effect of temperature on the scrubber performance. The results of these auxiliary experiments are presented in this section. High temperature particle collection is described in the next section.

PNEUMATIC TRANSPORT EXPERIMENTS

The PxP system with "delta" configuration does not require an external collector lifting system. From the PxP contactor, the collector granules are lifted up to the separator by the cleaned gas. To minimize particle reentrainment, collector attrition, and equipment erosion, the gas velocity should be kept as low as possible in the transport pipe. However, it should not be so low as to allow choking.

There are numerous correlations reported in the literature for predicting the choking gas velocity in vertical pneumatic transport and the saltation velocity in horizontal transport. Little information is available on transport in inclined pipes. Kunii and Levenspiel (1969) mentioned that the saltation velocity in inclined-pipe transport is 1 to 3 m/s higher than that for horizontal transport.

The correlations reported in the literature were used to calculate the minimum transport gas velocity but the results were inconclusive. For this reason, the apparatus shown in Figure 27 was built to determine that velocity.

The apparatus had a PxP contactor followed by either a 3.8 cm I.D. or a 7.8 cm I.D. transparent polycarbonate pipe. The length of the pipe was 2.44 m (8 ft.). The transport pipe was oriented either vertically or inclined 60° from the horizontal.

In starting the experiment, the gas flow rate was adjusted to a desired rate. Then, the collector granules were fed into the PxP contactor. The feed

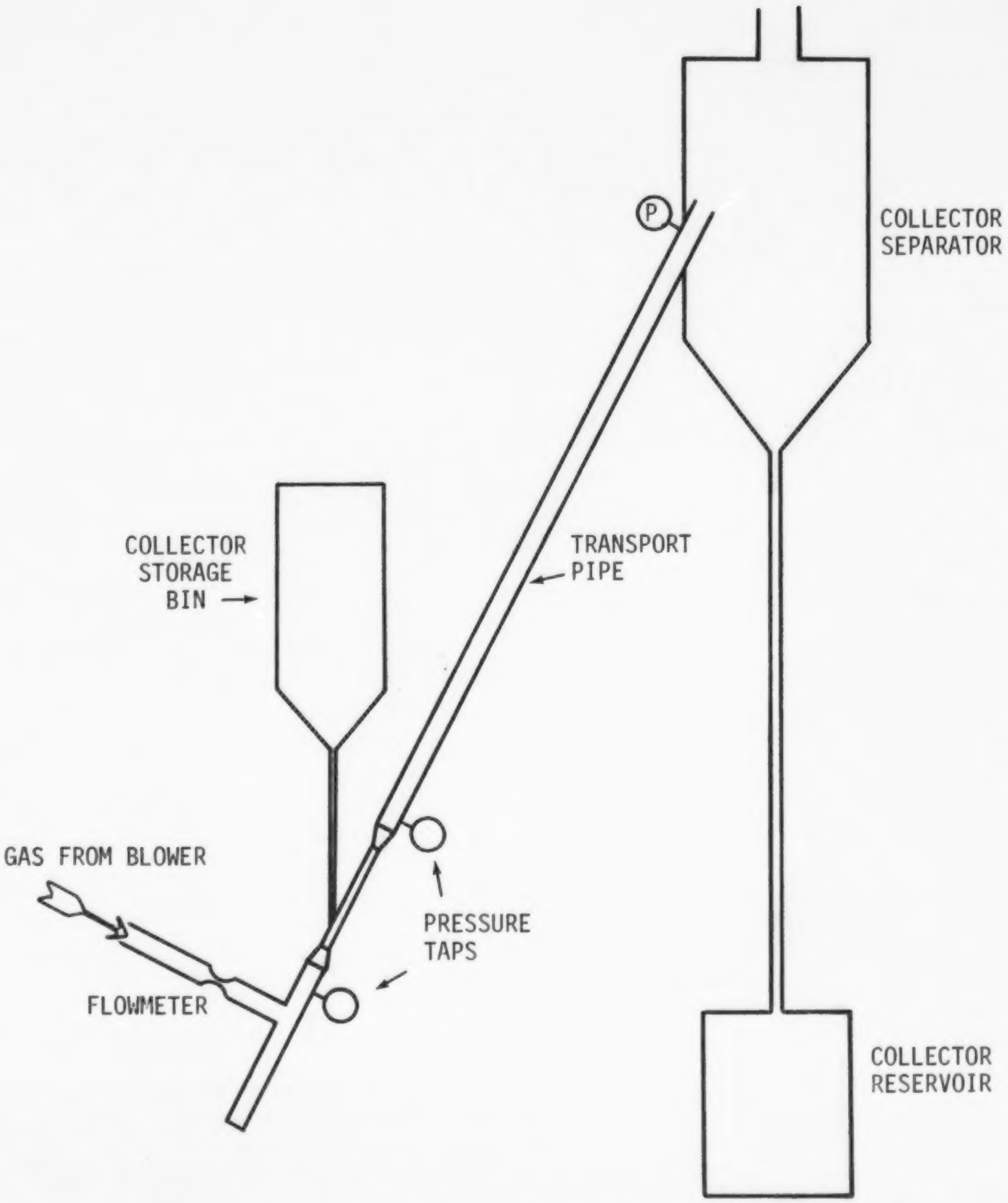
P
COLLECTOR
SEPARATOR
TRANSPORT
PIPE
COLLECTOR
STORAGE
BIN
GAS FROM BLOWER
PRESSURE
TAPS
FLOWMETER
COLLECTOR
RESERVOIR

Figure 27. Apparatus for studying pneumatic transport.

rate of the granules was gradually increased until choking was observed. Choking was defined as the condition at which granules settled out of the gas stream and slid backward into the contactor, forming a fluidized bed at the contactor throat exit. The collector flow rate was determined by weighing the collector reservoir before and after a known time interval.

Table 3 shows a summary of the experimental results. The collector granules were regular grade Florida zircon sand. It can be seen that there is a higher solid handling capacity with vertical transport. This is in good agreement with other researchers' findings.

Figure 28 shows a plot of the solids handling capacity versus transport velocity for an inclined transport pipe (60°). In the EPxP scrubber, the collector-mass/gas-volume ratio is 6 kg/m^3 or higher. From Figure 28, the superficial gas velocity in the transport pipe should be higher than 10 m/s.

COLLECTOR INJECTION

In an EPxP system, collector granules are separated from the gas stream in the collector separator, then passed through a cleaning device to remove collected particles, and reinjected into the gas stream at the EPxP contactor entrance. The collector flow is due to gravity only. No moving parts are used to control and regulate the collector flow.

Since the gas pressure in the contactor is always higher than that in the collector separator, some gas will bypass the contactor and flow through the collector circulation pipe to the collector separator. This bypassing should be kept at a mimimum for two reasons: (1) the bypassing will reduce the collection efficiency of the scrubber system; (2) the gas flow in the collector circulation pipe will restrict the collector flow.

To minimize the bypass, the collector flow in the circulation pipe should be maintained at a dense flow or stick-slip flow condition. A dense flow condition occurs when the gas phase pressure drop in the circulation pipe is higher than the scrubber pressure drop.

The minimum length of the dense phase collector transport pipe can be calculated from Ergun's equation for flow through packed beds. Dense flow will occur if the following equation is satisfied:

TABLE 3. PNEUMATIC TRANSPORT EXPERIMENTAL DATA

Run No.	Transport Pipe I.D., cm	Transport Pipe Orientation	Transport Pipe Gas Velocity, m/s	Collector Flow Rate, kg/min	$\frac{\rho_c Q_c}{Q_G}$, kg/m^3	Contactor Pressure Drop, cm W.C.
1	3.8	60° to horiz.	7.0	1.25	2.61	22
2	3.8	"	7.0	1.00	2.10	22
3	3.8	"	8.3	1.86	3.30	28
4	3.8	"	8.3	1.68	2.96	28
5	3.8	"	8.3	1.82	3.20	28
6	3.8	Vertical	4.1	0.68	2.43	14
7	3.8	"	5.6	2.04	5.33	19
8	3.8	"	5.6	2.00	5.21	19
9	3.8	"	5.6	2.04	4.86	19
10	3.8	"	5.6	2.04	5.33	19
11	3.8	"	7.8	3.95	7.40	38
12	3.8	"	7.8	3.90	7.30	38
13	7.8	60° to horiz.	8.4	8.30	3.5	30.5
14	7.8	"	8.9	15.7	6.2	45.7
15	7.8	"	9.7	16.1	5.8	45.7
16	7.8	"	8.9	14.1	5.5	45.7

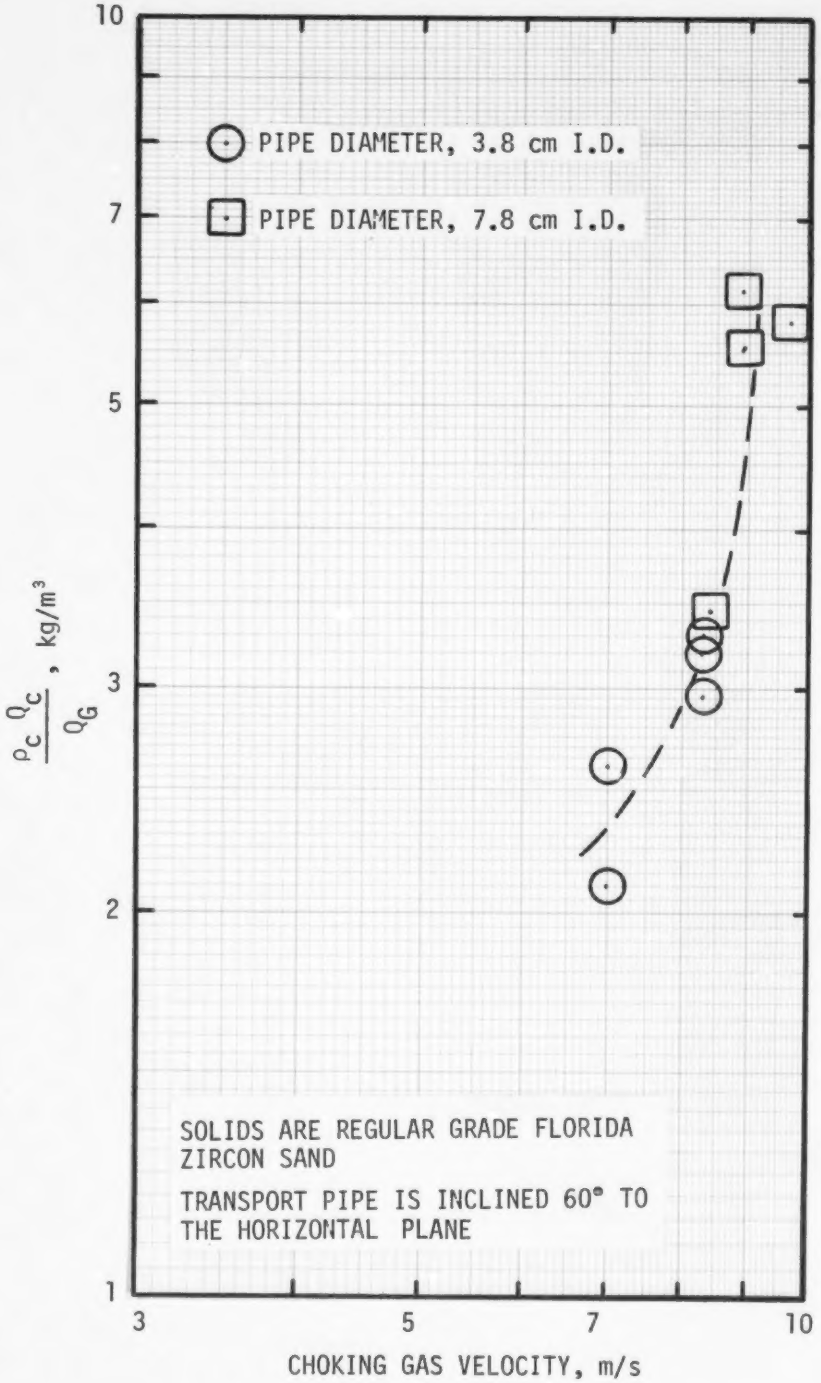

Figure 28. Inclined transport pipe solid handing capacity.

$$\Delta p < \rho_c (1-\varepsilon) L \tag{24}$$

where ρ_c = collector density, g/cm^3
ε = void fraction, fraction
L = dense phase transport pipe length, cm
Δp = scrubber pressure drop, Pa

Equation 24 gives information on the minimum required height for maintaining the dense flow condition. It does not yield information on collector flow rates. In an EPxP system, the collector flow rate is maintained at about 6.4 kg/m^3 (0.4 lb/ft^3) or higher, depending on the required pressure drop to clean the gas. The collector flow in the EPxP is due to gravity and no instruments are used to meter it. Therefore, some means to control the collector flow is required.

The collector feeding system in the EPxP is very similar to downward discharge from a vertical pipe. Therefore, collector flow can be controlled by having a restriction such as an orifice at the lower end of the pipe.

The discharge rate of solids from orifices has been studied by a number of investigators. The most exhaustive study is by Rausch (1948) (Kunii and Levenspiel, 1969). Rausch used tubes from 7.6 to 20.3 cm ID, orifices from 0.059 to 5.08 cm ID, and 10 different kinds of particles ranging in diameter from 0.127 to 12.7 mm with bulk densities from 0.73 to 6.74 g/cm^3. The correlation which accounts for his findings as well as those of several other investigators is:

$$\frac{F_S \tan(\theta_r)^{0.5}}{(C_w\, C_o\, g^{0.5}\, \rho\, d_c)^{2.5}} = 0.161\left(\frac{d_{or}}{d_c}\right)^{2.75} \tag{25}$$

where d_{or} = orifice diameter, cm
d_c = collector diameter, cm
F_S = discharge rate of solid, g/s
ρ = bulk density of solid, g/cm^3
g = 980 cm/s^2

θ_r = repose angle, degree

"C_w" and "C_o" are constants taken from Table 4. For a flat orifice plate where $d_{or}/d_c > 10$, $C_w \times C_o$ can be taken as unity.

Equation 25 cannot be applied to the EPxP system directly because the effect of the pressure gradient and the height of sand in the column were not included in the equation. A new or modified correlation is needed. To generate design data for the EPxP pilot plant, the setup shown in Figure 29 was built. It consisted of a gas-tight box fitted with a 3.8 cm ID, clear, polycarbonate tube. At the bottom of the tube was a flat orifice plate of known diameter.

In starting the experiment, the box was pressurized with compressed air to a desired value (the orifice was plugged). The sand hopper valve was opened to fill the polycarbonate tube to a known height. The plug under the orifice plate was then removed to start the collector flow. The collector level in the polycarbonate tube was kept constant by feeding collector granules from the sand hopper. The compressed air was adjusted to maintain a constant gas pressure in the box. The collector flow rate was determined by weighing the box before and after each time interval. The air flow through the polycarbonate tube was determined by measuring the amount of air flowing into and out of the box. The collector flow pattern (whether disperse or dense flow) in the polycarbonate tube was determined visually.

Figures 30 through 32 show the data for three pressure gradients. The granules were regular grade Florida zircon sand. The properties of the sand are shown in Table 1. The angle of repose of the sand was measured to be 35°.

As can be seen from these figures, there is a minimum column height, which corresponds to the minimum head needed to overcome the pressure gradient, for the collectors to start flowing. The required minimum column height is proportional to the pressure gradient across the column and inversely proportional to the orifice diameter.

When the column height was slightly larger than the minimum, the collector granules started flowing. The discharge rate increased as the height increased until an equilibrium height was reached. The discharge rate

TABLE 4. COEFFICIENTS C_w and C_o

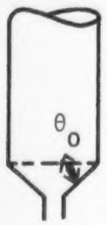

	d_{or}/d_c	10	20	40	100
	C_w	0.89	0.96	1	1
C_o	θ_o = 0-30°	1	1	1	1
	60°	1.3	1.2	1.1	1
	80°	2.1	1.8	1.5	1.2

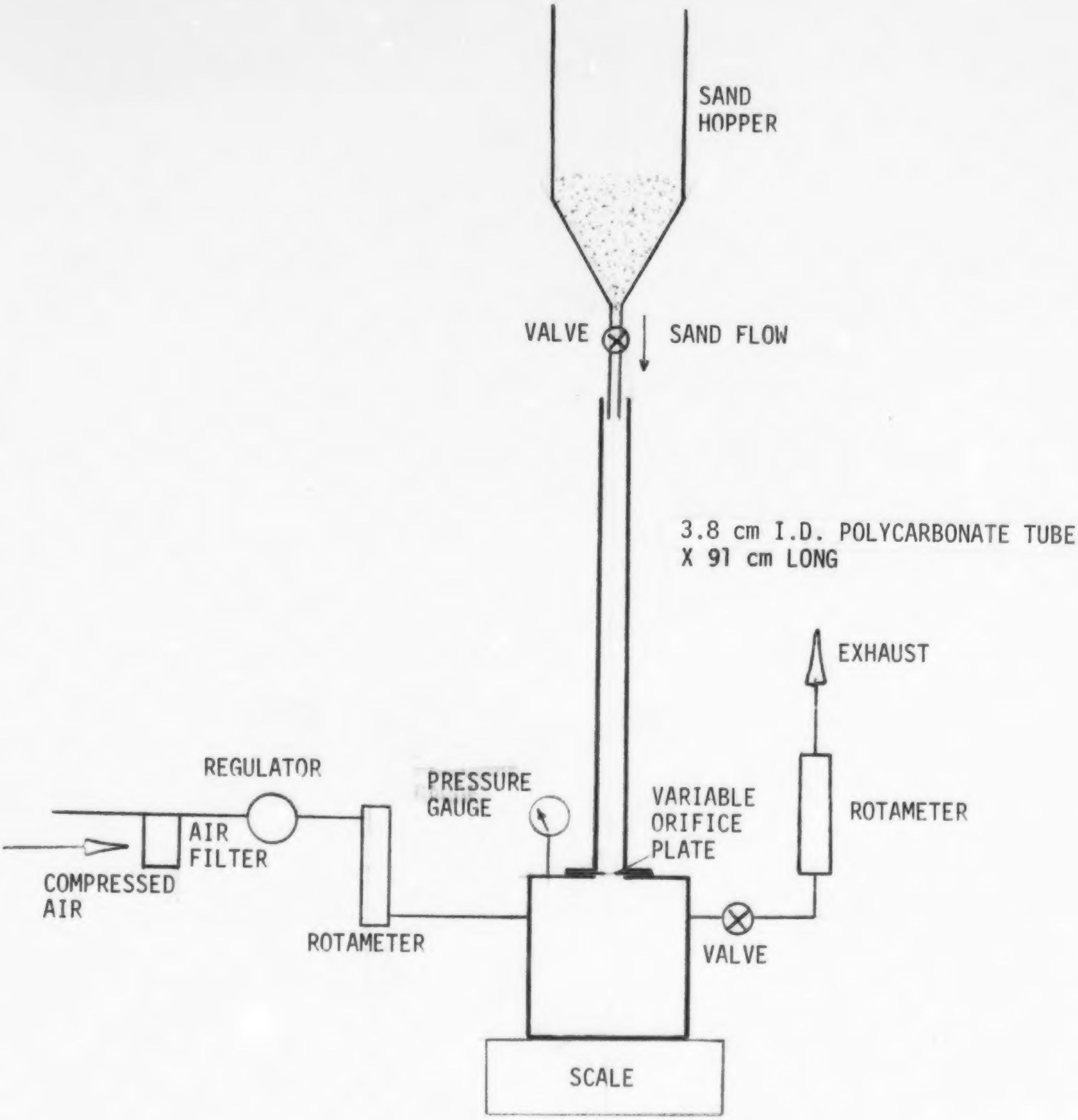
SAND
HOPPER
VALVE
SAND FLOW
3.8 cm I.D. POLYCARBONATE TUBE
X 91 cm LONG
EXHAUST
REGULATOR
PRESSURE
GAUGE
VARIABLE
ORIFICE
PLATE
ROTAMETER
AIR
FILTER
COMPRESSED
AIR
ROTAMETER
VALVE
SCALE

Figure 29. Sand flow experimental setup.

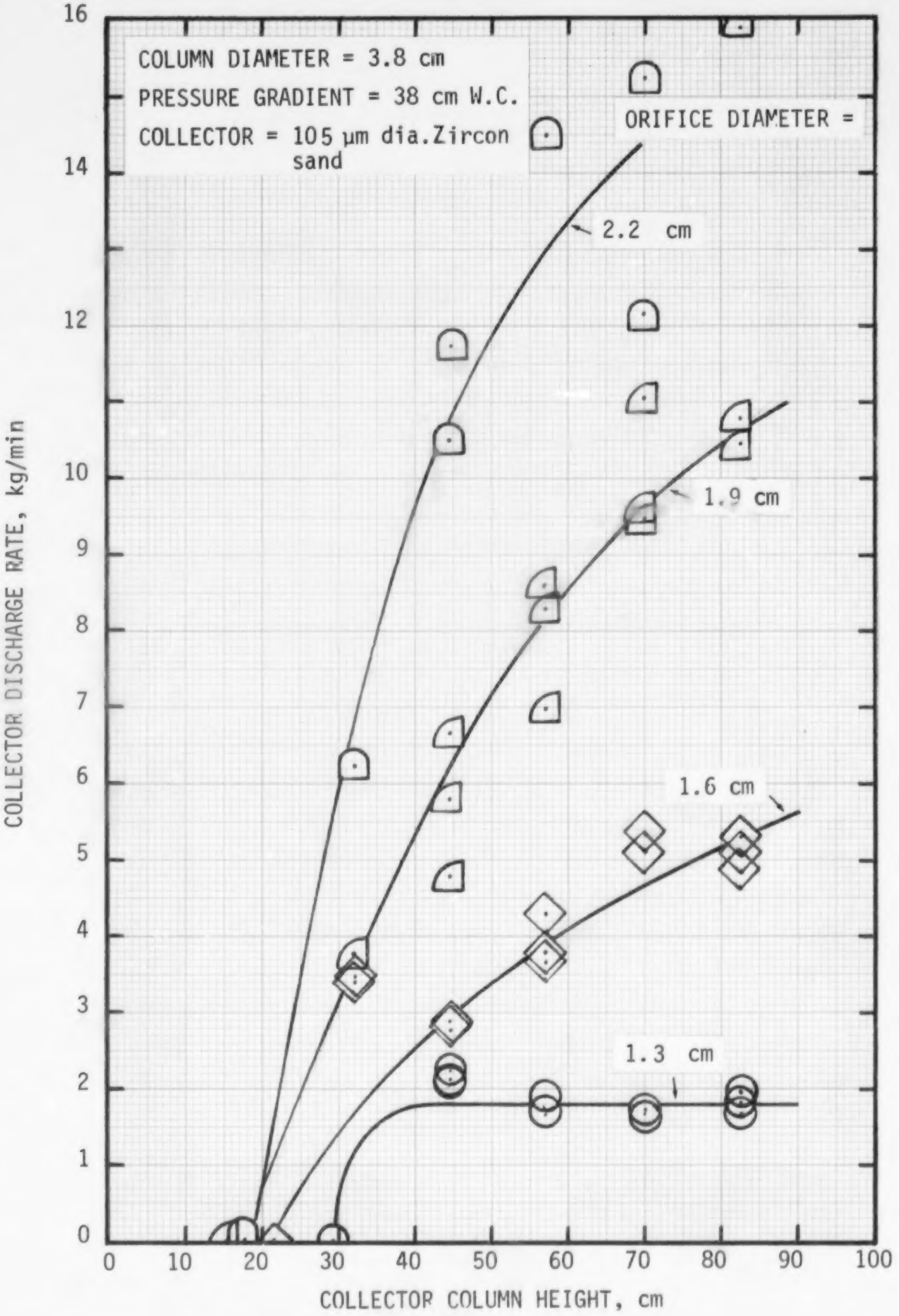

Figure 30. Experimental collector discharge rate.

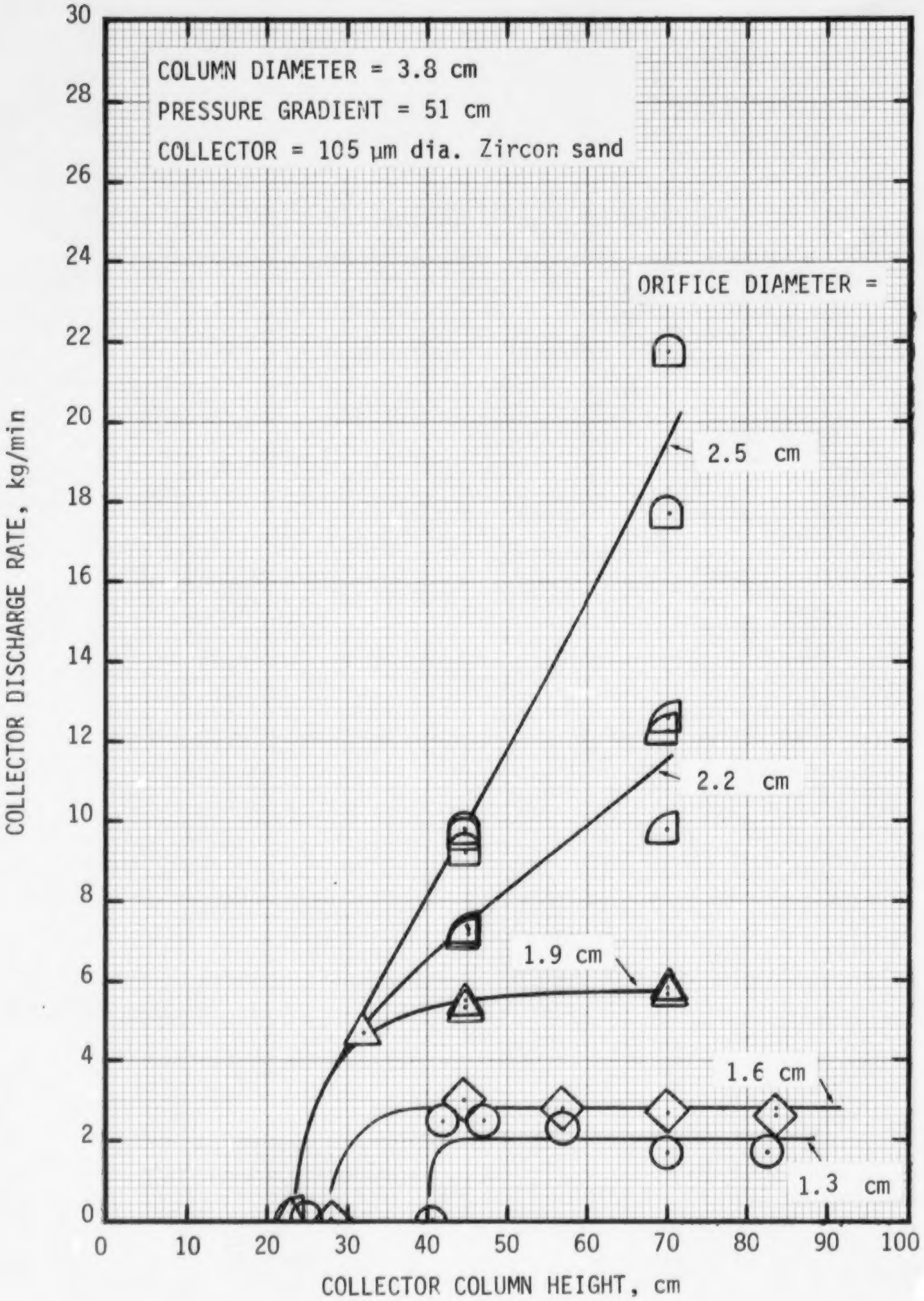

Figure 31. Experimental collector discharge rate.

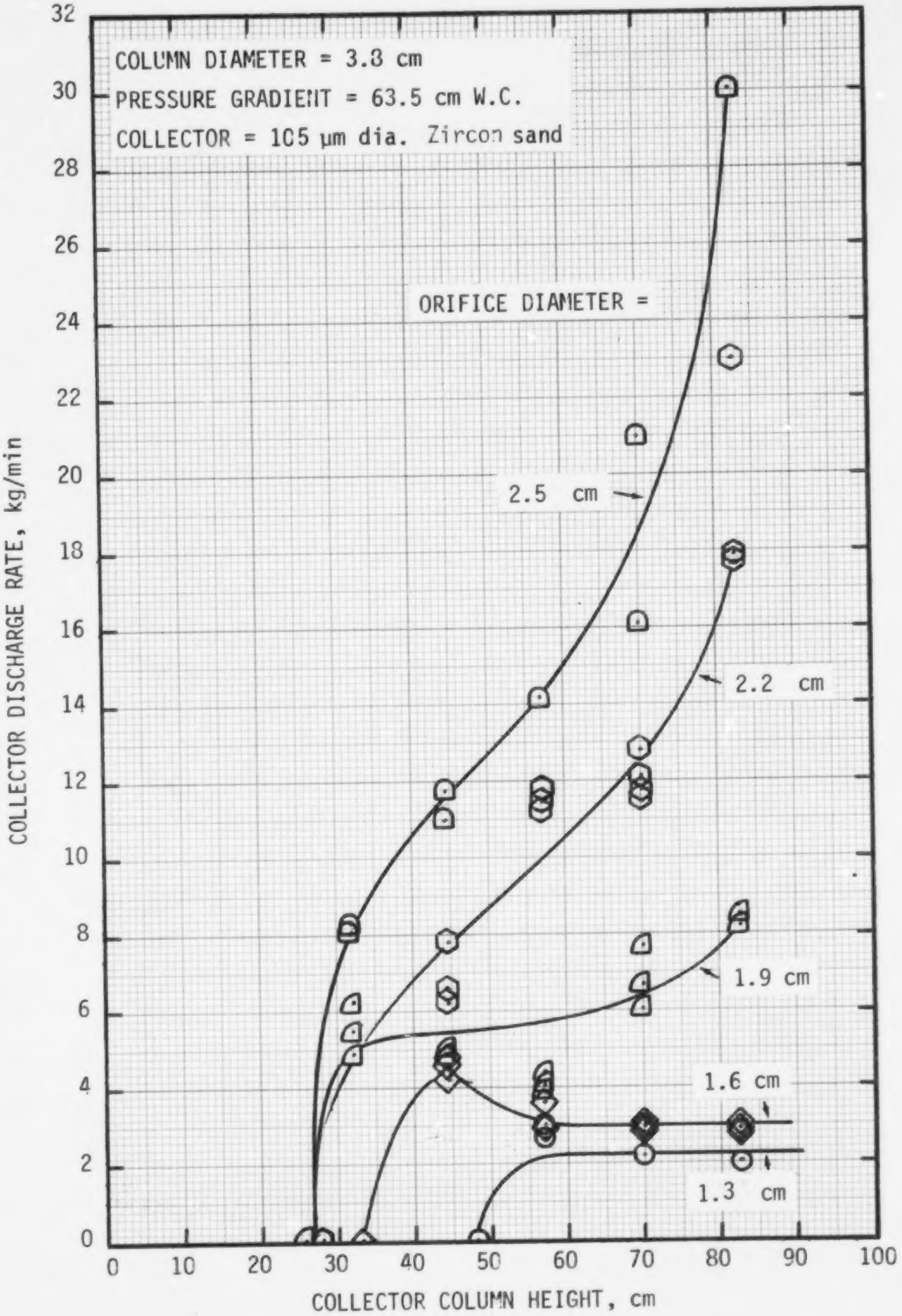

Figure 32. Experimental collector discharge rate.

no longer increased with increasing column height. This equilibrium discharge rate depended only on the orifice geometry and the properties of the granules. The measured collector discharge rate under this condition was compared with that calculated from equation (25). The rate calculated from equation (25) was about twice that measured in the experiments.

COLLECTOR CLEANING EXPERIMENTS

The collector granules from the collector separator flow downward by gravity through a collector cleaning device (bustle) before being re-injected into the gas stream at the EPxP contactor. The collector flow in this return line is maintained in dense flow to minimize gas by-passing.

Since the granules are in a dense flow mode, the inter-collector motion dislodges the collected particles. It is then possible to use a stream of air to elutriate the dislodged particles out of the system. The particles in the cleaning air stream can then be removed by conventional devices, such as filters and scrubbers, at low temperatures and pressures.

To determine the minimum length of the cleaning bustle, an experimental setup shown in Figure 33 was built. The sand was fed into a 2.54 cm x 10 cm x 60 cm long vertical box that contained an array of rods for promoting inter-collector motion. The depth of the rod bed was about 20 cm. Compressed air was injected below the rods to elutriate the fly ash. The collector-mass to cleaning air-volume ratio was maintained at about 400 kg/m^3, i.e. the cleaning air flow rate was about 2% of the gas flow rate in the EPxP.

Instead of mixing known amounts of sand and fly ash particles, which affects the adhesiveness of the collector granules, the sand from the hot bench-scale experiments was used in the collector cleaning experiments. The sand contained a unknown amount of fly ash particles. The same sand was re-used for a number of cycles through the bustle. The weight of fly ash particles separated from the sand was measured with a filter for each cycle. Figure 34 shows the amount of fly ash particle separated relative to the first pass. After the third cycle, the amount of fly ash collected by the filter decreased to about 40% of the first cycle. From Figure 34, it seems that a rod bed of 100 cm deep, which is equivalent to five passes, would be sufficient to clean the granules.

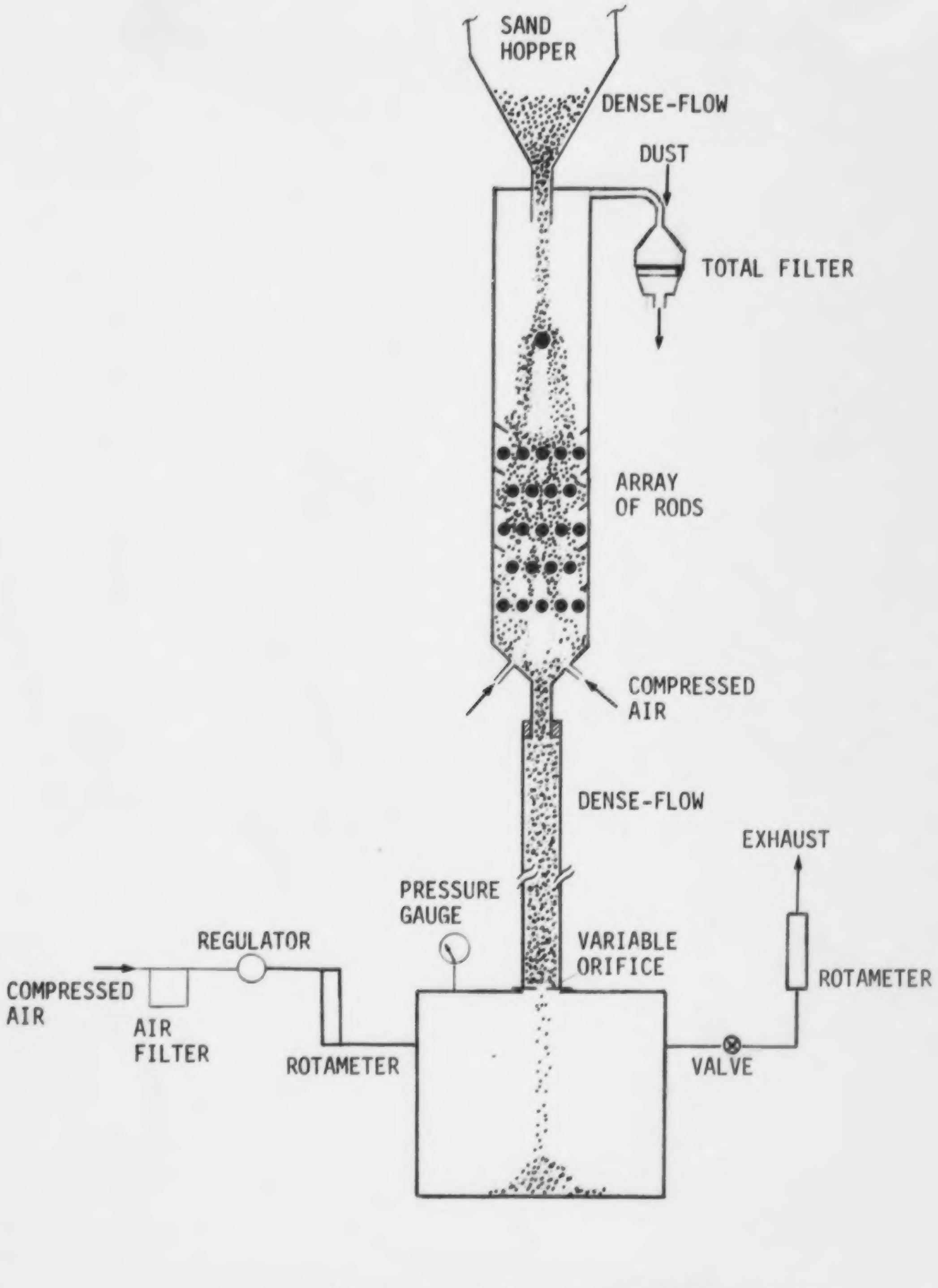
SAND HOPPER
DENSE-FLOW
DUST
TOTAL FILTER
ARRAY OF RODS
COMPRESSED AIR
DENSE-FLOW
EXHAUST
PRESSURE GAUGE
REGULATOR
VARIABLE ORIFICE
ROTAMETER
COMPRESSED AIR
AIR FILTER
ROTAMETER
VALVE

Figure 33. Study of sand cleaning bustle.

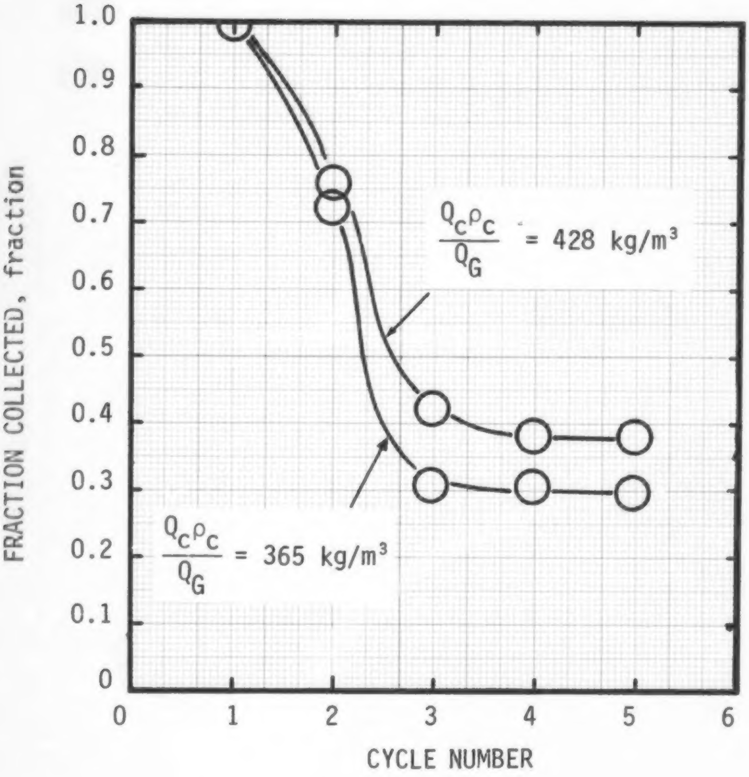

Figure 34. Measured fraction of fly ash as a function of cycle number.

COLLECTOR ATTRITION EXPERIMENTS

The wearing away of collector granules by friction affects not only the scrubber performance but also the operating cost. Therefore, the collector granules should be resistant to attrition.

Two experiments were done to characterize the attrition of collectors. In the first experiment, a sieve analysis was performed on a sample of regular grade "T" zirconium sand. The sand was then loaded into a ball mill without any balls. The milling speed was 10 RPM. After four hours of milling, the sand was resieved. Figure 35 shows the size distribution of the sand before and after ball mill grinding. The difference in size distribution is insignificant and is within the range of experimental error.

The mechanism of attrition in an EPxP scrubber is different from that in the ball mill. Therefore, a second attrition experiment was done on the hot, bench-scale EPxP. The scrubber design is presented in the next section. The bench-scale EPxP was operated with collector injection only; no fly ash particles were used. The outlet gas was sampled with a total filter. The attrition rate was then calculated from the filter weight gain and the volume of gas sampled.

The attrition rate was measured for Florida regular grade zircon sand at ambient and high temperature. The attrition rate increased with increasing temperature. At ambient temperatures, the concentration of dust resulting from attrition was 4.8 mg/m^3 for the first time through the EPxP system, and 2.3 mg/m^3 for the second time through the system. The attrition rate at 300°C was about 20.5 mg/m^3. It increased to 80.2 mg/m^3 at 600°C.

The high attrition rate of the zircon sand could be due to its irregular shape. It is known that smooth spheres would give a lower attrition rate. Other collector granules with spherical shape were evaluated. It was found that high density alumina spheres can stand high temperatures and resist attrition. However, alumina spheres of 0.1 mm in diameter have not been mass produced. Their high cost prohibits their use in the present study.

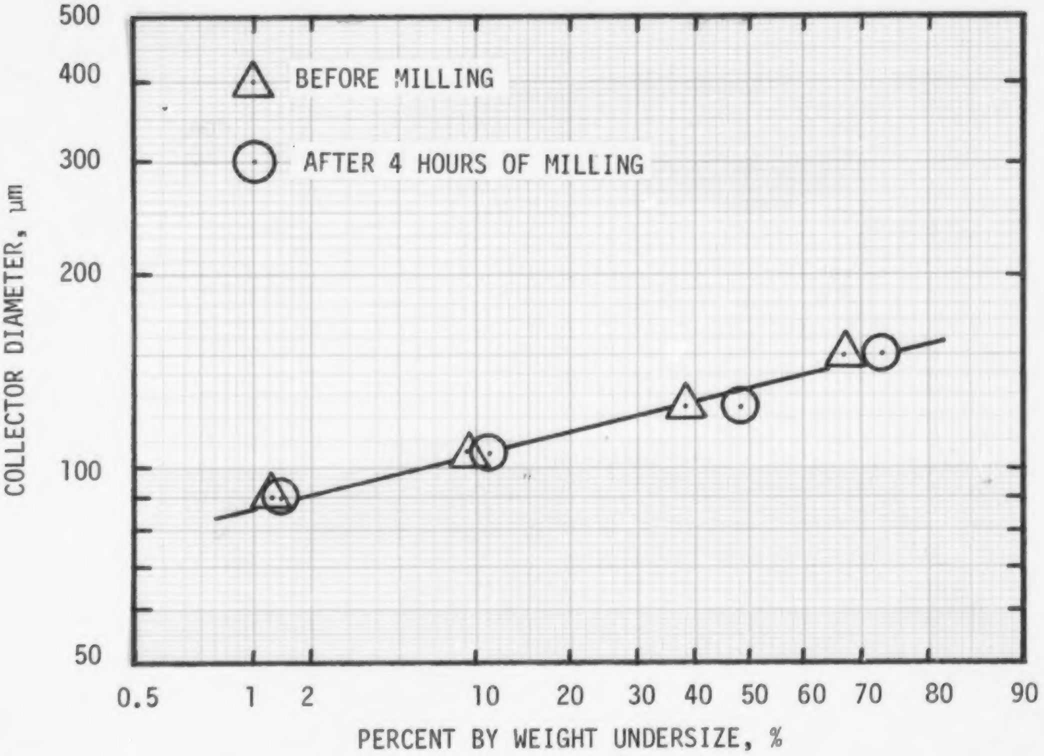

Figure 35. Particle size distribution zirconium T sand before and after grinding.

Section 6

HIGH TEMPERATURE BENCH SCALE EXPERIMENTS

The high temperature bench scale EPxP scrubber system shown in Figure 36 was built to obtain design information for the particle charger, contactor, and collector separator, under high temperature conditions. Its design was similar to the ambient temperature bench scale EPxP except for the addition of a furnace to produce the hot gas and a quencher to cool the gas before venting into the atmosphere.

The system was designed for a maximum volumetric gas flow rate of 1.1 Am^3/min (38 ACFM) and a maximum collector-mass/gas-volume ratio of 8 kg/m^3. All ducts were made from 309 s.s. and had square cross-sections. The duct dimensions were 7.5 cm x 7.5 cm (3 in. x 3 in.) before the contactor and 5.1 cm x 5.1 cm (2 in. x 2 in.) after the contactor.

The furnace was a rectangular box of insulating fire bricks. The frontal face of the furnace was open to the atmosphere for air to flow in. The furnace had a natural gas burner for heating the air to desired temperatures. Fly ash particles were injected into the flame to deagglomerate and mix the particles.

The particles next entered the particle charger, which was made from machinable ceramic. The charger was a wire-and-plate design (Figure 37). The particle charger was 7.1 cm high x 7.1 cm wide 15.2 cm (6 in.) long. Three 309 s.s. plates (0.34 cm thick) served as ground electrodes and were used to split the gas stream. The plate-to-plate spacing was 3.3 cm (1.3 in.). The corona wires were four 0.0178 cm (0.007 in.) diameter platinum wires spaced 2.5 cm (1 in.) apart. The high voltage could be applied to any one wire or any combination of wires. Sampling ports were provided before and after the particle charger to measure the amount of particles collected by the charger and the charge level on particles.

The particle charger was followed by the EPxP contactor which was made from machinable ceramic. The contactor was 1.91 cm high x 1.91 cm wide (0.75 in. x 0.75 in.) and 30.5 cm (12 in.) long. Two opposite surfaces were lined with 309 s.s. plates so that a high electric field could be applied to the gas. Collector granules were injected into the contactor at a location 8.9 cm

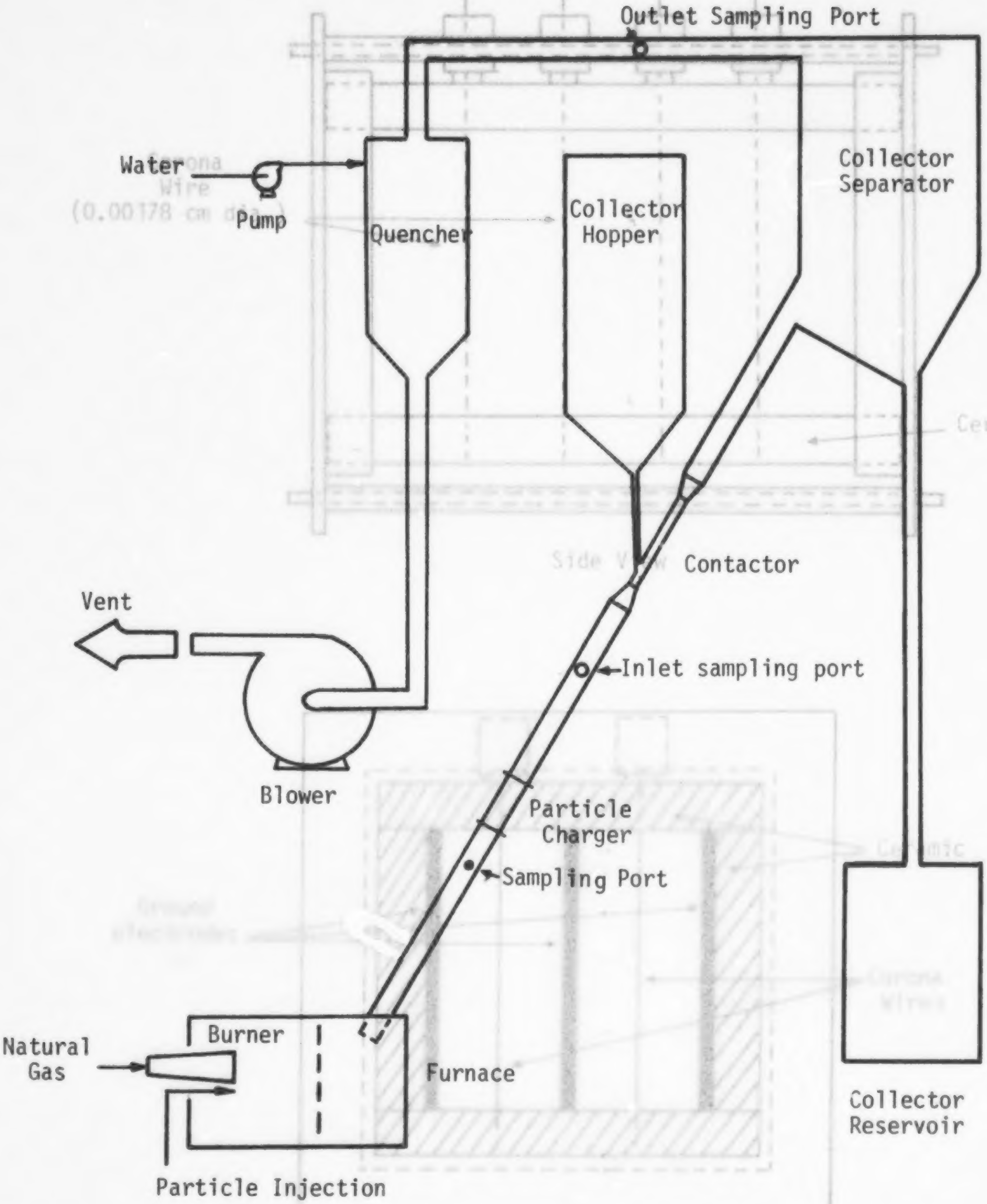
Outlet Sampling Port
Water
Pump
Quencher
Collector Hopper
Collector Separator
Contactor
Vent
Inlet sampling port
Blower
Particle Charger
Sampling Port
Natural Gas
Burner
Furnace
Particle Injection
Collector Reservoir

Figure 36. Hot EPxP bench scale system.

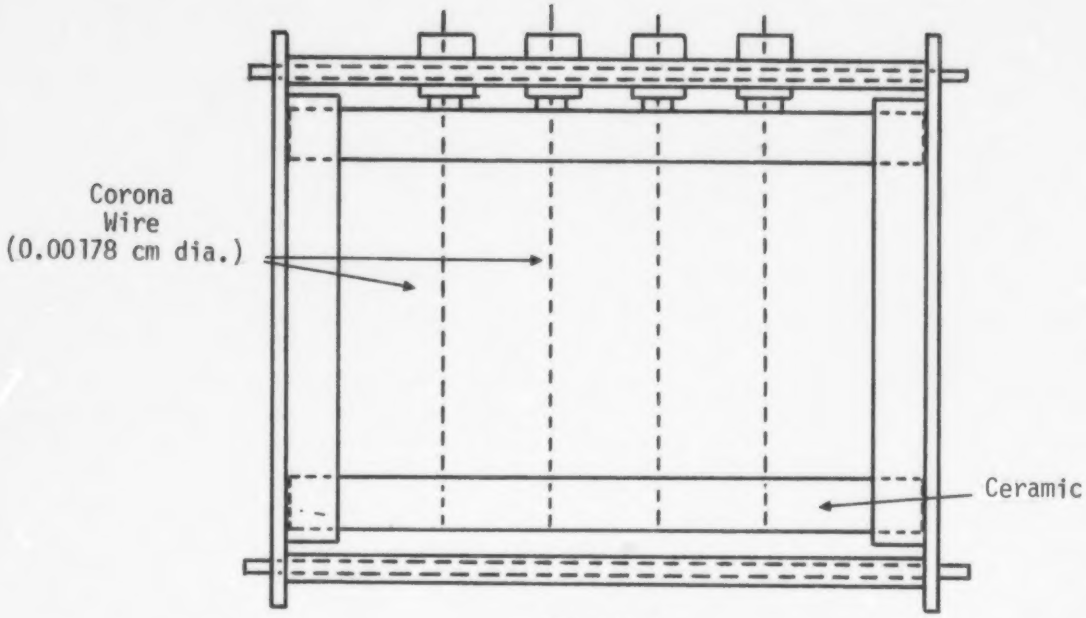
Corona
Wire
(0.00178 cm dia.)
Ceramic

Side View

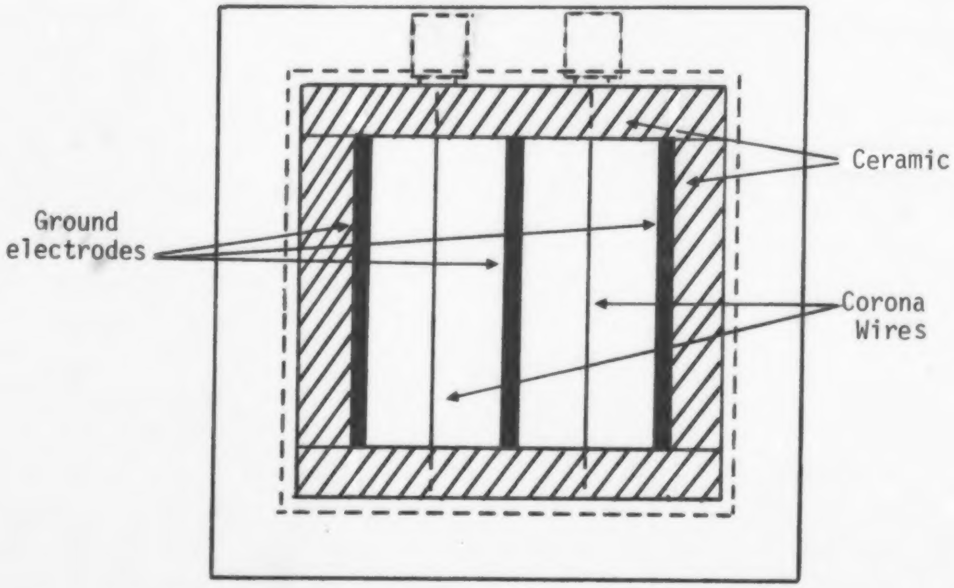
Ceramic
Ground
electrodes
Corona
Wires

End View

Figure 37. Particle charger design.

(3.5 in.) downsteam of the entrance. Therefore, the effective throat length was 21.6 cm (8.5 in.).

The granules and the collected particles were separated from the gas stream in a baffled gravity settler. A single row of baffles was placed at the top of the settler. The baffles were 7.5 cm x 5.1 cm (3 in. x 2 in.) 309 s.s. plates. Space between baffles was 5.1 cm (2 in.). Baffle plates were inclined 60° to the horizontal plane.

After the collector separator was a quencher to cool the gas and an entrainment separator to remove the water drops before the gas was vented to the atmosphere.

Thermocouples and pressure gauges were installed at each process step to monitor gas temperatures and pressures. Gas flow rates were monitored with a venturi meter and an electronic flow meter.

HIGH TEMPERATURE PARTICLE CHARGING EXPERIMENTS

Theory

It is generally acknowledged that the corona-starting voltage decreases as gas density decreases (or as gas temperature increases). There is also a narrower operating range between the corona-starting voltage and the spark-over voltage at lower gas densities (Robinson, 1971). It is not possible to predict the corona-starting voltage and the spark-over voltage with much accuracy in an industrial environment. The major disturbing factors include poor electrode alignment, surface irregularities, dust deposition, and non-uniform electric fields. Empirical formulas are available in the literature for predicting the corona-starting voltage. Cooperman (1960) presented the following expression for predicting the corona-starting voltage for wire-plate geometry:

$$V_c = r_o E_c \ln (d/r_o) \tag{26}$$

where r_o = wire radius, cm
E_c = corona starting field strength, kV/cm
d = characteristic dimension, cm
V_c = corona starting voltage, kV

The parameter, d, can be calculated from the following equations (Cooperman, 1960) and from Figure 38.

$$\text{For } \frac{b}{c} \leq 0.6, \quad d = \frac{4b}{\pi} \tag{27}$$

$$\text{For } \frac{b}{c} \geq 2.0, \quad d = \frac{c}{\pi} \exp \frac{\pi b}{2c} \tag{28}$$

For $0.6 < \frac{b}{c} < 2.0$, d calculate from Figure (38).

where 2b = plate-to-plate spacing, cm

2c = wire-to-wire spacing, cm

The corona starting field strength for several gases and mixtures was studied experimentally and can be calculated from the following empirical equation:

$$\frac{E_c}{\delta} = A_g + \frac{B_g}{(r_o \ \delta)^{0.5}} \tag{29}$$

where A_g = empirical constant, kV/cm

B_g = empirical constant, kV/cm$^{0.5}$

δ = relative gas density, dimensionless

Relative gas density, δ, is conventionally taken with respect to 1 atm and 25°C. The empirical constants, A_g and B_g, have been reported by Thornton (1939) for several gases. For negative corona in air and at ambient temperatures, $A_g = 3.22 \times 10^5$ V/m and $B_g = 8.46 \times 10^4$ V/m$^{0.5}$.

Figure 39 shows the calculated corona starting voltage versus relative air density for the bench scale EPxP particle charger. Empirical values of "A_g" and "B_g" at room temperatures were used in the calculations. It can be

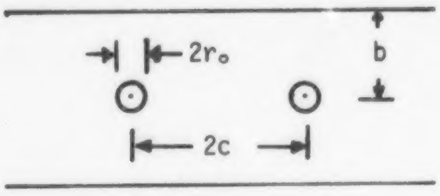

WIRE-PLATE GEOMETRY
PARTICLE CHARGER

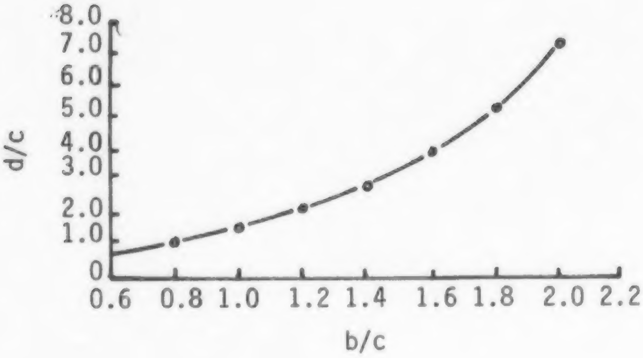

Figure 38. Calculated values of d/c vs. b/c for Wire-Plate Geometry (Cooperman 1960).

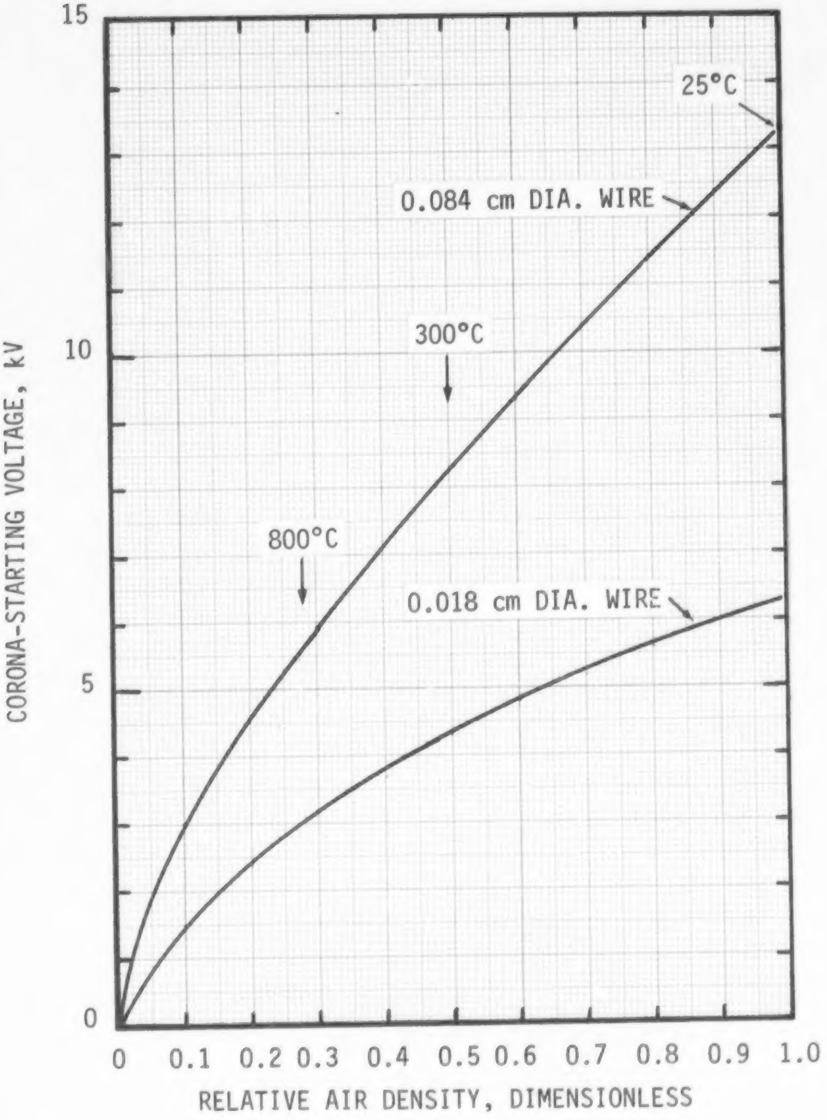

Figure 39. Calculated corona-starting voltage vs. relative air density for wire plate geometry.

seen from this figure that the corona starting voltage decreases with increasing gas temperature and decreasing wire diameter.

EXPERIMENTS

The particle charger was tested at temperatures up to 800°C and problems with the corona wire developed. The wire broke repeatedly at high temperatures. The wires were subsequently replaced with 0.084 cm diameter Nichrome wires. No problems occurred after wire replacement.

Figure 40 shows the experimental negative corona current-voltage curves at various gas temperatures. The results agree with the findings of other researchers that the operating range between the corona-starting voltage and the spark-over voltage narrows as the gas temperature increases. The measured spark-over voltage decreased from 19 kV DC at 20°C to 7.5 kV at 450°, and to 5 kV at 650°C.

A Faraday cup (Figure 41), which consisted of a shielded, isolated glass fiber filter connected to an electrometer, was used to measure the charge/mass ratio at various temperatures. When sampling at high temperatures, a dilution cooling system shown in Figure 42 was used to cool the gas to prevent damaging the filter. The sample stream was surrounded by a stream of sheath air in laminar flow for minimizing the wall losses of particles.

Figure 43 shows the measured charge/mass ratios at various temperatures. The obtainable charge level on particles decreases with increasing temperature. It was about -7×10^{-5} C/g at ambient temperatures and about -1×10^{-5} C/g at 800^{0}C. Even though the obtainable charge level at high temperatures is 7 times lower than that at low temperatures, it is still acceptable.

The measured charge/mass ratios were higher than those reported for ESP's in coal-fired power plants because finer particles were used in the present experiments. The particles were measured with cascade impactors to have a mass median diameter of about 1.5 µmA and a geometric standard deviation of about 2.0.

PARTICLE COLLECTION EXPERIMENTS

Particle penetration was determined for the EPxP scrubber at several gas temperatures. The scrubber was operated at a pressure drop of 50 cm W.C. for all experiments due to blower limitations. Table 5 shows a summary of experi-

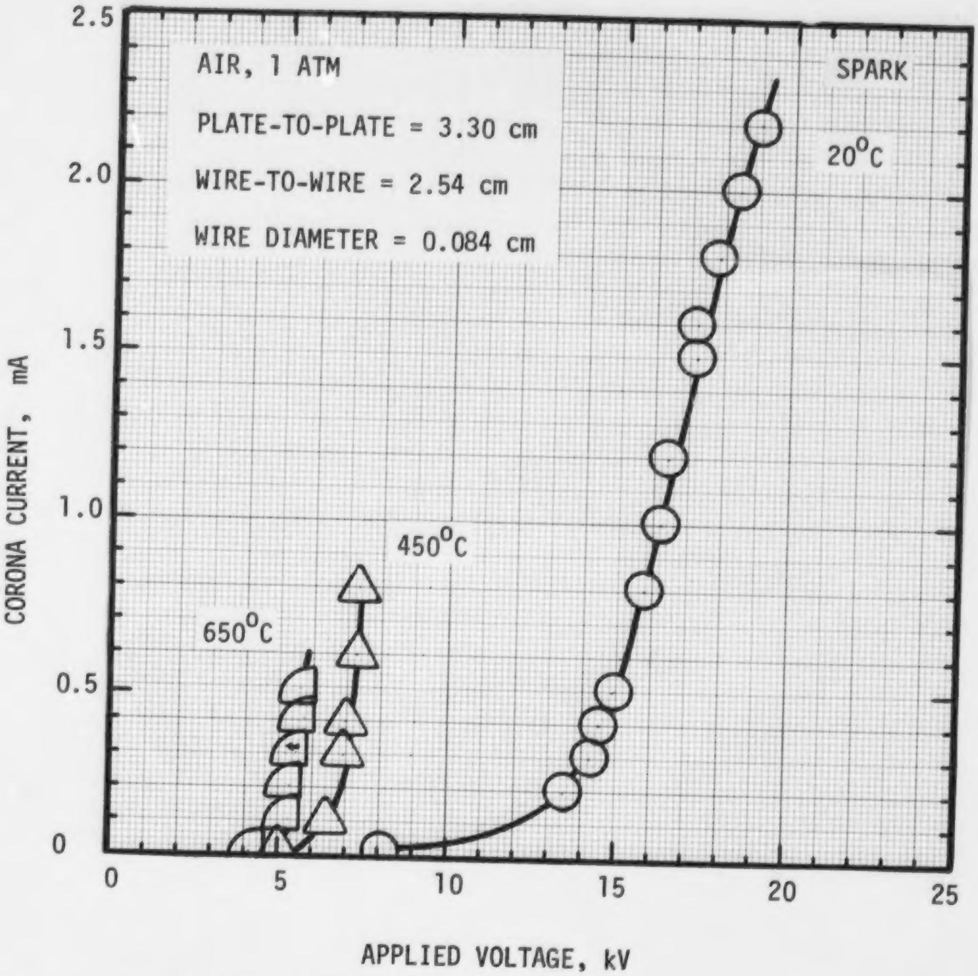

Figure 40. Measured negative corona current-voltage curves at various gas temperatures in the bench-scale, EPXP particle charger.

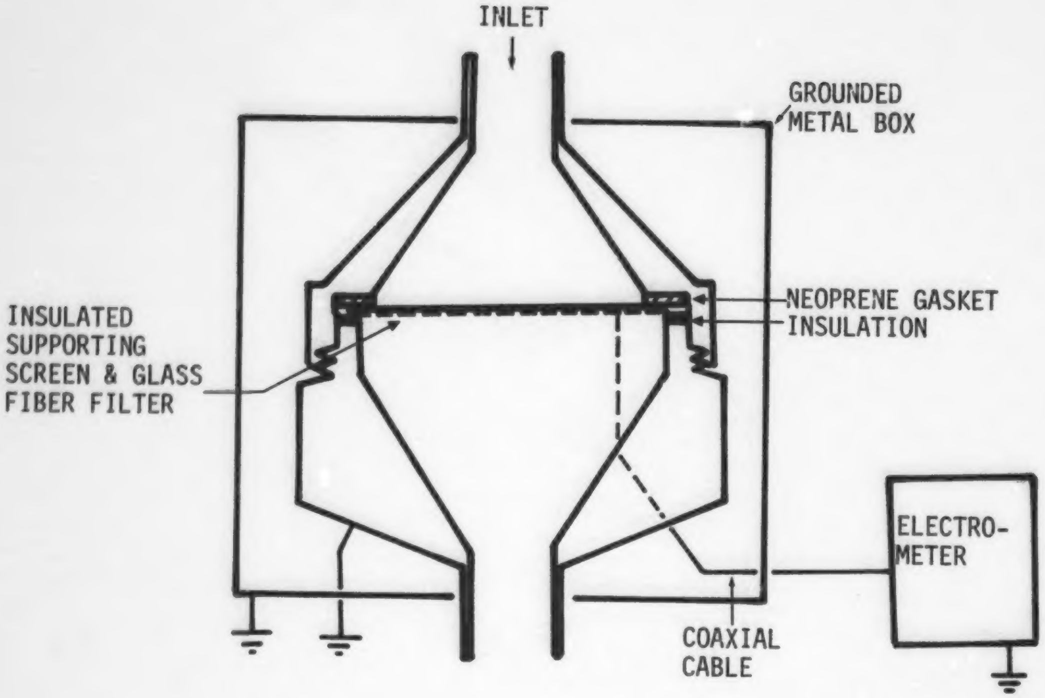
INLET
GROUNDED METAL BOX
NEOPRENE GASKET
INSULATION
INSULATED SUPPORTING SCREEN & GLASS FIBER FILTER
ELECTRO-METER
COAXIAL CABLE

Figure 41. Faraday Cup for charge measurements.

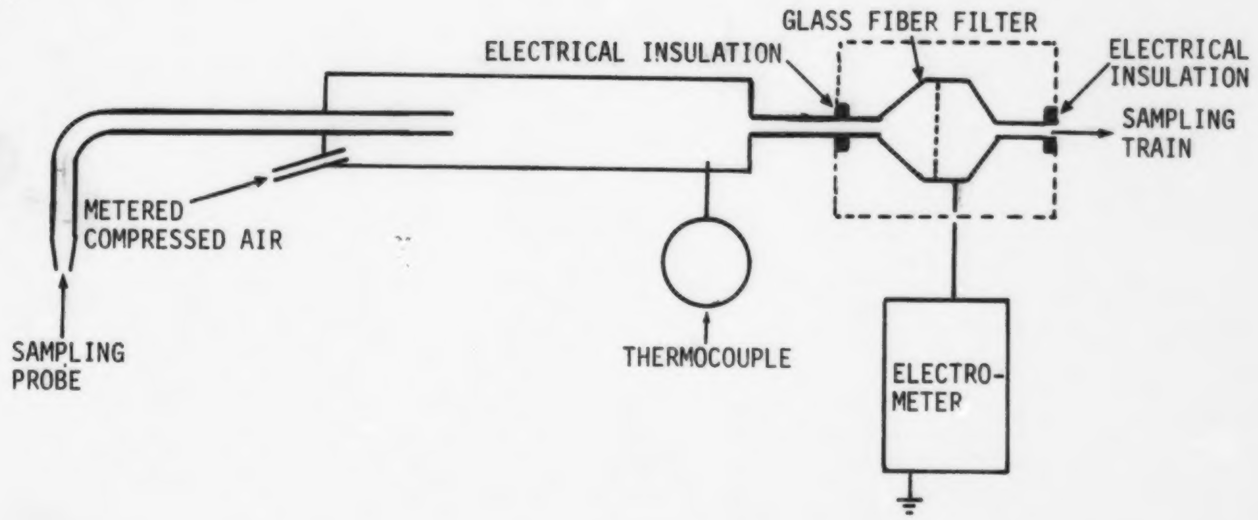
GLASS FIBER FILTER
ELECTRICAL INSULATION
ELECTRICAL INSULATION
SAMPLING TRAIN
METERED COMPRESSED AIR
SAMPLING PROBE
THERMOCOUPLE
ELECTRO-METER

Figure 42. Dilution and Faraday cup for high-temperature charge measurements.

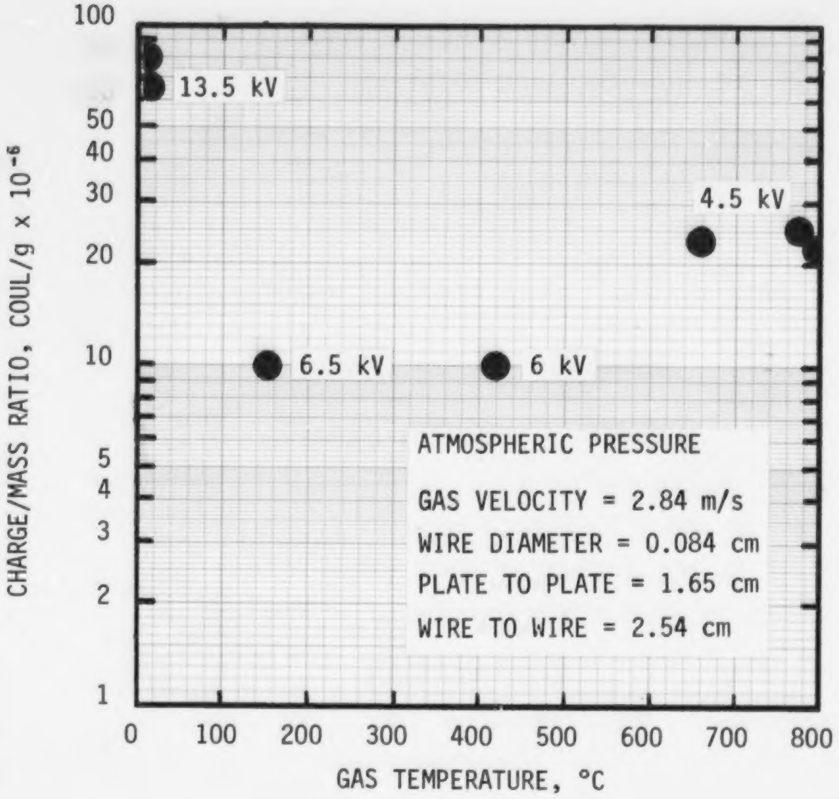

Figure 43. Experimental charge to mass ratio vs. gas temperature in the bench-scale EPxP wire-plate particle charger, at the obtainable operating negative corona applied voltage.

Table 5. Hot Bench Scale EPxP Test Summary

								Inlet Part. Size Dist.		Part Conc. mg/DNm^3			
Run No.	U_{Gt}, m/s	Q_G Am^3/min	$\frac{Q_c \rho_c}{Q_G}$, kg/m^3	ΔP, cm W.C.	T_G, °C	E_C, kV/cm	E_p kV/cm	d_{pg} μmA	σ_g	Inlet	Outlet	$\overline{Pt}$, %	Test Part.
16/8	29.3	0.65	7.6	51	Ambient	0	0	1.4	2.2	3,560	383.9	10.8	TiO2
16/9	32.8	0.71	7.6	52	Ambient	0	0	1.6	2.6	1,338.8	66.3	5.0	TiO2
16/10	35.1	0.76	6.1	51	Ambient	0	0	1.2	2.2	2,495.5	678.5		TiO2
16/12	36.5	0.79	5.0	51	Ambient	0	7.9	2.0	2.6	759.5	236.2	31.1	Fly ash
16/13	48.5	1.05	2.5	51	Ambient	6.1	0	3.3	4.1	748.6	159.0	21.2	Fly ash
17/2	30.5	0.66	7.5	51	Ambient	6.1	7.9	2.8	2.2	86.0	7.4	8.6	Fly ash
17/3	31.6	0.69	7.0	51	Ambient	6.1	7.9	2.6	2.5	617.6	66.8	10.8	Fly ash
17/4	29.8	0.65	7.7	51	Ambient	0	0	3.6	2.5	2,321.8	417.6	18.0	Fly ash
17/5	29.8	0.65	8.8	51	Ambient	6.1	7.9	3.3	2.8	1,001.4	92.7	9.3	Fly ash
17/7	29.8	0.65	9.2	51	Ambient	0	7.9	3.8	2.5	888.2	249.3	28.1	Fly ash
17/8	29.8	0.65	8.9	51	Ambient	6.1	0	3.4	2.5	1,057.6	56.9	5.4	Fly ash
17/17	41.0	0.91	5.2	49.5	280	3.0	0	4.2	3.9	839.6	467.4	55.7	Fly ash
18/1	42.4	0.94	5.0	49.5	302	3.0	0	4.0	2.6	726.9	138.1	19.0	Fly ash
18/2	46.3	1.0	5.2	49.5	356	0	0	4.5	2.6	583.8	138.3	23.7	Fly ash
18/3	45.3	1.0	5.5	49.5	338	0	0	4.6	2.4	535.5	143.9	26.9	Fly ash
18/4	45.3	1.0	5.5	49.5	342	0	0	5.1	2.3	787.4	153.1	19.4	Fly ash
18/5	44.1	0.98	5.2	49.5	325	0	0	4.2	2.5	716.1	157.3	22	Fly ash
18/6	43.6	0.97	5.1	49.5	317	2.4	6.3	4.1	2.6	650.9	147.9	22.7	Fly ash

Table 5. Hot Bench Scale EPxP Test Summary (Continued)

								Inlet Part. Size Dist.		Part Conc. mg/DNm^3			
Run No.	U_{Gt}, m/s	Q_G Am^3/min	$\frac{Q_c \rho_c}{Q_G}$, kg/m^3	ΔP, cm W.C.	T_G, °C	E_C, kV/cm	E_p kV/cm	d_{pg} µmA	σ_g	Inlet	Outlet	$\overline{Pt}$, %	Test Part.
18/7	42.7	0.95	5.4	49.5	307	2.4	6.3	4.6	2.4	731.5	131.9	18.0	Fly ash
18/8	44.8	0.99	5.2	49.5	334	2.4	5.8	4.2	2.3	491.8	80.7	16.4	Fly ash
18/9	43.8	0.97	5.4	49.5	320	2.4	6.3	4.2	2.7	642.2	120.3	18.7	Fly ash
18/10	44.5	0.99	5.2	49.5	330	0	0	4.5	2.5	474.1	107.3	22.6	Fly ash
18/11	43.8	0.97	5.5	49.5	322	0	6.3	4.2	2.8	481.9	124.6	25.6	Fly ash
18/12	43.8	0.97	6.0	51.0	302	0	6.3	4.2	2.5	417.3	82.3	19.7	Fly ash
18/13	43.8	0.97	5.3	49.5	321	0	6.3	4.4	2.6	480.4	98.0	20.4	Fly ash
18/14	42.8	0.95	5.8	49.5	345	0	6.3	3.8	2.3	178.7	92.1	51.5	Fly ash
18/16	45.1	1.0	5.4	49.5	494	0	0	3.6	2.3	178.7	92.1	51.5	Fly ash
18/17	45.1	1.0	5.4	49.5	550	0	0	4.2	2.2	308.7	92.5	30	Fly ash
18/18	45.1	1.0	5.4	49.5	517	0	0	5.1	2.2	411.7	121.9	29.6	Fly ash
18/19	44.7	0.99	5.8	50.8	502	0	0	4.8	2.4	460.0	112.1	24.4	Fly ash
18/20	45.1	1.0	5.3	49.5	512	3.0	0	4.7	2.4	326.0	82.5	25.3	Fly ash
18/21	44.4	0.99	5.8	49.5	497	3.0	0	4.4	2.4	262.8	60.0	22.8	Fly ash
18/22	44.8	0.99	5.5	49.5	503	2.9	0	5.0	2.3	294.0	64.3	21.9	Fly ash
18/23	42.5	0.94	5.9	49.5	481	3.0	4.7	4.9	2.4	364.1	69.7	19.1	Fly ash
18/27	45.7	1.0	5.9	49.5	519	0	0	4.7	2.2	658.5	158.9	24.1	Fly ash
18/30	44.7	0.99	5.7	49.5	500	3.0	4.7	5.3	2.9	1,714.2	415.5	24.2	Fly ash

Table 5. Hot Bench Scale EPxP Test Summary

Run No.	U_{Gt}, m/s	Q_G Am^3/min	$\frac{Q_c \rho_c}{Q_G}$, kg/m^3	ΔP, cm W.C.	T_G, °C	E_C, kV/cm	E_p kV/cm	Inlet Part. Size Dist. d_{pg} µmA	σ_g	Part Conc. mg/DNm^3 Inlet	Outlet	$\overline{Pt}$, %	Test Part.
18/31	45.3	1.0	6.0	49.5	530	0	0	6.2	2.1	1,111.8	281.1	25.3	Fly ash
19/01	44.7	0.99	6.5	49.5	516	3.0	0	7.1	3.9	1,092.0	298.2	27.3	Fly ash
19/02	45.6	1.01	6.3	49.5	506	3.0	0	6.3	3.6	1,501.2	344.6	23.0	Fly ash
19/03	44.7	0.99	5.9	49.5	508	0	4.5	3.6	2.5	2,348.4	445.3	19.0	Fly ash
19/05	44.9	1.0	5.1	49.5	494	0	4.7	4.5	2.9	2,419.0	547.8	22.6	Fly ash
19/06	44.9	1.0	5.1	49.5	498	0	4.7	4.8	2.8	2,313.0	555.1	24.0	Fly ash
19/12	44.2	0.98	6.0	49.5	481	3.0	4.5	4.3	2.8	2,513.8	579.1	23.0	Fly ash
19/13	44.7	0.99	6.3	49.5	504	0	4.2	3.8	4.1	2,868.7	490.6	17.1	Fly ash
19/14	44.7	0.99	6.0	49.5	490	3.0	4.5	5.7	3.2	1,935.2	489.2	25.3	Fly ash
19/18	44.7	0.99	6.2	49.5	693	0	0	7.9	2.9	2,849.2	647.3	22.7	Fly ash
19/20	44.7	0.99	6.6	49.5	583	3.0	3.7	10.5	3.1	4,475.3	904.4	20.2	Fly ash
20/4	44.7	0.99	6.4	49.5	619	0	2.6	3.3	2.1	780.4	325.2	41.7	Fly ash
20/6	44.7	0.99	7.2	48.3	600	2.4	0	7.0	2.9	1,421.1	400.6	28.2	Fly ash
20/7	44.7	0.99	6.1	49.5	628	0	0	0.67	9.4	3,987.8	330.1	8.3	Fly ash
20/9	44.7	0.99	5.1	48.3	621	0	0	5.4	2.9	998.0	253.6	25.4	Fly ash
20/10	49.8	1.1	5.3	48.3	610	3.0	0	15.1	4.7	3,613.9	933.5	25.8	Fly ash
20/11	44.7	0.99	6.0	48.3	605	0	3.1	10.4	2.8	7,764.6	1,082.9	20.3	Fly ash
20/12	44.7	0.99	6.9	48.3	612	0	2.6	20.6	3.4	4,095.8	831.1	20.3	Fly ash
20/13	44.7	0.99	6.9	48.3	571	0	2.6	19.8	3.2	2,683.5	474.5	17.7	Fly ash
20/14	44.7	0.99	5.6	48.3	612	3.0	0	26.5	3.6	3,858.3	697.4	18.1	Fly ash
20/15	44.7	0.99	6.7	49.5	610	3.0	2.6	18.4	4.4	2,542.1	721.5	28.4	Fly ash

mental conditions and results. Particle samples were taken simultaneously at the inlet and outlet of the scrubber with cascade impactors. Inlet samples were taken downstream of the particle charger; therefore collection in the charger was excluded.

Cascade impactor data have been reduced into plots of grade penetration. Experimental grade penetration curves are presented in Appendix "A".

Figures 44 and 45 show the experimental penetration for ambient gas temperature and 500°C; respectively. The particle collection efficiency of the PxP scrubber increased by augmenting the scrubber with electrostatic forces, even under high temperature conditions. The improvement was greater with small particles. For particles larger than 5μmA diameter, the improvement was minimal.

The measured collection efficiency decreased with increasing temperature as shown in Figure 46. This is consistent with the findings of Calvert and Parker (1977) that particle collection is more difficult at high temperatures than that at low temperatures. The lower efficiency at high temperatures could be partly due to attrition. As mentioned earlier, the attrition of zircon sand increased with increasing gas temperature. At gas temperatures above 600°C, attrition was excessive. The penetration measured for the EPxP at temperatures around 600°C was erratic and non-reproducible. For some runs the particle penetration increased with increasing particle diameter and exceeded 100% for some experiments.

The particles used in the experiments were re-dispersed power plant fly ash. The properties of power plant fly ash differ from pressurized fluidized bed combustor (PFBC) fly ash. PFBC fly ash is sticky; therefore, particle bounce and re-entrainment would be less with PFBC particles. A few experiments were done using titanium dioxide particles, which are sticky. Experimental results indicated that the EPxP was more efficient in removing titanium dioxide particles (Figure 47).

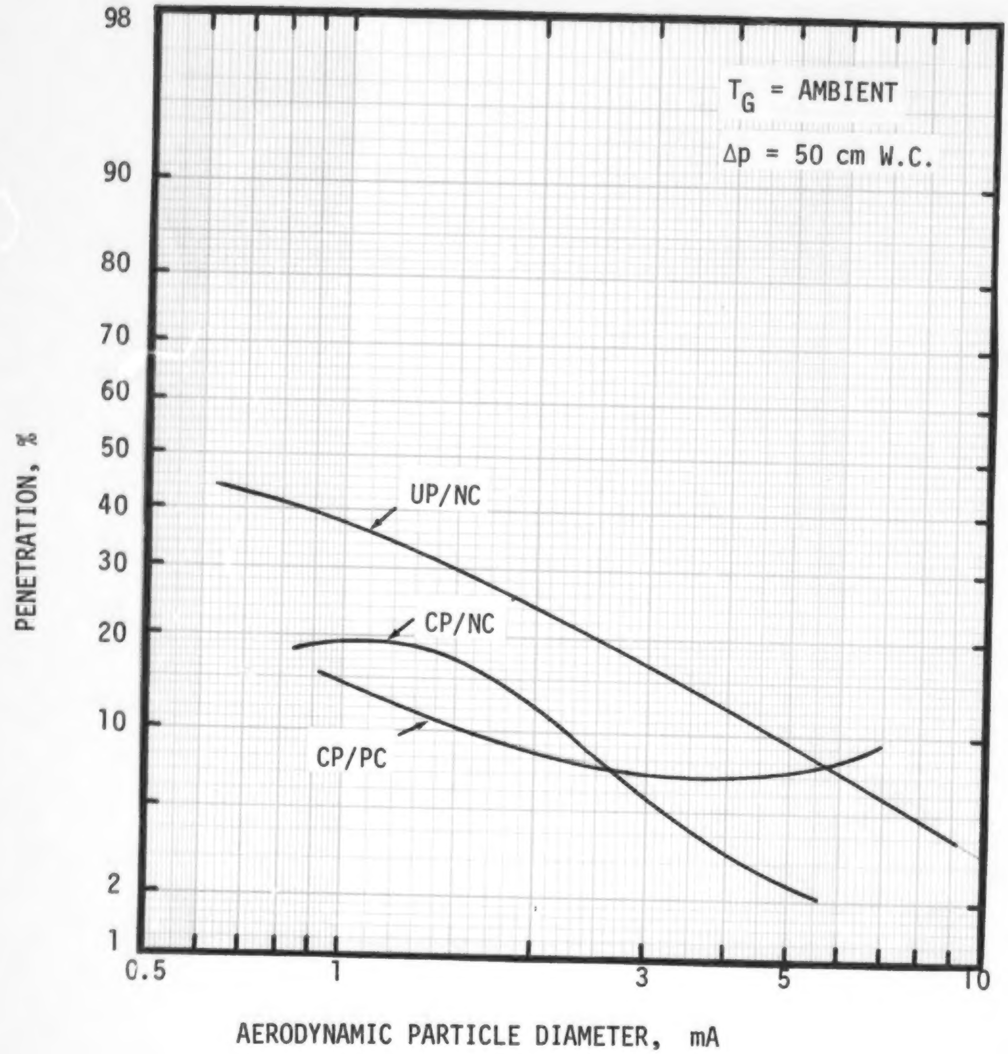

Figure 44. Measured EPxP penetration.

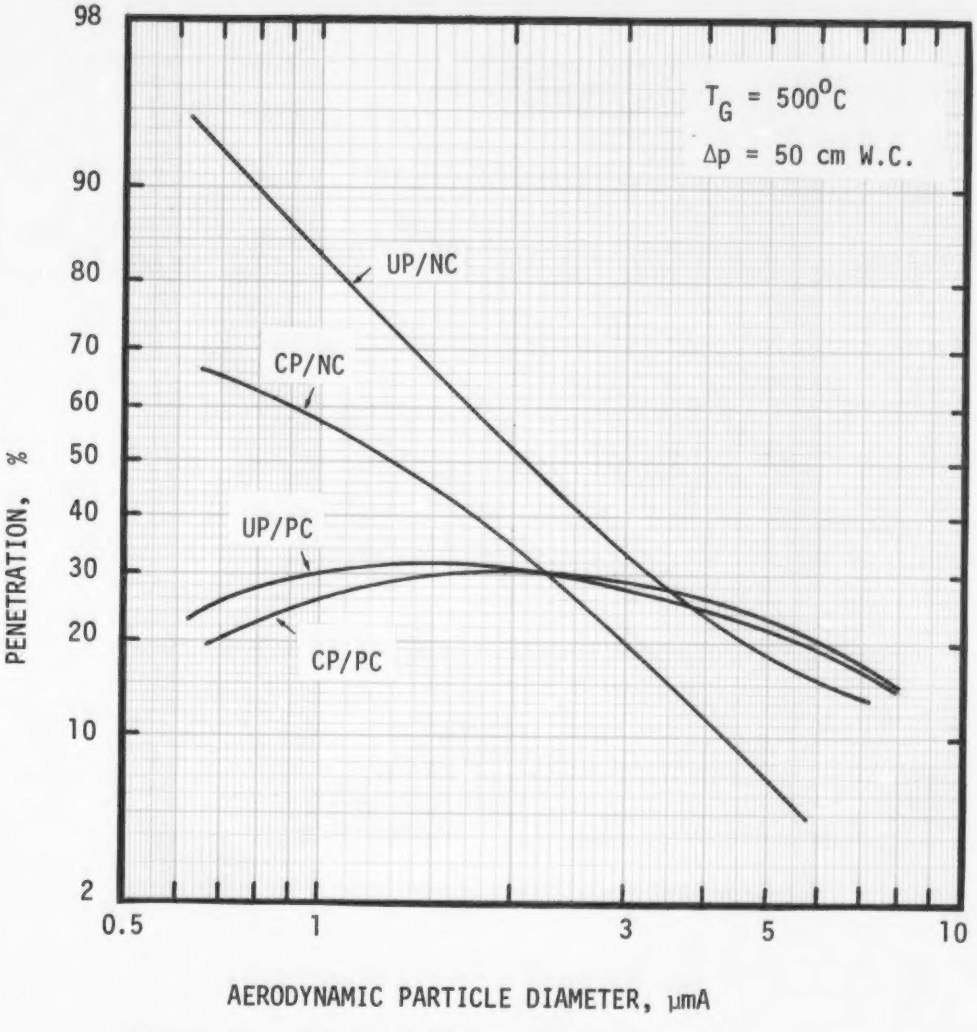

Figure 45. Measured EPxP penetration.

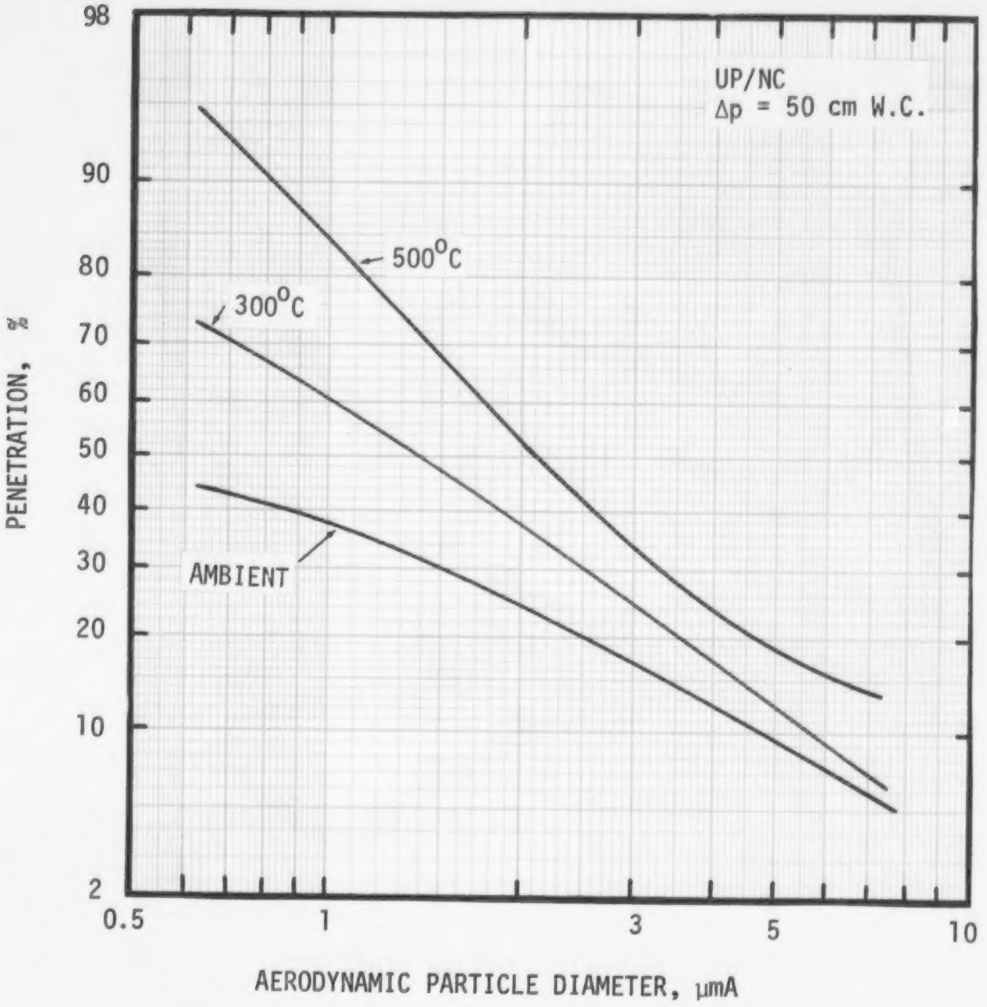

Figure 46. Effect of temperature on penetration.

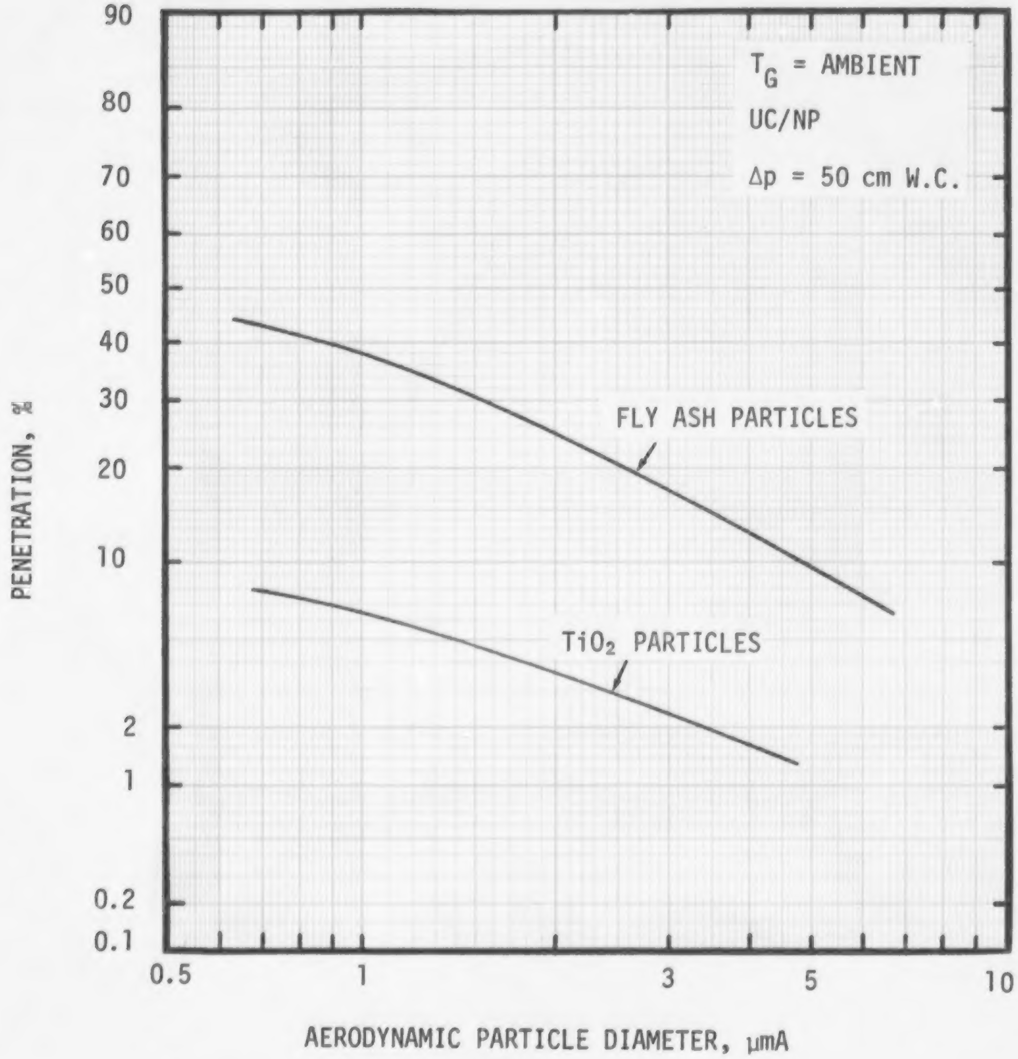

Figure 47. Effect of particle type on EPxP penetration.

Section 7

PILOT PLANT STUDIES

PILOT PLANT DESIGN

An EPxP pilot plant was designed and built based on the design information generated in the auxiliary experiments and the bench scale studies. The EPxP was used to control the emissions from an A.P.T. atmospheric fluidized bed combuster (AFBC). The flue gas from the AFBC had a volumetric flowrate of 14.2 Am^3/min at 870°C (500 ACFM at 1,600°F). The design and operation of the AFBC have been described in the report by Patterson et al. (1980).

Figure 48 shows the process flow diagram for the EPxP pilot plant. The pilot plant was primarily a scale-up of the hot bench scale system. In actual industrial installations, three EPxPs would be arranged in a "delta" arrangement as a unit. Each handles one-third of the gas flow. In the pilot plant, only one EPxP was built. The gas capacity of this EPxP was 4.8 Am^3/min at 870°C (170 ACFM at 1,600°F). Therefore, only one third of the AFBC flue gas was passed through the EPxP pilot plant. The remaining flue gas was quenched and passed through a regular venturi scrubber.

In the delta arrangement, the collector granules separated from one EPxP are cleaned and re-injected into another EPxP contactor. Since only one EPxP was built, it was designed so that the collectors could be passed through the system in a once-through mode or in a continuous circulation mode. In the continuous mode, granules were injected at the EPxP throat entrance and were lifted by the cleaned gas to a gravity settler. Collector granules separated by the settler were cleaned in a bustle and were re-injected into the throat.

The main components of the EPxP scrubber system were:

1. Particle charger
2. EPxP contactor
3. Gravity settler
4. Collector re-circulating and cleaning system
5. Quencher, and

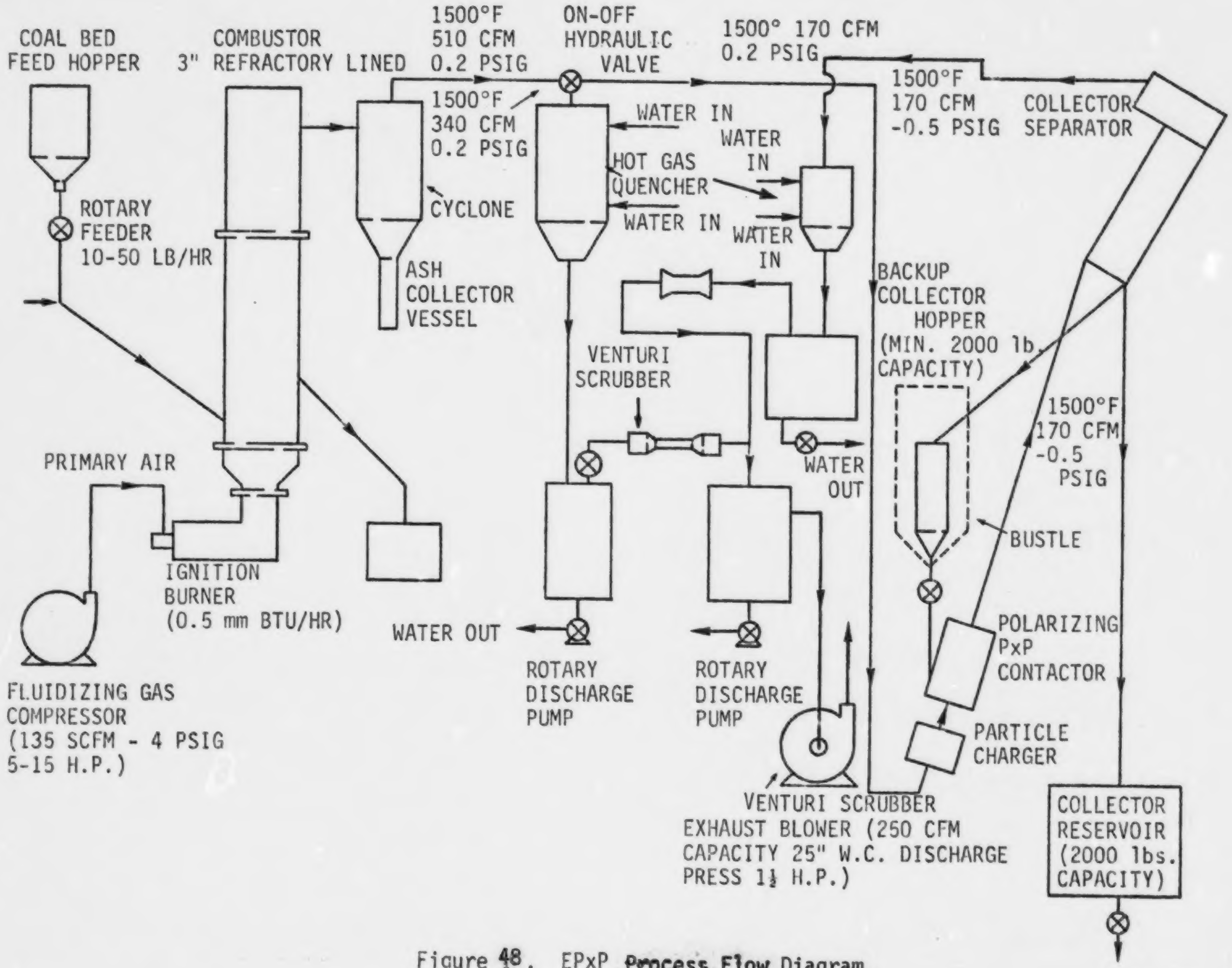
COAL BED FEED HOPPER
ROTARY FEEDER 10-50 LB/HR
COMBUSTOR 3" REFRACTORY LINED
PRIMARY AIR
IGNITION BURNER (0.5 mm BTU/HR)
FLUIDIZING GAS COMPRESSOR (135 SCFM - 4 PSIG 5-15 H.P.)
1500°F 510 CFM 0.2 PSIG
1500°F 340 CFM 0.2 PSIG
CYCLONE
ASH COLLECTOR VESSEL
ON-OFF HYDRAULIC VALVE
WATER IN
HOT GAS QUENCHER
WATER IN
WATER IN
WATER IN
1500° 170 CFM 0.2 PSIG
VENTURI SCRUBBER
WATER OUT
ROTARY DISCHARGE PUMP
ROTARY DISCHARGE PUMP
WATER OUT
VENTURI SCRUBBER EXHAUST BLOWER (250 CFM CAPACITY 25" W.C. DISCHARGE PRESS 1½ H.P.)
1500°F 170 CFM -0.5 PSIG
COLLECTOR SEPARATOR
BACKUP COLLECTOR HOPPER (MIN. 2000 lb. CAPACITY)
BUSTLE
1500°F 170 CFM -0.5 PSIG
POLARIZING PxP CONTACTOR
PARTICLE CHARGER
COLLECTOR RESERVOIR (2000 lbs. CAPACITY)

Figure 48. EPxP Process Flow Diagram.

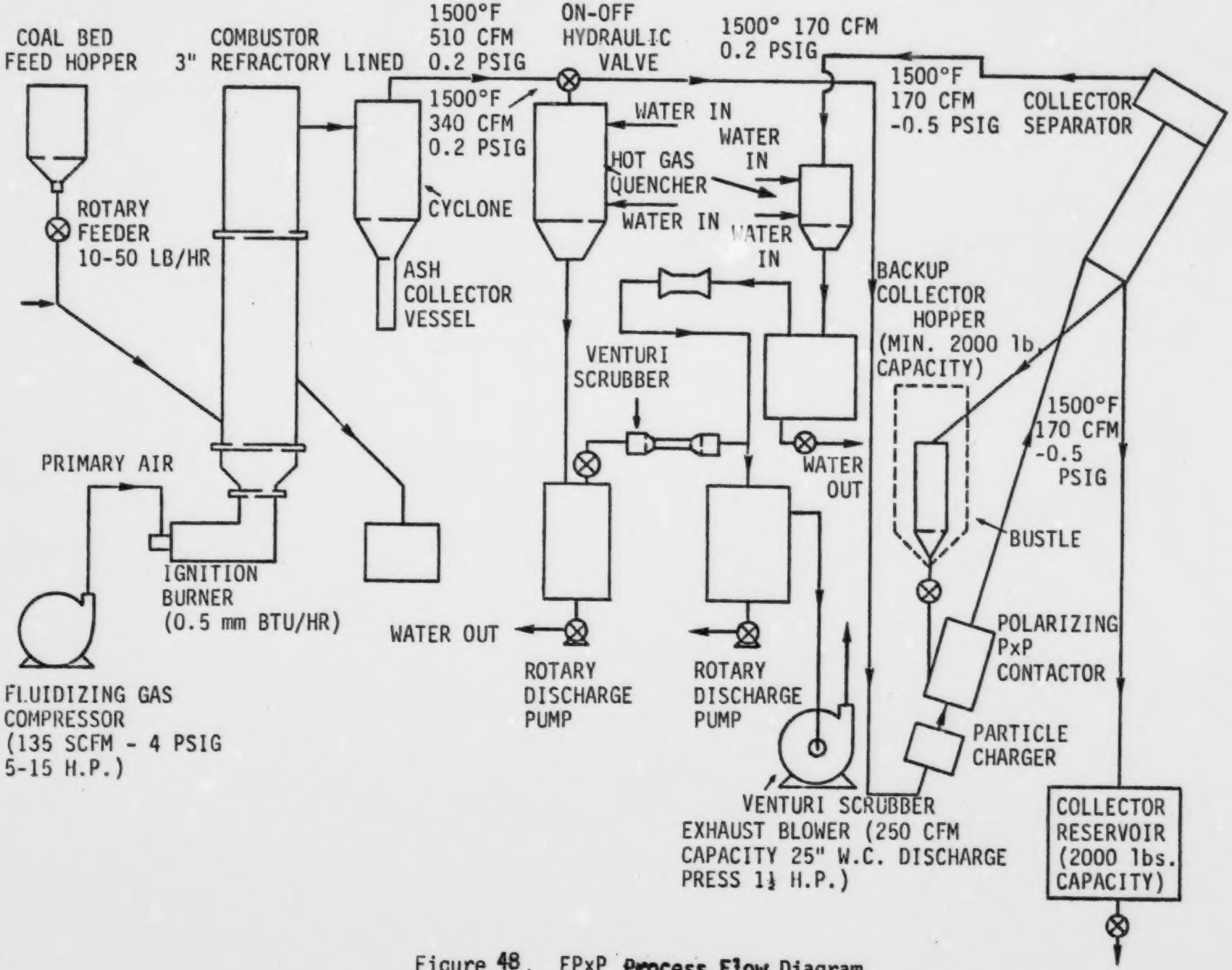
COAL BED FEED HOPPER
ROTARY FEEDER 10-50 LB/HR
COMBUSTOR 3" REFRACTORY LINED
PRIMARY AIR
IGNITION BURNER (0.5 mm BTU/HR)
FLUIDIZING GAS COMPRESSOR (135 SCFM - 4 PSIG 5-15 H.P.)
1500°F 510 CFM 0.2 PSIG
1500°F 340 CFM 0.2 PSIG
CYCLONE
ASH COLLECTOR VESSEL
ON-OFF HYDRAULIC VALVE
WATER IN
HOT GAS QUENCHER
WATER IN
WATER IN
WATER IN
1500° 170 CFM 0.2 PSIG
VENTURI SCRUBBER
WATER OUT
WATER OUT
ROTARY DISCHARGE PUMP
ROTARY DISCHARGE PUMP
VENTURI SCRUBBER EXHAUST BLOWER (250 CFM CAPACITY 25" W.C. DISCHARGE PRESS 1½ H.P.)
1500°F 170 CFM -0.5 PSIG
BACKUP COLLECTOR HOPPER (MIN. 2000 lb. CAPACITY)
BUSTLE
COLLECTOR SEPARATOR
1500°F 170 CFM -0.5 PSIG
POLARIZING PxP CONTACTOR
PARTICLE CHARGER
COLLECTOR RESERVOIR (2000 lbs. CAPACITY)

Figure 48. EPxP Process Flow Diagram.

6. Instruments for measuring temperatures, pressures, and flow rates.

The particle charger in the pilot plant was similar to the charger in the bench scale EPxP. It was of wire-plate geometry and was made from 309 s.s., ceramic, and Nichrome wires. The following data were used in the design:

Gas velocity = 5 m/s at 870°C
Residence time of particle in the electric field = 10-15 ms.
Plate-to-plate spacing = 3.8 cm.
Wire-to-wire spacing = 2.5 cm.

The EPxP contactor was also made from ceramic. It had a rectangular cross-section with two opposing sides of the throat lined with 309 s.s. plates for producing a high electric field. The design parameters for the EPxP contactor are as follows:

Gas velocity in the throat = 48 m/s at 870°C
Collector flow rate = 31 kg/min (70 lb/min)
Throat dimensions = 3.8 cm (polarizing plate separation) x 4.5 cm x 33 cm long

The gravity settler was a 35 cm x 35 cm x 427 cm long rectangular duct. It was inclined at an angle of 60° to the horizon. Gas entered at the bottom and left horizontally near the top. Six rows of zig-zag baffles were installed in the duct near the exit to remove the collector granules.

The quencher was used for cooling the gas before venting it to the atmosphere. In it water was sprayed downward co-currently with the gas.

The gas temperatures and pressures were monitored at various locations with thermocouples and calibrated gauges. The gas flow rate was controlled with valves downstream of the quencher and was monitored with a venturi meter.

The pilot plant was operated for several days at 870°C (1,600°F) in continuously circulating mode with no difficulties.

The attrition problem mentioned earlier prevented the determination of particle collection efficiency. Figure 49 shows the measured cumulative particle concentrations at the EPxP inlet and outlet. The outlet particle

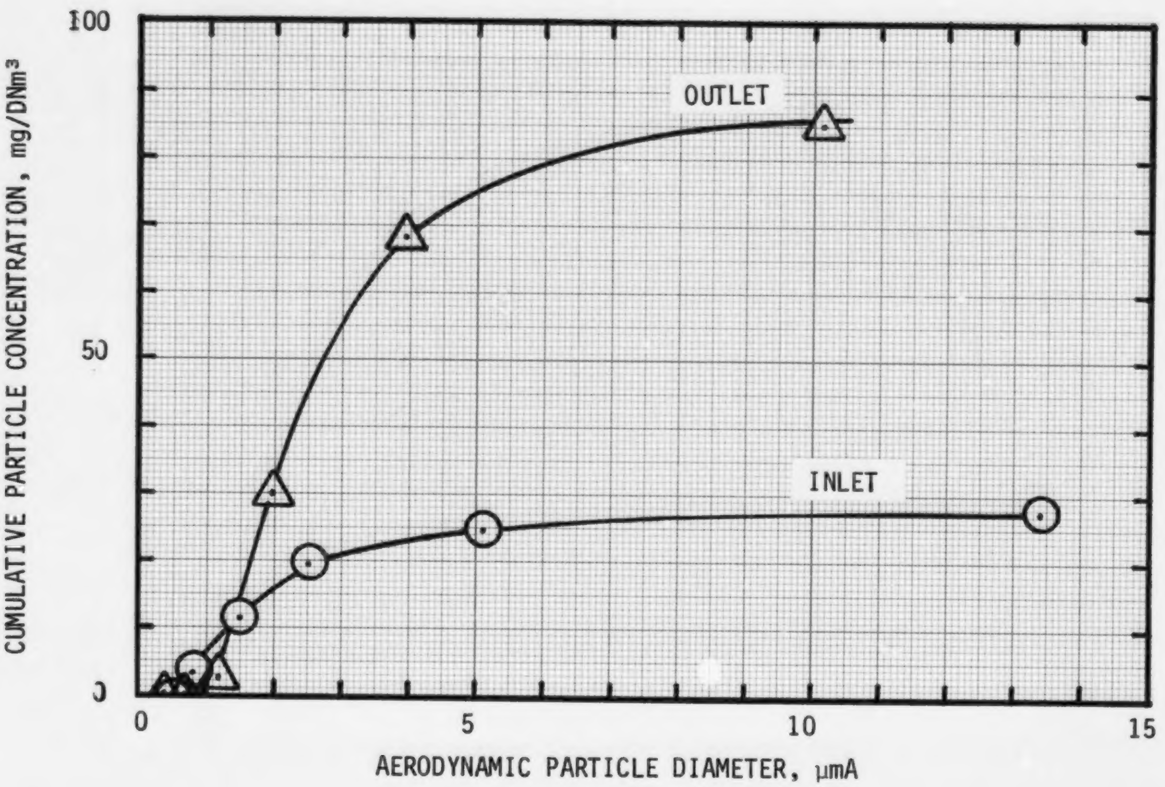

Figure 49. Measured EPxP inlet and outlet particle concentrations with no coal feed to combustor.

concentration was much higher than at the inlet. This indicated that the collector granules (zircon sand) were breaking up at high temperatures. Particle samples collected by cascade impactors showed two distinct colors, black in lower stages and sandy brown in the upper. This indicates either attrition or reentrainment of fine dust contained in the sand. Cleaning the sand by passing it through the system several times helped but did not completely alleviate the problem.

Figure 50 shows the measured particle penetration for the EPxP. The particles were charged and throat was polarized for this run. The gas velocity in the throat was 45 m/s and the gas phase pressure drop was 51 cm W.C. Due to attrition of the sand, the particle penetration increased with increasing particle diameter.

Attrition did not produce particles smaller than 0.5 μmA (Figure 49). Therefore, the measured penetration curve was valid for $d_{pa} < 0.5$ μmA. From Figure 50, the particle penetration is 0.25 for $d_{pa} = 0.5$ μmA, which is close to that measured in the bench scale EPxP at a lower gas temperature.

In order for the EPxP to be operated successfully, attrition-resistant granules, such as high density alumina spheres, are needed. The cost of 0.1 μm diameter alumina spheres was too high to be used in this study. For this reason, no additional particle sampling experiments were done.

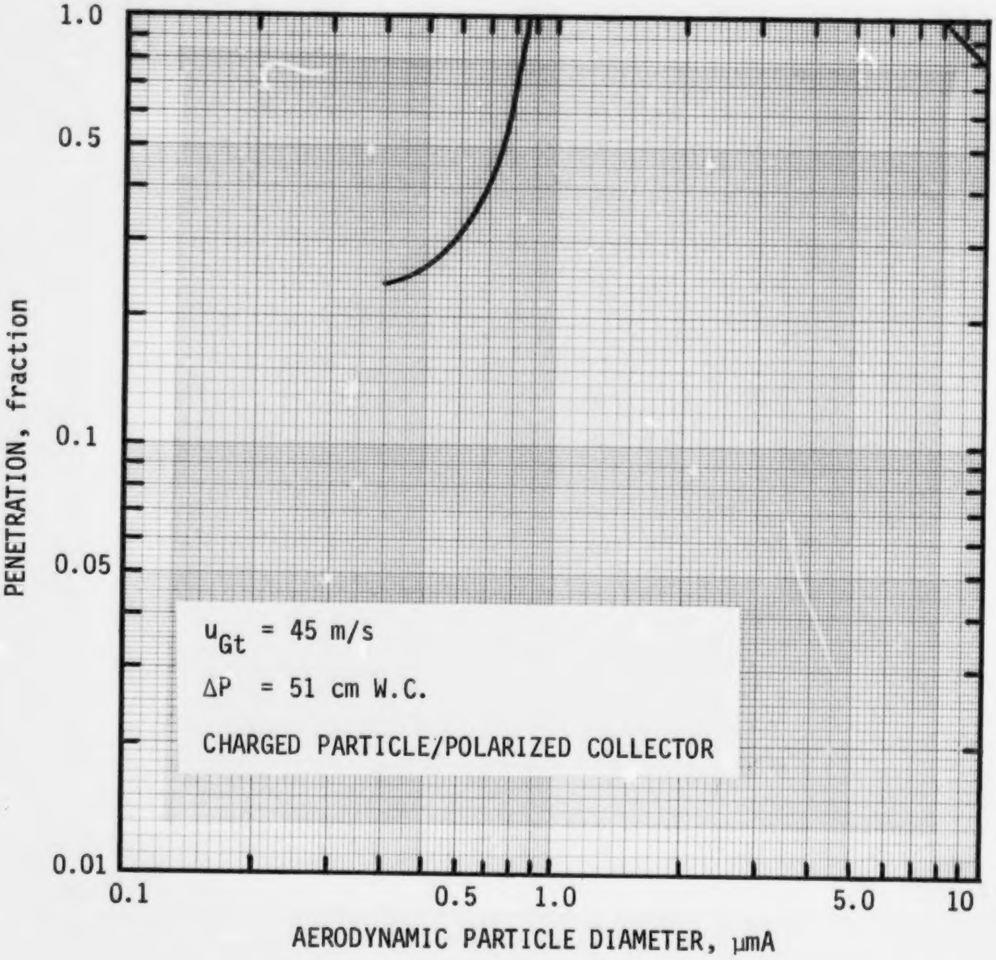

Figure 50. Measured EPxP penetration.

Section 8

EVALUATIONS

A detailed economic and engineering evaluation of the PxP Dry Scrubber has been presented by Patterson et al. (1980). This evaluation will not be repeated here. In the following sections, the feasibility of using the EPxP to control the emissions from a pressurized, fluidized bed combuster (PFBC) to meet the turbine requirements and the EPA emission limit is evaluated.

HTP CLEANUP REQUIREMENTS

Particle cleanup requirements for HTP processes vary depending on the intended use of the gas. If it is to be vented, the gas must be cleaned sufficiently to meet the EPA emission standards. The NSPS (new source performance standards) for fossil fuel-fired boiler is being lowered to 13 mg/MJ. This would correspond to a mass concentration of about 0.03 g/Nm^3 for a typical PFBC.

If the hot gas is to be expanded through a gas turbine, the gas should be cleaned to meet NSPS as well as turbine requirements. There is a great deal of uncertainty among experts as to the particle tolerance of industrial gas turbines.

Researchers at the Westinghouse Research Laboratories (Sverdrup et al., 1977) have looked at this problem from a theoretical basis, considering the effects of hot corrosion, erosion, and fine particle deposition on turbine performance. While acknowledging that much additional experimental work is needed, they concluded that an order of magnitude estimate of the gas cleanliness required to operate a large industrial gas turbine in a combined-cycle system is a mass concentration below about 0.0046 g/Nm^3 (0.002 gr/SCF).

United Technologies Research Center has conducted an investigation of the gas cleanup requirements for combined-cycle systems (Robson and Blecher, 1976). They concluded that the best estimate for the allowable particle mass concentration passing through a gas turbine is 0.0028 g/Nm^3 (0.0012 gr/SCF).

General Electric Company (Boericke et al., 1980) considered the experimental results of coal-fired locomotive turbine tests, GE erosion rig tests, and PFBC cascade experiments performed by GE at Exxon and NCB/CURL. They estimated that a GE heavy duty industrial gas turbine could tolerate particle concentration in the range of 0.1 g/Nm^3, provided 98% or more of the particles is under 10 μm in diameter. Figure 51 shows the projected turbine tolerance by General Electric (1981).

Parker and Calvert (1977) reviewed the literature thoroughly and found estimates ranging from 40 ppb (about 0.000023 g/Nm^3) to 0.35 g/Nm^3 (0.15 gr/SCF). This range is not so surprising when we consider that the actual allowable mass concentration will depend on the chemical composition of the gas and particulate matter, the size of the particles, the hardness or abrasiveness of the particles and turbine blades, the aerodynamic design of the turbine, turbine inlet temperature and very likely many other parameters.

The turbine requirement estimated by Westinghouse and United Technologies is approximately 10 times more stringent than the EPA NSPS. The GE projected turbine tolerance is less stringent than EPA emission standard. Therefore, even though a particle control device can clean the gas to meet the GE projected turbine tolerance, additional cleaning (which could be done at lower gas temperatures and pressures) is needed if the gas is vented to the atmosphere after the turbine.

EMISSIONS FROM PFBC

Most proposed HTP particle control systems use one or two stages of cyclones for primary and secondary particle removal. The primary cyclone recycles unreacted carbon to the combuster. The secondary cyclone reduces the particle concentration and size of the particles to the final collection stage, such as an EPxP scrubber.

To evaluate the potential of EPxP scrubber to clean the gas to meet NSPS and turbine requirements, information on particle size distribution and concentration of particles in the gas stream from the secondary cyclone is needed. Exxon (Hoke, 1980) collected the particles with filters and determined the size distribution of the collected particles with a Coulter Counter. The average size distribution has a mass median diameter of 4.8 micrometers and a geometric standard deviation of 3.2. The mass concentration varied from 0.23 to 2.3 g/Nm^3 (0.1 to 1.0 gr/SCF).

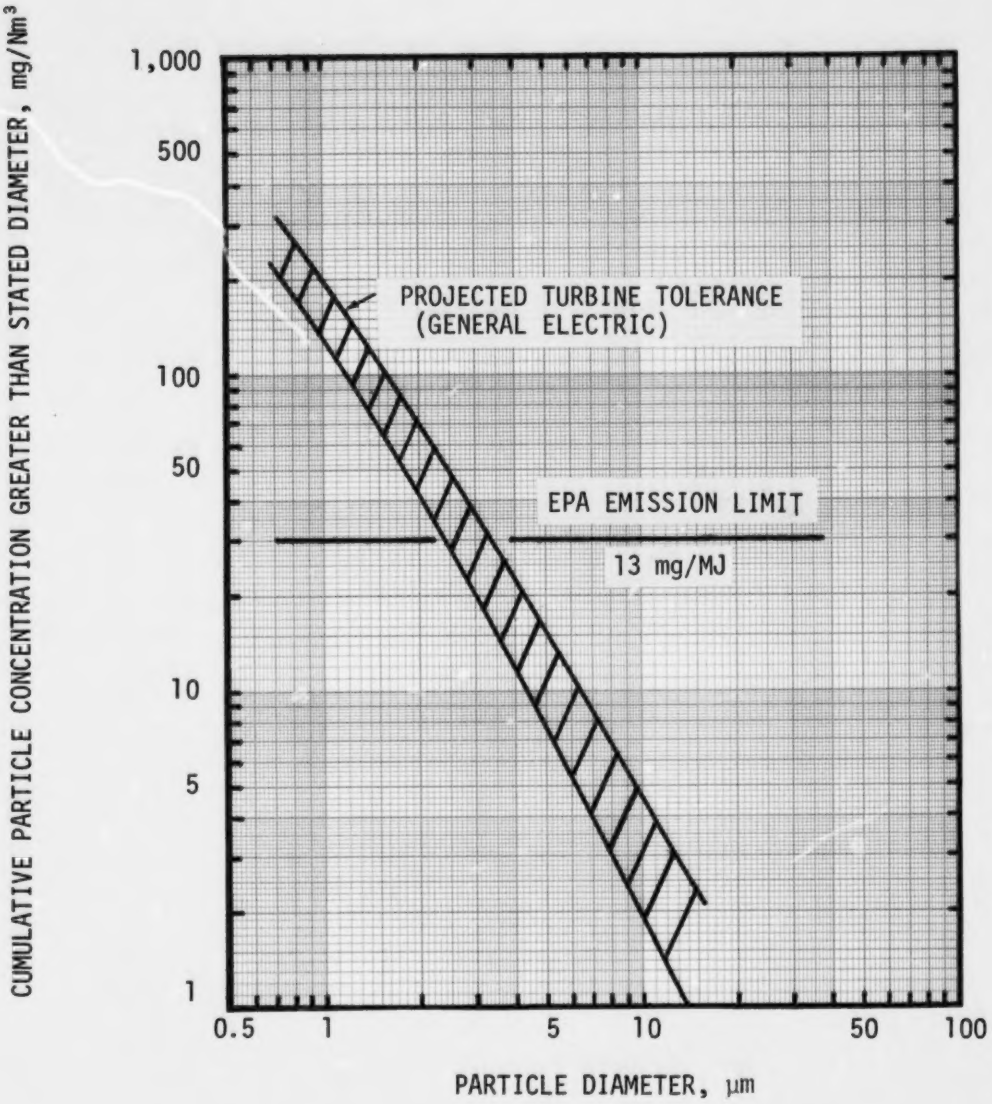

Figure 51. Projected turbine tolerance.

A.P.T. in cooperation with Exxon and SoRI did a performance test of a tertiary cyclone of the PFBC miniplant using the A.P.T. HTP cascade impactors. Figure 52 shows the cumulative mass concentration measured at the inlet of the tertiary cyclone (outlet of the secondary cyclone). The mass median diameter is about 2.5 μmA and the concentration is about 2.3 g/Nm^3.

In the following evaluations, the particle size distribution reported by A.P.T. (Figure 52) will be used. The particle concentration is taken to be 2.3 g/Nm^3.

PERFORMANCE EVALUATION

Figure 53 shows the maximum allowable penetration to meet GE's projected turbine requirement. It was calculated using Figures 51 and 52 as the outlet and inlet cumulative mass concentration of a control device, respectively.

Given the experimental grade penetration curve at ambient temperatures, the EPxP is capable of meeting the GE projected turbine tolerance with a scrubber pressure drop of 50 cm W.C. The EPxP cannot meet the GE requirement at high temperature with the same pressure drop. The EPxP also cannot meet NSPS and turbine requirements estimated by Westinghouse and United Technologies at a pressure drop of 50 cm W.C. To meet the NSPS and turbine requirements by Westinghouse and United Technologies, the EPxP should be operated at a higher pressure drop. Since neither experimental data nor a reliable mathematical model is available for higher pressure drops, the required pressure drop is not known.

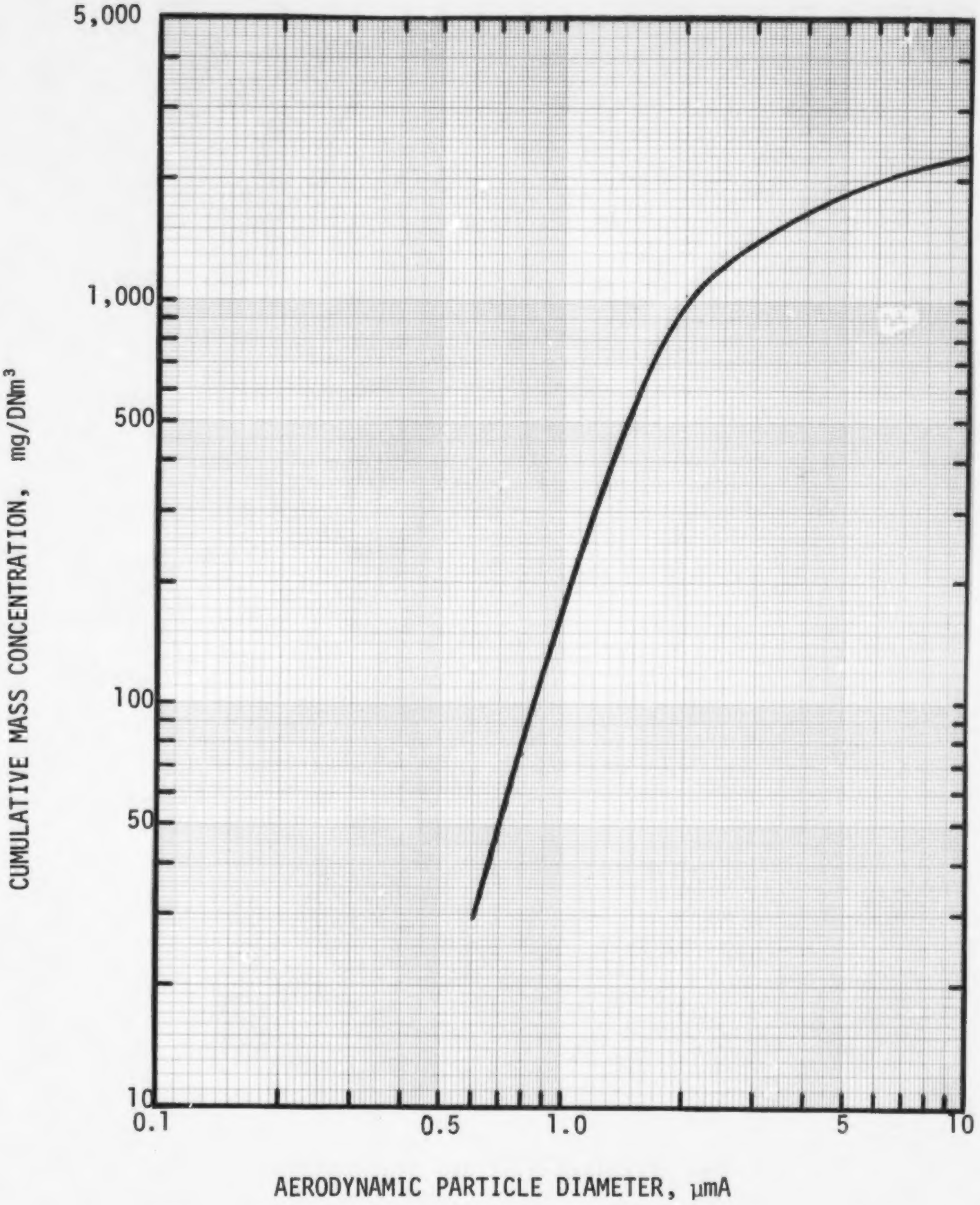

Figure 52. Particle size distribution in gas stream from secondary cyclone.

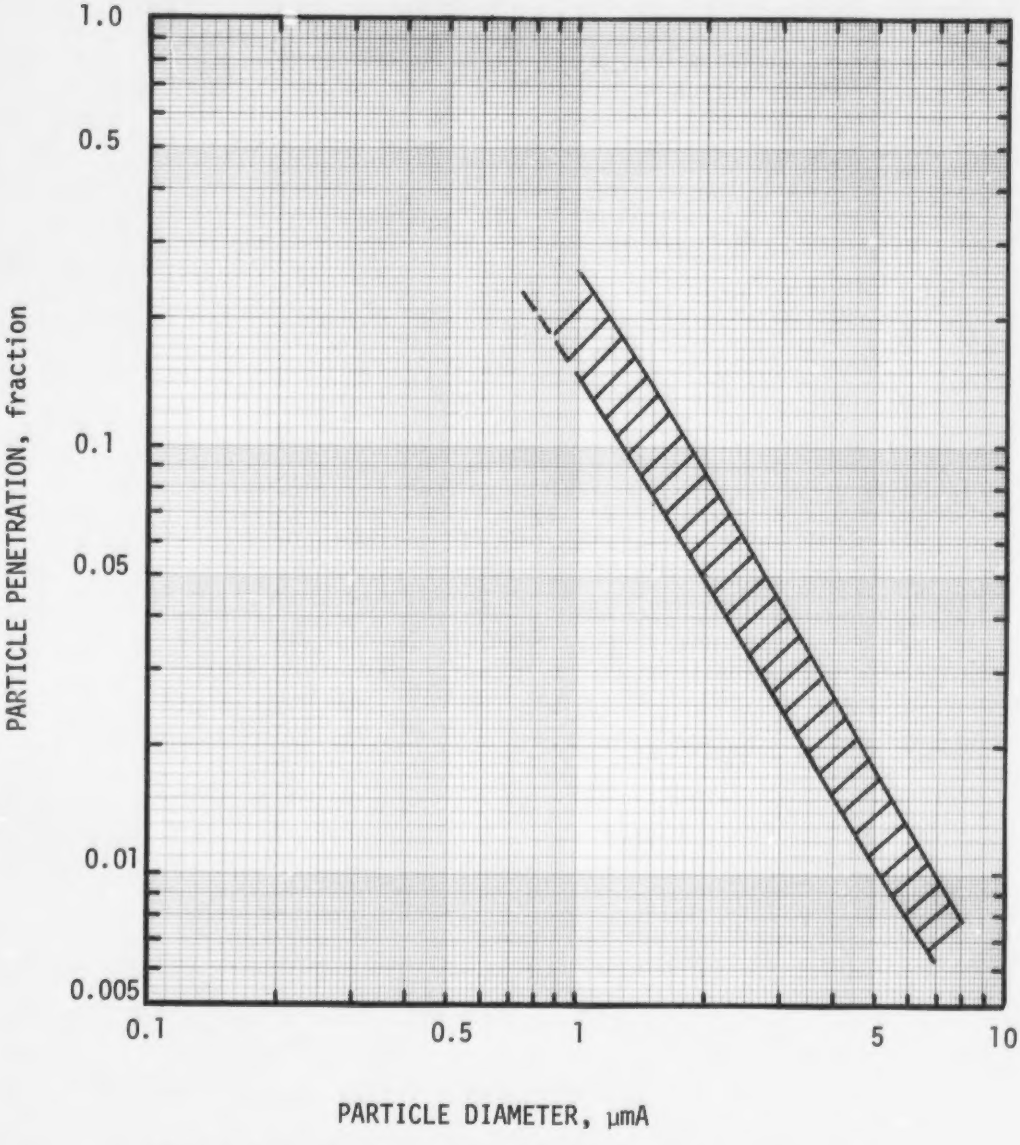

Figure 53. Maximum allowable penetration to meet GE's turbine requirement.

Section 9

RECOMMENDATIONS

Electrostatic augmentation is a feasible way of improving the high temperature performance of the PxP scrubber. When the particles are pre-charged and the collector granules polarized, the EPxP has the potential to clean the gas to meet the turbine requirements.

For successful operation, the EPxP needs attrition-resistant materials, such as high density alumina spheres. Alumina spheres of 0.1 mm diameter are not mass produced at this time. Therefore, their cost is high and they are not yet economically feasible for use in the EPxP.

The price of 0.1 mm diameter alumina spheres is expected to become economic for use in the EPxP scrubber in the near future. It is recommended to re-evaluate the EPxP scrubber when alumina spheres are available and to determine the operating conditions for the EPxP scrubber to meet the NSPS requirements.

The particle penetration predicted from the Venturi scrubber performance model did not agree with experimental measurements. A better design model for the EPxP is needed and its development is recommended.

REFERENCES

Boericke, R. R., R. Hartman, and J. Kuo, Assessment of Gas Turbine Erosion by PFB Combustion Products Paper presented at the 6th International Conference on Fluidized Bed Combustion, Atlanta, Georgia, April 9-11, 1980.

Boll, R.H. Particle Collection and Pressure Drop in Venturi Scrubber. Ind. Eng. Chem. Fundam. 12:40-50 (1973).

Calvert, S. Source Control by Liquid Scrubbing. Chapter 46 in Air Pollution, Arthur Stern, ed. Academic Press, N.Y. 1968.

Calvert, S. Venturi and Other Atomizing Scrubbers: Efficiency and Pressure Drop. A.I.Ch.E. Journal, 16:392-396, 1970.

Calvert, S. Engineering Design of Fine Particle Scrubbers, J. of Air Pollution Control Association, 24:929-934, 1974.

Calvert, S. and R. Parker. Effects of Temperature and Pressure on Particle Collection Mechanisms: Theoretical Review. EPA-600/7-77-002, NTIS PB 264203, January, 1977.

Cooperman, P. A Theory for Space-Charge-Limited Currents with Application to Electrical Precipitation. Trans. Am. Inst. Elec. Engrs. 79: 47-50 (1960).

George, H.F. and G.W. Poehlein. Capture of Aerosol Particles by Spherical Collectors, Electrostatic, Inertial, Interception and Viscous Effects. Environ. Sci. and Tech. 8: 46-49, 1974.

Herne, H. International Journal of Air Pollution, Vol. 3, No. 1-3, 26-34, 1960.

Knettig, P. and J.M. Beeckmans. Inertial Capture of Aerosol Particles by Swarms of Accelerating Spheres. J. of Aerosol Science, 5:225-233 (1974).

Kraemer, H.F. and H.F. Johnstone. Collection of Aerosol Particles in the Presence of Electrostatic Fields. Ind. and Eng. Chem. 47:2, 426-2, 434, 1955.

Kunii, D. and O. Levenspiel. Fluidization Engineering. John Wiley and Sons. N.Y. 1969.

Langmuir, I. and K.B. Blodgett, Army Air Forces Technical Report 5418, 1946.

Lawless, P. Analysis of Cascade Impactor Data for Calculating Particle Penetration. EPA-600/7-78-189, 1978.

Nielsen, K.A. Effect of Electrical Forces on Target Efficiencies for Spheres. Eng. Research Institute Technical Report 74127, Iowa State University, 1974.

Nielsen, K.A. and J.C. Hill. Collection of Inertialess Particles on Spheres and Electrical Forces. Ind. Eng. Chem. Fundam. 15:149-157, 1976a.

Nielsen, K.A. and J.C. Hill. Capture of Particles on Spheres and Electrical Forces. Ind. Eng. Chem. Fundam. 15:157-163, 1976b.

Patterson, R., M. Taheri, and S. Calvert. The A.P.T. PXP Dry Scrubber for High Temperature, High Pressure Particulate Control. EPA contract 68-02-22164 final report, August, 1980.

Ranz, W.E. and J.B. Wong. Impaction of Dust and Smoke Particles on Surface and Body Collectors. Ind. and Eng. Chem. 44:1371-1381, 1952.

Robinson, M. Electrostatic Precipitation in Air Pollution Control, Part 1, Strauss (ed.). Wiley-Interscience, N.Y. 1971.

Robson, F. L. and W. A. Blecher, Particulate Control Requirements for Gasified Coal-Combined Cycle Power Plants. Proceedings of Particulate Control in Energy Processes Symposium, San Francisco, May, 1976. NTIS p B260499.

Smith, W.B., K.M. Cushing, and J.D. McCain. Procedure Manual for Electrostatic Precipitator Evaluation. EPA-600/7-77-059, 1977.

Sverdrup, E. F., et al. The Tolerance of Large Gas Turbines to "Rocks", "Dusts" and "Chemical Corrodants," EPA/DOE Symposium on High Temperature High Pressure Particulate Control, EPA-600/9-78-004, September 1977.

Thorton, W. Phil. Mag. 28:666 (1939).

Walton, W.H. and A. Woolcock, in Aerodynamic Capture of Particles, E.G. Richardson, ed., Pergamon Press, Oxford, 129-153,, 1960.

Yung, S., S. Calvert, and H. Barbarika. Venturi Scrubber Performance Model. EPA-600/2-77-172, August 1977.

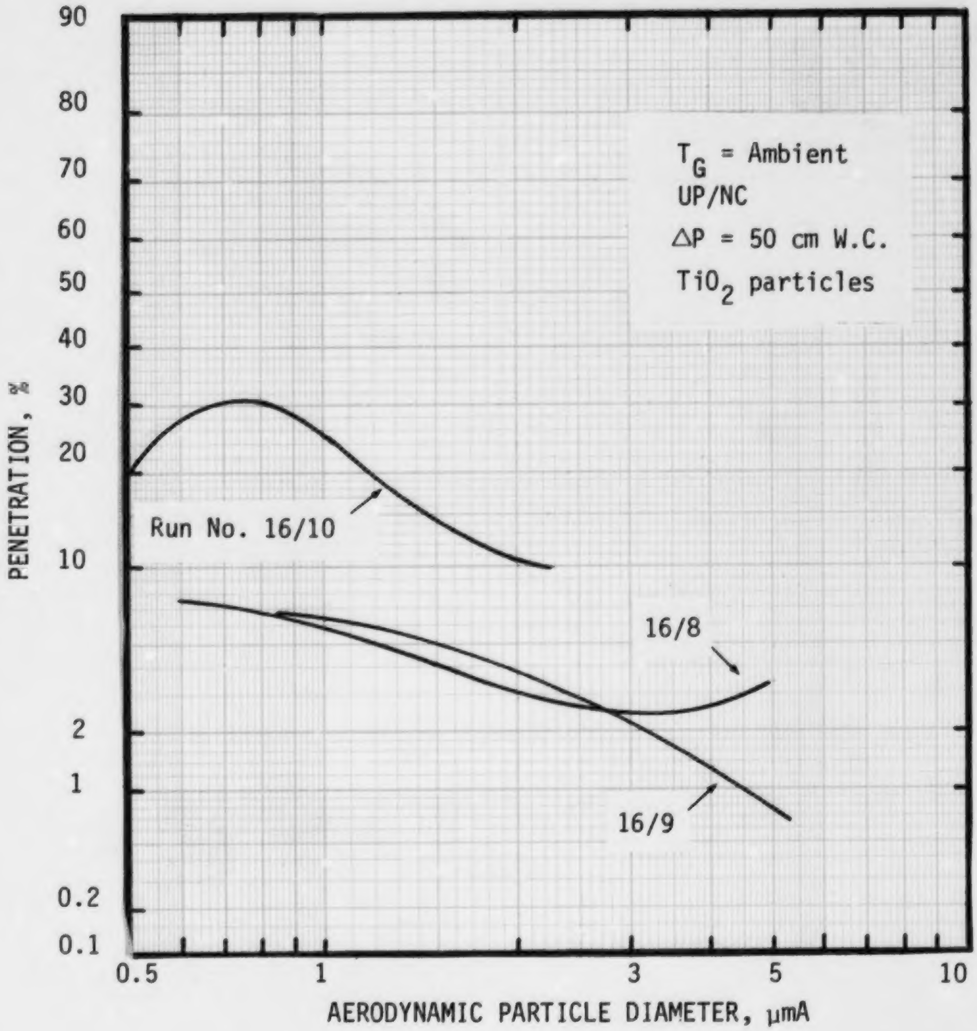

Figure A1: Measured penetration for bench scale EPXP scrubber.

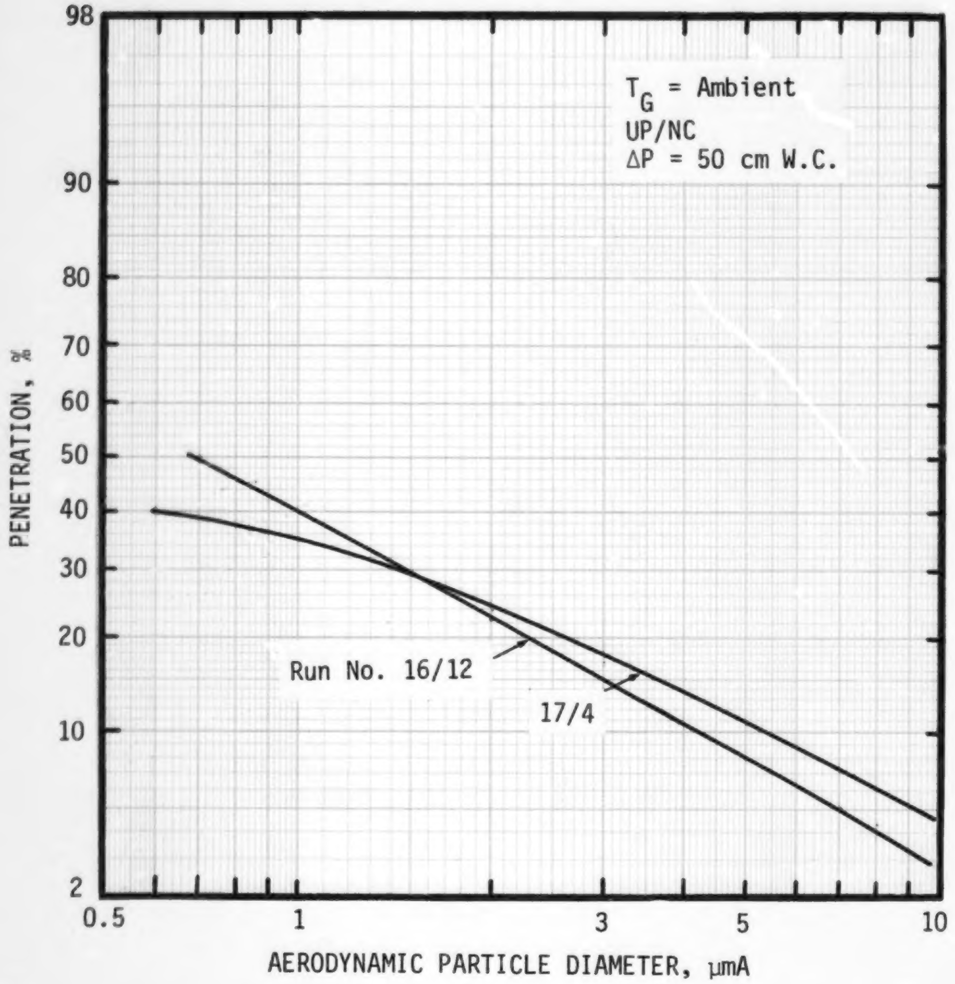

Figure A2: Measured penetration for bench scale EPXP scrubber.

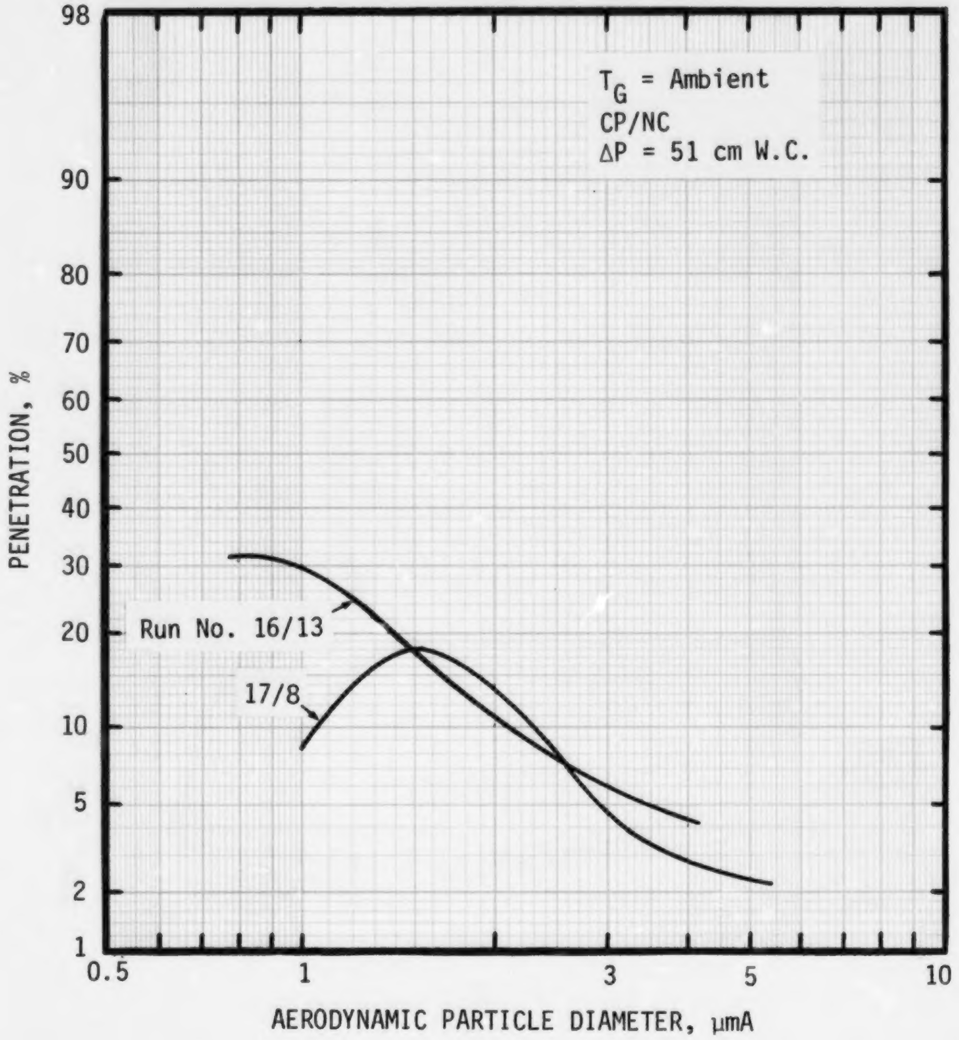

Figure A3: Measured penetration for bench scale EPXP scrubber.

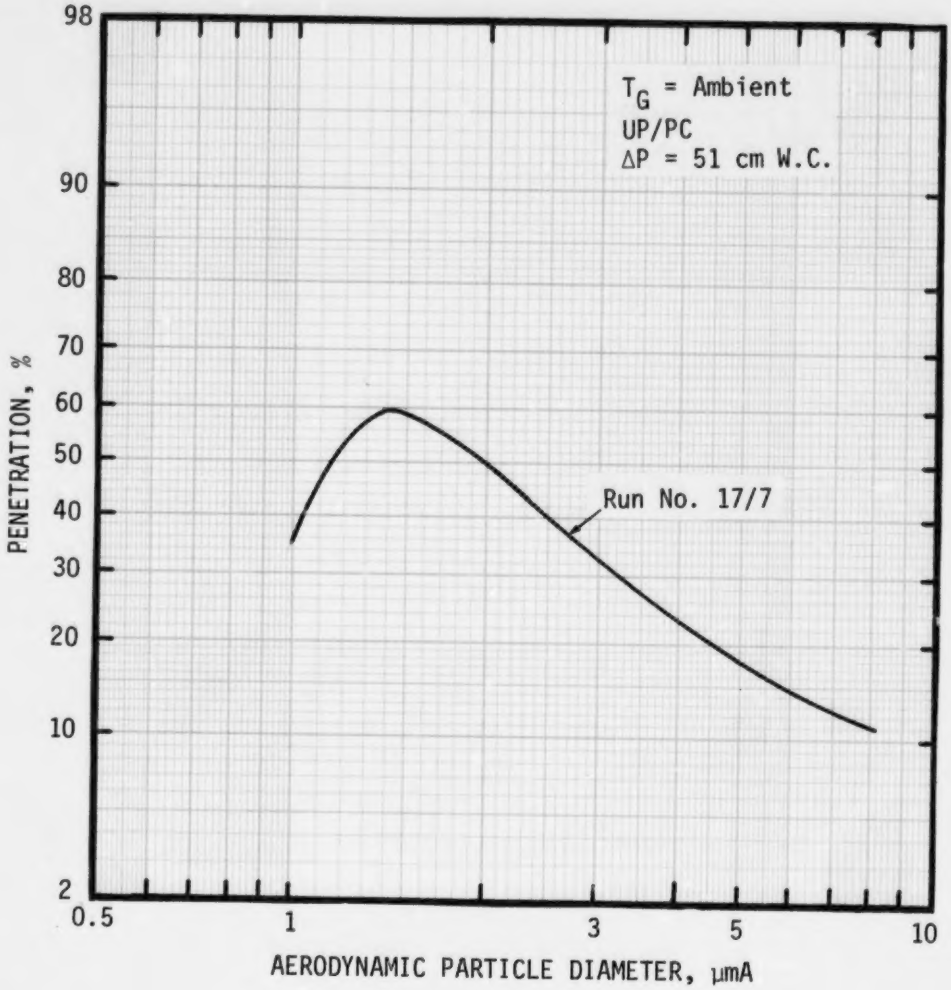

Figure A4: Measured penetration for bench scale EPXP scrubber.

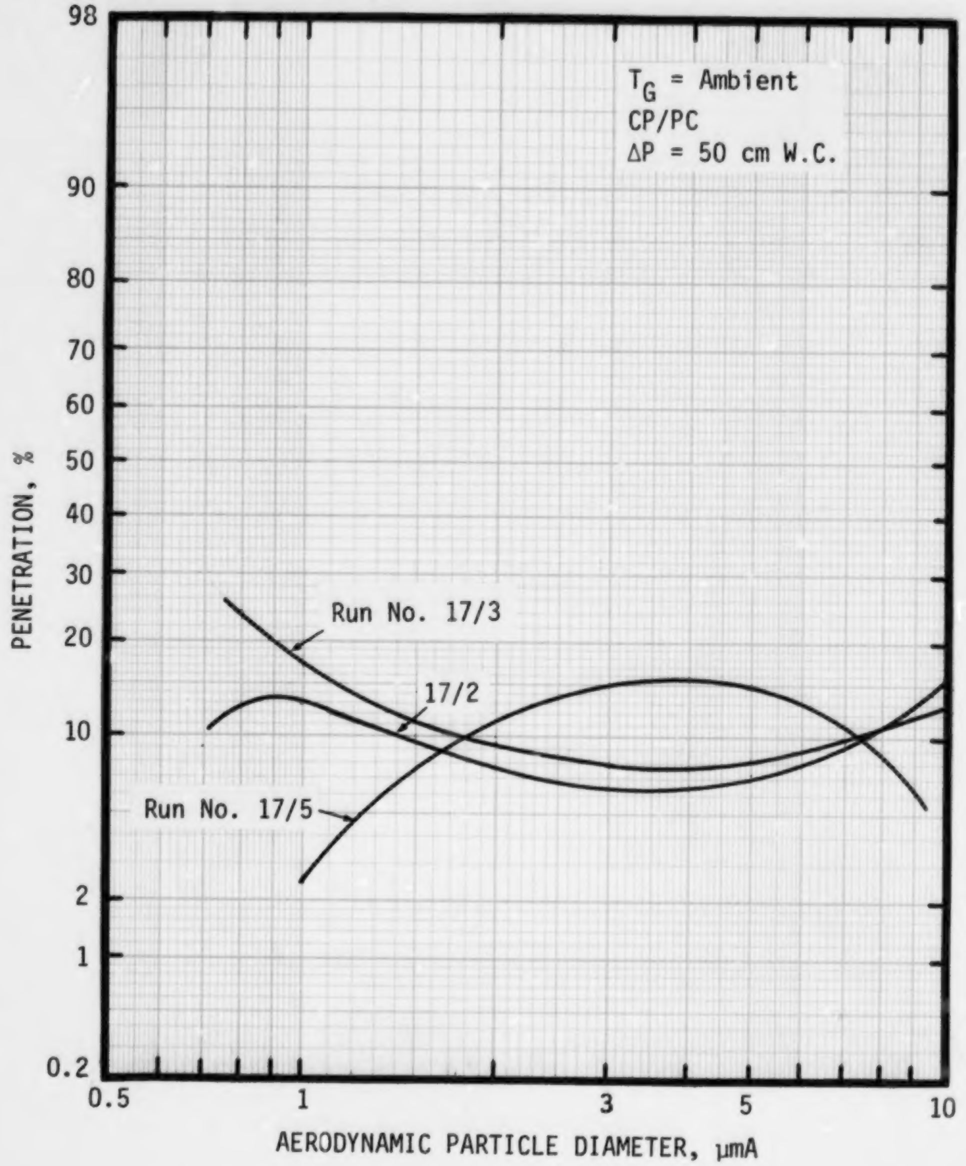

Figure A5: Measured penetration for bench scale EPXP scrubber.

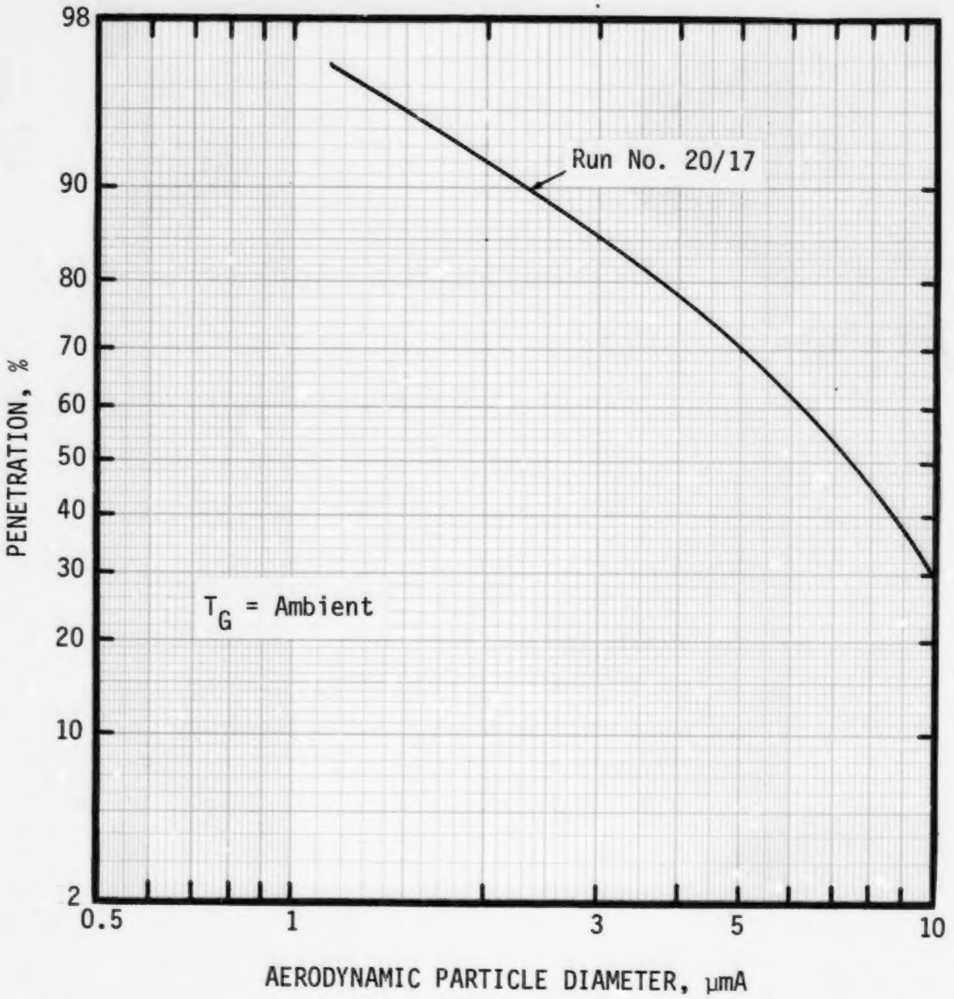

Figure A6: Particle loss in the EPXP scrubber.

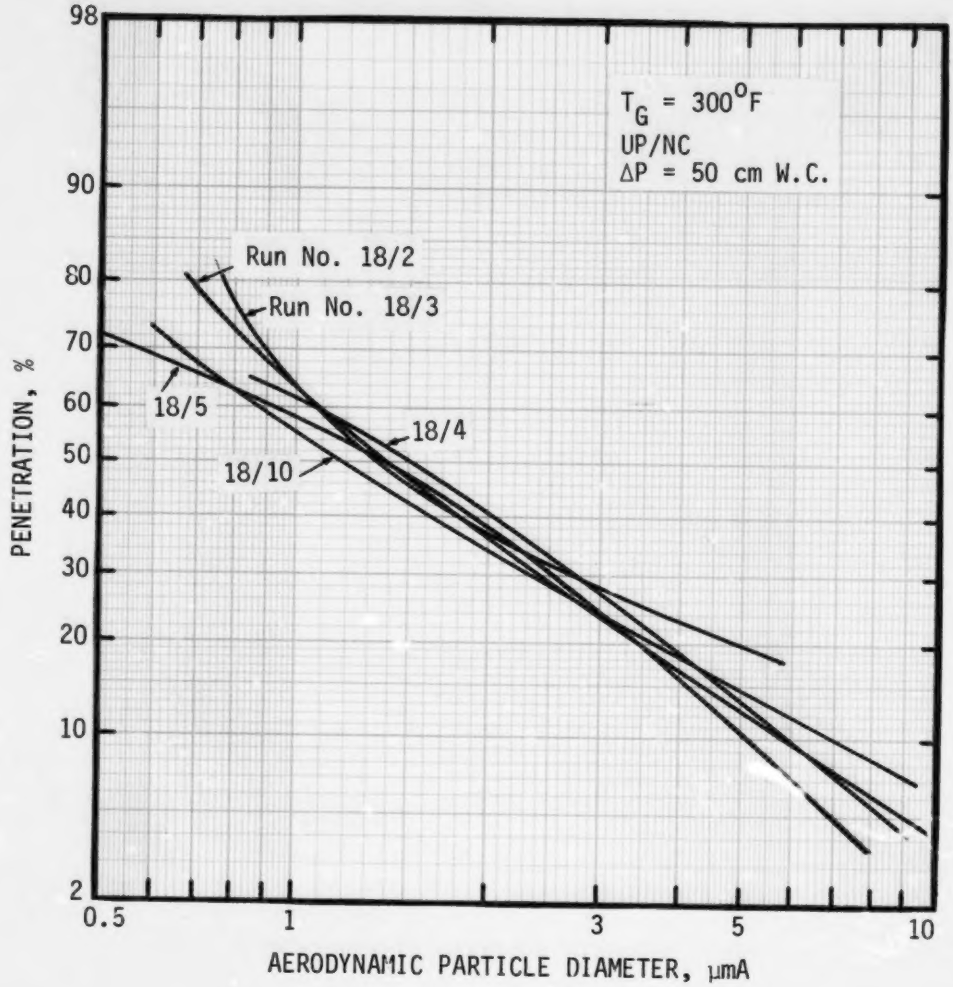

Figure A7: Measured penetration for bench scale EPXP scrubber.

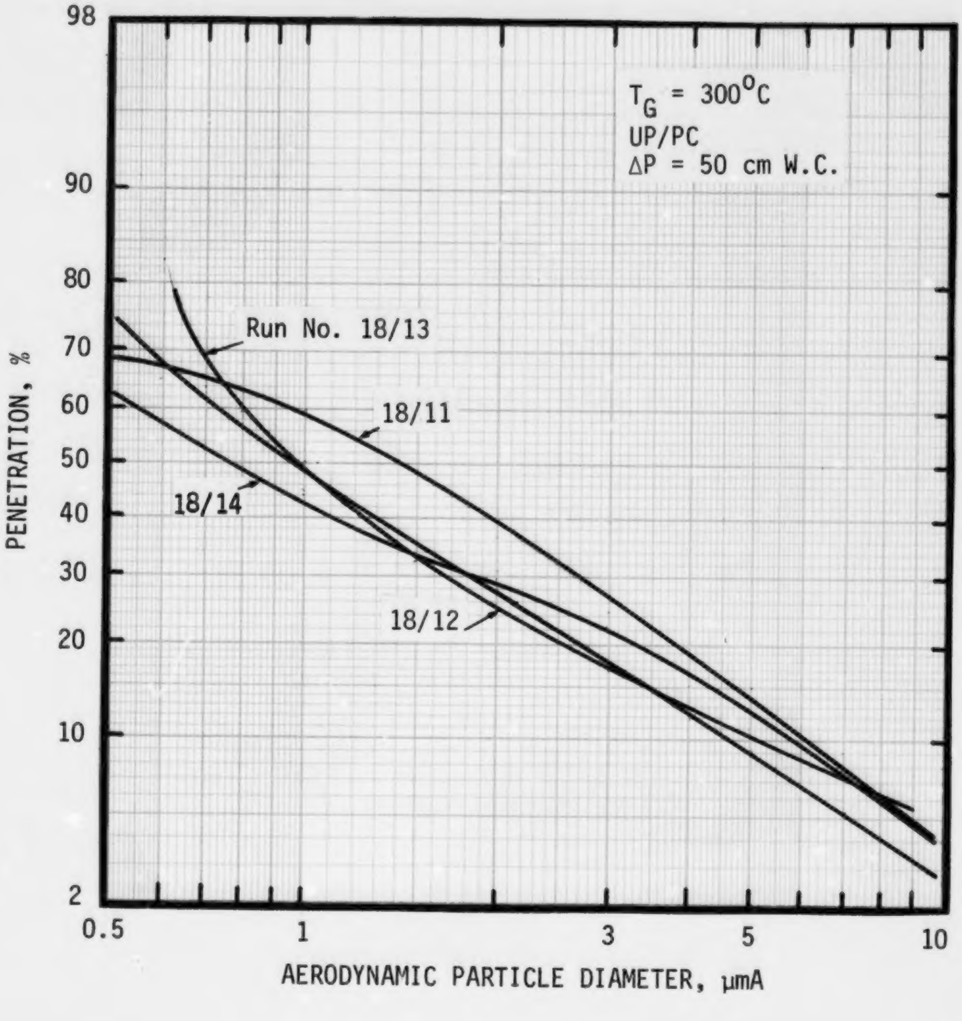

Figure A8: Measured penetration for bench scale EPXP scrubber.

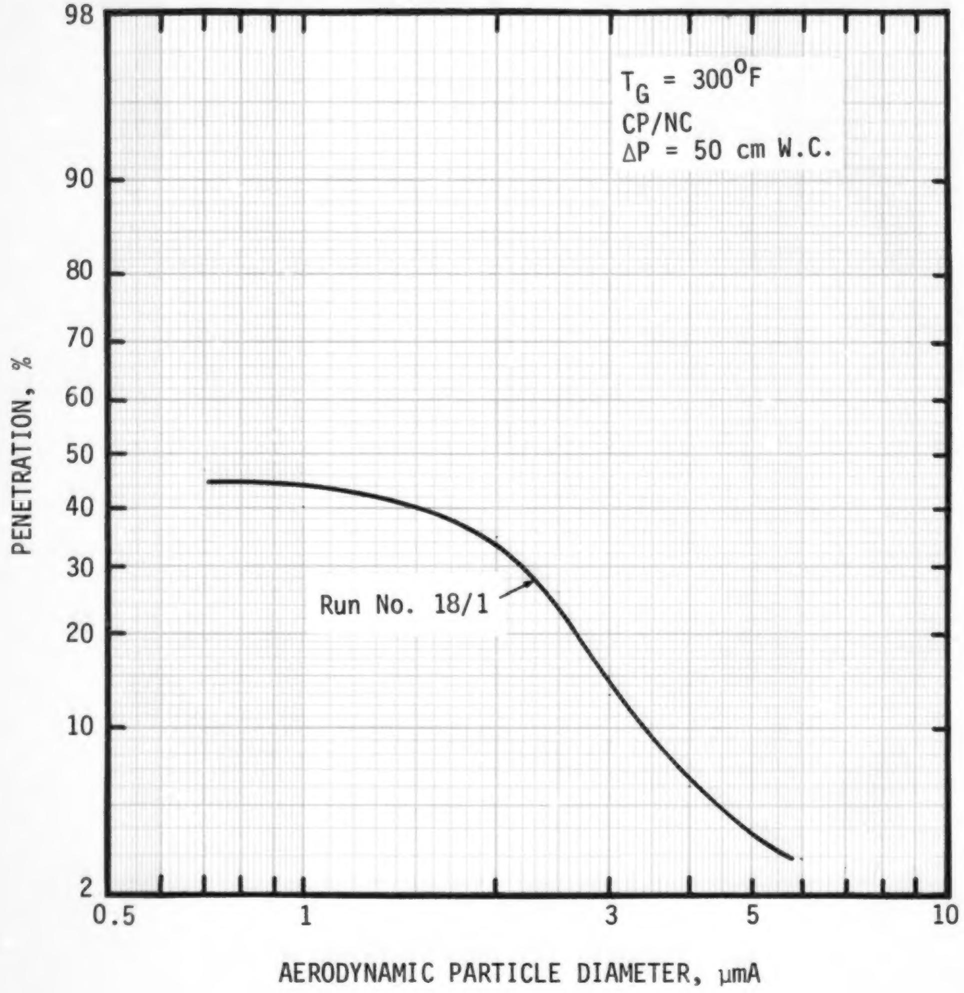

Figure A9: Measured penetration for bench scale EPXP scrubber.

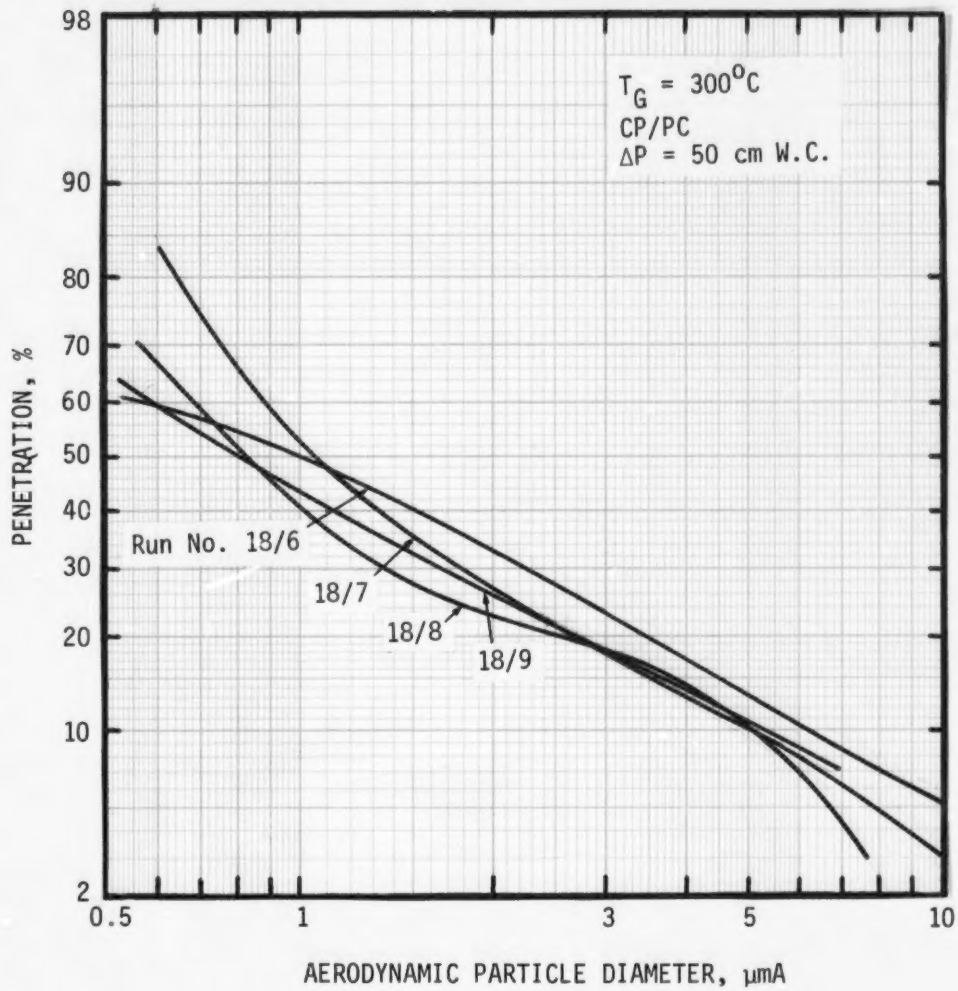

Figure A10: Measured penetration for bench scale EPXP scrubber.

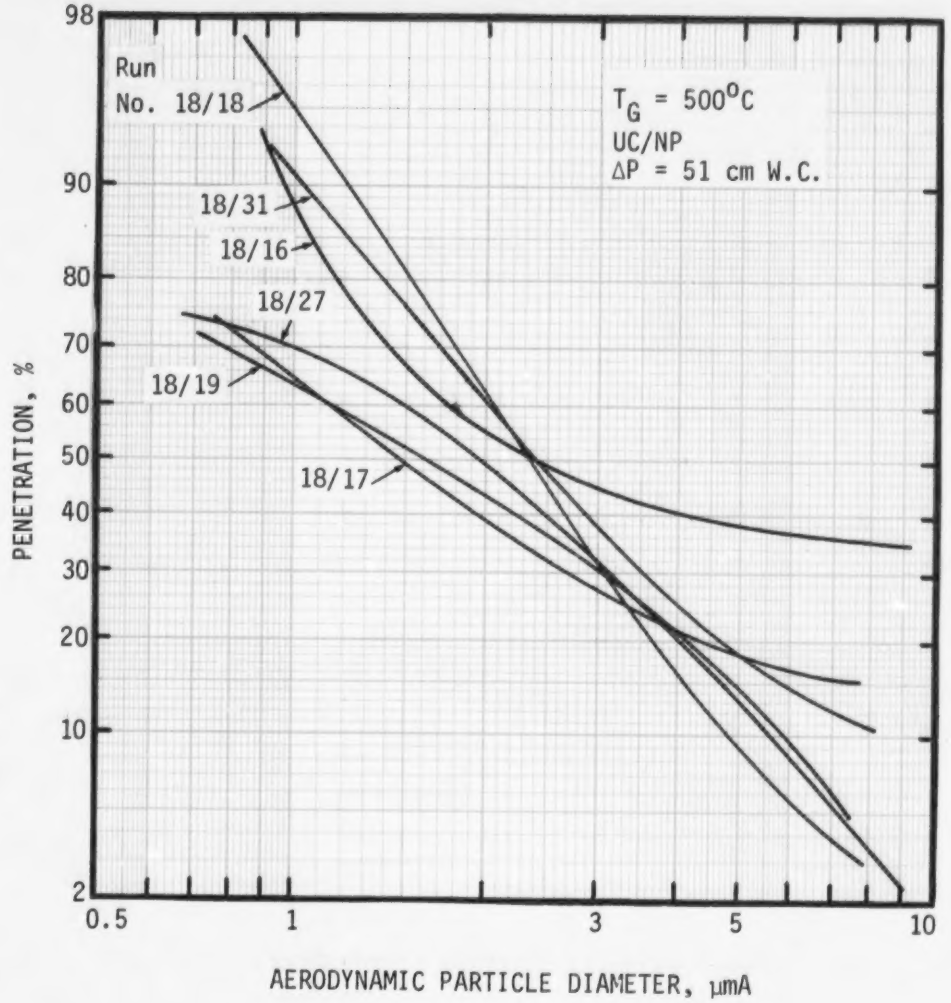

Figure A11: Measured penetration for bench scale EPXP scrubber.

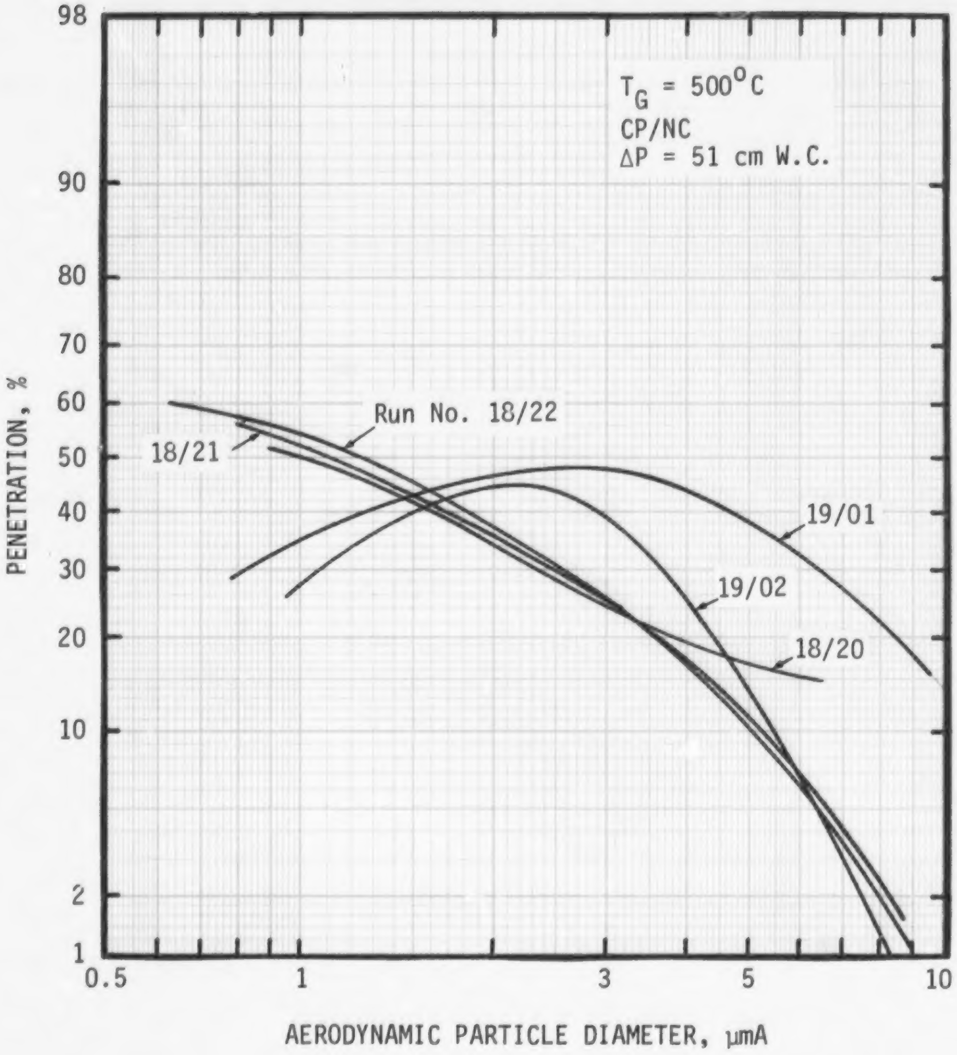

Figure A12: Measured penetration for bench scale EPXP scrubber.

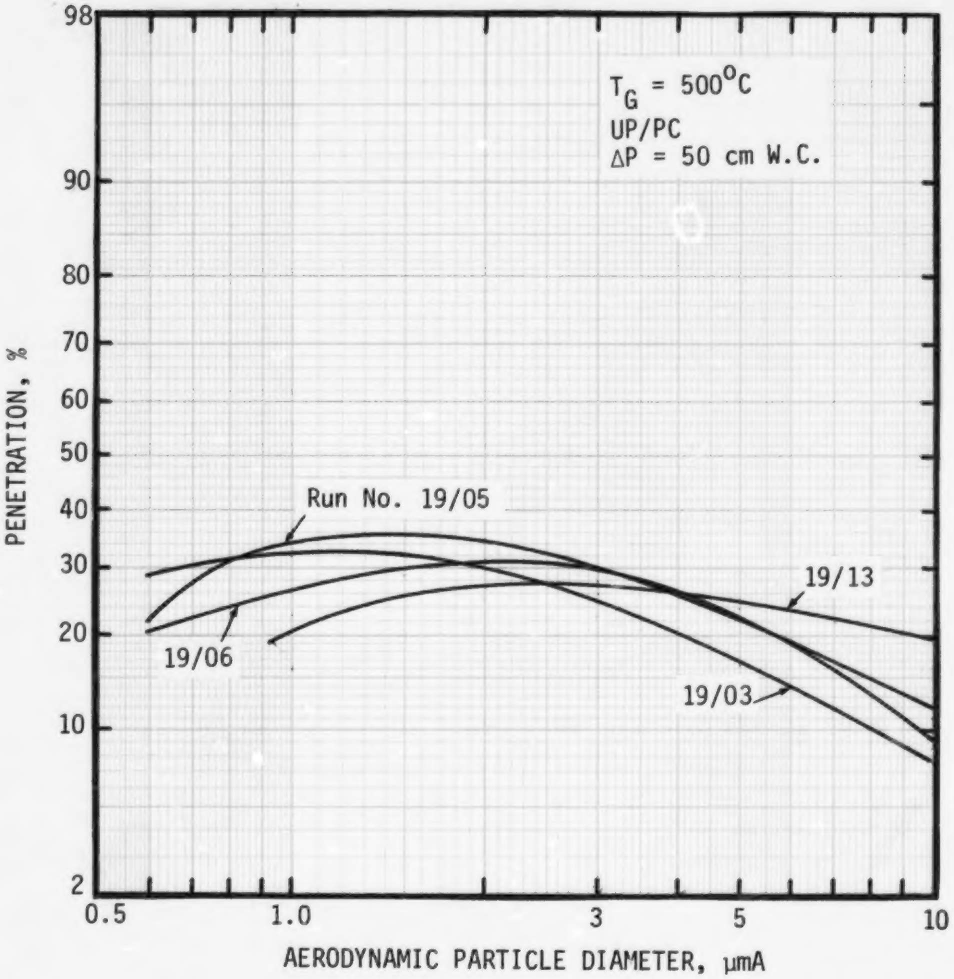

Figure A13: Measured penetration for bench scale EPXP scrubber.

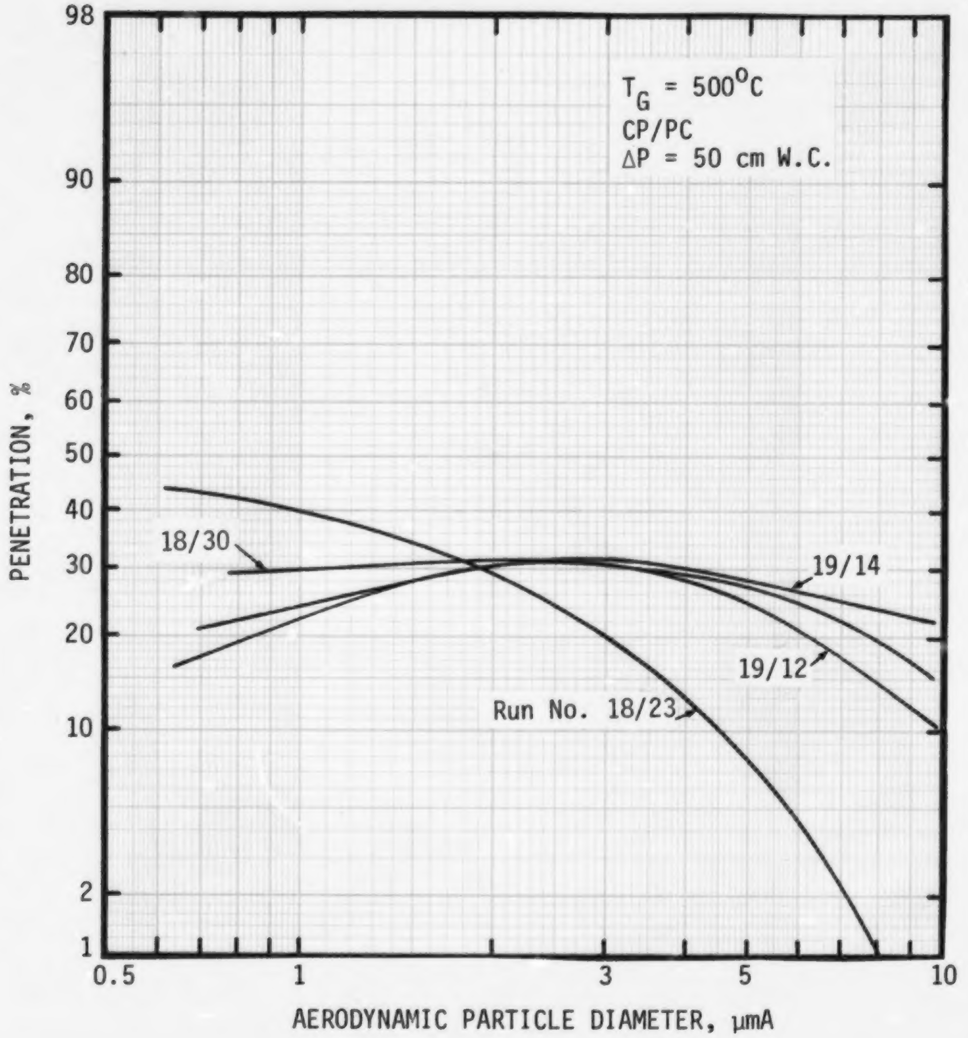

Figure A14: Measured penetration for bench scale EPXP scrubber.